UNIVERSITAT DE BARCELONA

Ni-based catalysts for H_2 production from ethanol steam reforming: Effect of the support and use of CO_2 as regenerating agent and reactant

Łukasz Bednarczuk

UNIVERSITAT DE BARCELONA

Facultat de Química

Departament de Química Inorgànica i Orgànica

Secció de Química Inorgànica

Programa de Doctorat: Química Inorgànica Molecular

Ni-based catalysts for H_2 production from ethanol steam reforming: Effect of the support and use of CO_2 as regenerating agent and reactant

Łukasz Bednarczuk

Directors:

Dr. Narcís Homs Martí, Universitat de Barcelona

Dra. Pilar Ramírez de la Piscina Millán, Universitat de Barcelona

SETEMBRE DE 2016

El Dr. Narcís Homs Martí y la Dra. Pilar Ramírez de la Piscina Millán, Catedráticos de la Universitat de Barcelona, CERTIFICAN:

Que la memoria titulada ***"Ni-based catalysts for H_2 production from ethanol steam reforming: Effect of the support and use of CO_2 as regenerating agent and reactant",*** presentada por Łukasz Bednarczuk para optar al título de Doctor en el programa de Química Inorgànica Molecular de la Universitat de Barcelona ha sido realizada bajo su dirección en el Grup de Materials Catalítics del Departament de Química Inorgànica i Orgànica, en la Secció de Química Inorgànica, de la Universitat de Barcelona.

Dr. Narcís Homs Martí Dra. Pilar Ramírez de la Piscina Millán

Quiero agradecer a todos los que me soportaron durante los estudios y la escritura, os dedico este pequeño poema

El once de septiembre, una fecha para recordar
¡Volvámonos a Erasmus para rememorar!
Un calor tremendo, la gente habla raro
Quizá sea el sol ¿algo le ha pasado?
¡Oxida glucosa! ¡Vamos, date prisa!
Y Raquel me pide una media sonrisa
No fue tan malo para no volver
Mil euros en mano ayudan a pensarlo bien
Y de nuevo septiembre, el veinte ahora
One-way ticket y de paciencia dosificadora
Es un hecho, seis años han pasado
Y el café, Muchacho, ¿Te lo has acabado?
Si fuera posible…sí, de nuevo lo haría
Un té con Xianyun es una pura alegría
¡Pero basta de eso, ponte manos a la obra!
Aunque con Marco y David el trabajo no sobra
Madrugadas frías y noches oscuras
Anuncian que las tareas serán duras
A seiscientos grados, presión atmosférica
¡Decid a los niños que rica es la química!
Y ahora escribe, algo menos tonto
¡Que Sonia te lo preguntara pronto!
Ya ha llegado el día, y aquí lo estoy mostrando,
¡No, No! ¡No solo yo he aguantado tanto!

Un grupo de gente me iba acompañando

De aquí, de allá siempre preguntando

¿Lukas, ya estas acabando?

La pregunta fácil, la respuesta no tanto…

Mejor cojo los resultados y me voy sentando

Poner tablas, crear figuras, determinar factores

Todo fue bien gracias a soporte de mis Directores

Las mañanas y las tardes, los fines de semana

¡Más fácil sería ganar contra Blaugrana¡

Pero ya se ha acabado ese camino duro

Que nos ha dejado como una pizca de cianuro

Mañana hará buen día, yo la bici monto

¡A ver si nos regeneramos pronto!

INDEX

1. Introduction 1

1.1. Application of hydrogen in road transport 3

1.2. Alternative ways of hydrogen production 4

1.3. Hydrogen production by ethanol steam reforming 6

1.4. Objective and structure of the thesis 13

1.5. References 15

2. Experimental 23

2.1. Characterization techniques 25

2.1.1. Chemical analysis by inductively-coupled plasma atomic emission spectroscopy (ICP- AES) 26

2.1.2. Physisorption of nitrogen (BET) 27

2.1.3. Powder X-ray diffraction (XRD) 28

2.1.4. Temperature-programmed reduction with H_2 (H_2-TPR) 30

2.1.5. Temperature-programmed desorption of CO_2 (CO_2-TPD) 31

2.1.6. CO_2 adsorption calorimetry 32

2.1.7. X-ray photoelectron spectroscopy (XPS) 32

2.1.8. Raman spectroscopy 33

2.1.9. Temperature-programmed oxidation coupled with mass spectrometry (TPO-MS) 34

2.1.10. Diffuse reflectance infrared Fourier transform spectroscopy (DRIFTS) 35

2.2. Reaction system and experimental procedures for ethanol steam reforming (ESR) and CO_2-assisted ethanol steam reforming (CDESR) 35

2.3. References 42

3. Preparation and characterization of supports 43

3.1. References 52

4. Study of Ni/Me_xO_y (Me = Mg, Al, Y, La, Zr) catalysts under CO_2-assisted substoichiometric ethanol steam reforming (CDESR); Regeneration of catalysts by CO_2-treatment..... 53

4.1. Preparation and characterization of Ni/Me_xO_y (Me = Mg, Al, Y, La, Zr) catalysts..... 55

4.2. Catalytic behaviour under CO_2-assisted substoichiometric ethanol steam reforming (CDESR); Characterization of spent catalysts and carbon deposits 69

4.3. Studies of regeneration of Ni/Me_xO_y catalysts by CO_2-treatment after ESR 88

4.4. References..... 96

5. Study of Ni/ZrY, Ni/ZrLa and Ni/ZrYLa catalysts under substoichiometric ethanol steam reforming (ESR); Regeneration of catalysts by CO_2-treatment.....101

5.1. Preparation and characterization of Ni/ZrY, Ni/ZrLa and Ni/ZrYLa catalysts..... 103

5.2. Catalytic behaviour under substoichiometric ethanol steam reforming (ESR); the effect of CO_2-treatment regeneration 118

5.3. Characterization of spent catalysts and carbon deposits 133

5.4. References..... 142

6. Conclusions 145

Annex 151

1. Introduction

1.1. Application of hydrogen in road transport

The constantly growing consumption of energy generated from fossil fuels causes different problems related to environmental pollution. One of the most affected sector is road transportation, which has a negative impact on the environment, mainly in air quality, due to emissions of undesired gases and dusts [1]. Nowadays, according to the International Energy Agency, about 65% of oil products are used for transportation, and more than 95% of transportation fuels are made from oil [2,3]. The substitution of cars with internal combustion engines by electric cars is considered as a solution for environmental contamination. Even though electricity still is mainly based on fossil fuels, the use of electric cars could help to solve the contamination problems in the city centres, where air pollution is higher. In this context, hydrogen has been proposed as an energy carrier in a similar way. The first attempt of hydrogen application in car combustion engines was carried out by different companies but final results were not completely positive. Direct substitution of petrol by hydrogen in combustion engines obviously diminished formation of pollutants. However, the high temperature of hydrogen combustion causes, in the presence of nitrogen coming from air, formation of considerable amounts of nitrogen oxides, and also CO_2 and CO by partial combustion of engine lubricants [4]. A different concept for application of hydrogen in electric cars assumes the use of electricity produced in fuel cells on board of the vehicle, such as in newly offered Toyota Mirai. The fuel cells would be fed with renewable hydrogen which is

not produced from fossil fuels. In this way, it could significantly reduce contamination because the only on-site product will be water. Moreover, a resignation from an oil-based economy would give an opportunity to a wider range of countries to reach independence from foreign fuel supply.

Currently, the only significant method of renewable hydrogen production is from electrolysis of water with use of expensive "green" electric energy, and only about 5% of worldwide hydrogen is generated in this way. The remaining 95% is produced upon natural gas and oil reforming and coal gasification. The H_2 obtained by electrolysis of water is about 7 times more expensive than that coming from steam reforming of natural gas. Competitive ways of hydrogen production based e.g. on transformation of biomass derivatives, such as alcohols, are still under intensive research [5]. Therefore, the main issue that must be solved, in order to fulfil numerous expectations related mainly with environmental protection, is a reliable production of renewable hydrogen.

1.2. Alternative ways of hydrogen production

Nowadays, more than half of the hydrogen produced is used for ammonia synthesis; the rest is mainly consumed for petrol and methanol production. In order to implement the hydrogen technology in the transportation, finding new methods of renewable hydrogen production is necessary. That

would lead to clean fuel production and avoidance of disadvantages characteristic for fossil fuels or use of expensive electric energy.

The methods of renewable hydrogen production are diverse. However, nowadays, they are still rather difficult to be applied at large scale. Among the different methods proposed we can distinguish those based on H_2 production from biomass conversion or on direct use of solar energy. Electrolysis of water may be ascribed to the solar group due to the possibility of using solar heat e.g. in high-temperature electrolysis, or just using photovoltaic cells for electricity production. The methods based on solar energy are considered as a long-term solution [6].

Mid-term pathways of renewable hydrogen production are proposed to be based on the use of biomass. The direct biomass gasification is investigated due to its similarity to the process of coal gasification [7]. Biomass may be also transformed into derivative products, in order to obtain more refined material for further processing. Steam reforming processes of different biomass derivative substrates could be applied for hydrogen production.

Although ethanol has been widely studied in reforming processes, other alcohols such as glycerol, propanol, butanol and other substrates such as acetone, bio oil, etc. could be also used in reforming processes for H_2 production [8–10]. This variety of potential raw materials for steam reforming makes this general process interesting not only due to the possible use of a wide range of renewable sources but also because of avoiding dependency on a specific substrate. Moreover, the well-known H_2

production from methane steam reforming can efficiently contribute to developing new processes using other substrates.

Nowadays, ethanol is the alcohol produced in a greatest scale. The traditional technology of production of ethanol is well developed [11]. However, when thinking about the amount of ethanol which would satisfy the worldwide demand on "green" hydrogen, some changes related with raw materials used in this process should be done to avoid competition between food and fuel industries. This subject has already been deeply discussed [12,13].

1.3. Hydrogen production by ethanol steam reforming

The ethanol steam reforming is an endothermic process [14]. The general equation is presented as follows:

$$C_2H_5OH + 3H_2O \rightarrow 6H_2 + 2CO_2 \qquad \Delta H° = 173 \text{ kJ/mol} \qquad (1.1)$$

However, under ethanol steam reforming conditions, different reactions can take place, depending on reaction temperature, reaction mixture composition and properties of the catalyst [14–16]. The first step is usually dehydrogenation of ethanol

$$C_2H_5OH \rightarrow CH_3CHO + H_2 \qquad (1.2)$$

Then CH_3CHO can be reformed

$$CH_3CHO + H_2O \rightarrow 3H_2 + 2CO \quad (1.3)$$

Or it can decompose

$$CH_3CHO \rightarrow CH_4 + CO \quad (1.4)$$

Methane could be reformed at appropriate temperature

$$CH_4 + H_2O \rightarrow 3H_2 + CO \quad (1.5)$$

However, ethanol may directly decompose into methane, carbon monoxide and hydrogen

$$C_2H_5OH \rightarrow CH_4 + CO + H_2 \quad (1.6)$$

Moreover, acid centres may participate in formation of carbon deposits through ethanol dehydration to ethene

$$C_2H_5OH \rightarrow C_2H_4 + H_2O \quad (1.7)$$

And further dehydrogenation or polymerization of the hydrocarbons

$$C_nH_m \rightarrow \frac{m}{2}H_2 + nC \quad (1.8)$$

Other by-products, such as acetone, can be produced [17]

$$2C_2H_5OH + H_2O \rightarrow CH_3COCH_3 + CO_2 + 4H_2 \quad (1.9)$$

In certain cases, the methanation reaction can occur, rather at moderate temperature [18]

$CO + 3H_2 \rightarrow CH_4 + H_2O$ $\Delta H° = -206$ kJ/mol (1.10)

The water gas shift reaction (WGS) (Eq. 1.11) plays an important role in the transformation of CO and H_2O into CO_2 and H_2.

$CO + H_2O \leftrightarrow CO_2 + H_2$ $\Delta H° = -41$ kJ/mol (1.11)

Furthermore, carbon monoxide can cause carbon deposits formation, through the Boudouard disproportionation

$2CO \rightarrow CO_2 + C$ $\Delta H° = -173$ kJ/mol (1.12)

Moreover, as stated above, at high temperature, decomposition of methane and other hydrocarbons also may contribute to the carbon formation (Eq. 1.8) [19,20].

The formation of carbon deposits is one of the main difficulties to overcome to carry out an effective ethanol steam reforming process. Coke covers surface active sites, deactivating catalyst, and also can worsen the circulation inside the reactor.

This short description shows that ethanol steam reforming is a complex process, combination of numerous pathways, and the obtained products may vary depending on the reaction conditions.

During more than 20 years, reforming of ethanol has been widely studied in different catalytic systems, under different conditions of temperature,

pressure and reactant composition. Emphasis has been put also into studies of ethanol steam reforming, using, besides H_2O, other reactants as O_2. The obtained results showed the main influence of catalyst on the reaction products [14,16,20].

Catalysts based on transition metals have been widely studied for application in ethanol steam reforming. Noble metals, such as Ru, Rh, Pd, Ir and Pt present good catalytic properties but are not so attractive in economic terms for applicability. Although bimetallic catalysts containing both, a noble and a non-noble metal, have been also studied in steam reforming of different substrates, including ethanol, many studies are focused on non-noble transitions metals, such as nickel and cobalt [21–24].

Nickel-based catalysts are widely used in industrial processes of hydrocarbon steam reforming. Nickel is known due to its ability to break C-C bonds, participation in water gas shift reaction and effective actuation in methane reforming [17,25–27]. The low price of nickel, easy incorporation of precursor to a support and facile activation makes this metal attractive for catalyst developing purposes. However, their main drawback is related with the formation of carbon deposits [17,26,28].

Besides the metal, the influence of the support on the catalytic behaviour under the reforming conditions has been determined. In this role, metal oxides-based systems are commonly applied. Their individual properties, related to chemical and physical characteristics, influence on the products of the reaction [29]. The use of acidic supports may promote formation of

carbon deposits because of decomposition of ethene, formed during dehydration of ethanol [30]. Doping with alkali metals was reported in different studies as an effective way of prevention of coke formation [31–33]. On the other hand, excess of basic centres may lead to higher oxygenates production such as acetone [34]. The control and modification of the above-mentioned characteristics is carried out by using adequate methods of catalyst preparation: manner of support preparation, incorporation of the active metal precursor and conditions of calcination and activation [33,35–40].

For ethanol steam reforming MgO has been reported to present good resistance to carbon deposits formation [41–43]. Al_2O_3-supported nickel catalysts have been already studied in ethanol steam reforming showing serious carbon deposition [44,45]. Y_2O_3- and ZrO_2-supported catalysts could participate in gasification of carbon deposits due to the presence of active oxygen surface species [40,46–48]. When La_2O_3 is used as a support for Ni catalysts in ethanol steam reforming the formation of carbonate $La_2O_2CO_3$ species can take place. These species can decorate the metallic particles and may react with carbon deposits (Eq. 1.13) [18,49,50].

$$La_2O_3 + CO_2 \rightarrow La_2O_2CO_3 + C_{dep} \rightarrow La_2O_3 + 2CO \qquad (1.13)$$

In terms of reactant mixture composition, the water/ethanol ratio and the presence of other reactants, such as O_2 or CO_2, may vary the final reaction product distribution. An excess of water, compared with stoichiometric values, is a method of prevention of coke formation, commonly used in

reforming of methane and ethanol [19]. Moreover, an excess of water shifts the reforming reaction toward CO and H_2 formation (Eq. 1.1 and 1.5), and further, in WGS reaction, favours H_2 formation (Eq. 1.11). However, besides all these positive aspects, an increase in the amount of water will affect negatively the energy balance of the process because of the necessary consumption of energy in water vaporization [9,51,52].

In the oxidative ethanol steam reforming (Eq. 1.14), oxygen or air is introduced in the reactant mixture; this is performed in order to oxidize carbon deposits and, due to the endothermic character of the ethanol steam reforming, to provide energy.

$$C_2H_5OH + 0.75O_2 + 1.5H_2O \rightarrow 4.5H_2 + 2CO_2 \qquad (1.14)$$

However, the amount of H_2 obtained per mol of ethanol is lower and the extra heat coming from the carbon deposits combustion may accelerate the sintering of the active phase [21,53].

There are few studies reporting about CO_2 application in reforming of alcohols [47,50,54–57]. CO_2 could be used in reforming processes as a mild oxidant helping to reduce coke formation according to the reverse Boudouard reaction.

$$CO_2 + C \rightarrow 2CO \qquad (1.15)$$

In ethanol dry reforming, CO_2 reacts with the substrate toward the partial oxidation of ethanol and leads to formation of H_2 and CO [47,55–57](Eq. 1.16), as in the methane dry reforming (Eq. 1.17) [58]

$C_2H_5OH + CO_2 \rightarrow 3H_2 + 3CO$ (1.16)

$CH_4 + CO_2 \rightarrow 2H_2 + 2CO$ (1.17)

Moreover, the CO_2-assisted ethanol steam reforming is possible

$2C_2H_5OH + H_2O + CO_2 \rightarrow 7H_2 + 5CO$ (1.18)

In these processes, CO_2 can be involved in the carbon deposits oxidation over supports rich in oxygen vacancies, such as ZrO_2, which may activate CO_2, catalysing the oxidation process [47]. Under ethanol steam reforming with excess of water, a small amount of CO_2 may participate in dry reforming of methane [50]. Moreover, for $PtSn/CeO_2$ and Rh/CeO_2 catalysts, the incorporation of CO_2 to the reactants has been shown to limit the access of the other carbon-containing substrates to the surface active centres. This contributed to the reduction of carbon deposits formation due to a decrease of the rate of decomposition of carbon-containing products [54,55].

Taking into account all this information, in this work we report on the valorisation of CO_2 through its use in the ethanol steam reforming process over Ni-based catalysts. We analyse the properties of different oxides (Al_2O_3, MgO, Y_2O_3, La_2O_3, ZrO_2, ZrO_2-Y_2O_3, ZrO_2-La_2O_3 and ZrO_2-Y_2O_3-La_2O_3) as supports of Ni-based catalysts. In order to analyse the resistance to carbon deposits formation, MgO, Al_2O_3 and Y_2O_3-supported catalysts were additionally doped with K_2O.

1.4. Objective and structure of the thesis

The objective of this thesis was to study the effect of CO_2 on the hydrogen production under substoichiometric ethanol steam reforming (ESR) conditions over nickel-based catalysts. For such purpose, new supported Ni catalysts were prepared using different single (Al_2O_3, MgO, Y_2O_3, La_2O_3, and ZrO_2), binary (ZrO_2-Y_2O_3 and ZrO_2-La_2O_3) and ternary (ZrO_2-Y_2O_3-La_2O_3) oxide systems as supports.

Several tasks were carried out for the determination of the influence of the characteristics of the catalyst on the carbon deposits formation, under these conditions. Different reaction methodologies were used for the introduction of CO_2. Namely, as a reactant in the CO_2-assisted ethanol steam reforming (CDESR). Moreover, the study of the regeneration of deactivated catalysts after ESR was also carried out using independent CO_2-treatments.

Specific objectives have been purposed:

- Preparation of nickel catalysts supported on new oxide systems prepared by nanocasting, and their characterization by different techniques.
- Study of the effect of carbon dioxide introduction as a reactant in the CO_2-assisted substoichiometric ethanol steam reforming (CDESR).
- Study the effect of CO_2-treatments in the regeneration of catalysts used in substoichiometric ethanol steam reforming.

This thesis has been divided into six chapters. Each chapter contains the references used. The introduction chapter briefly summarizes the background of the studied subject.

In Chapter 2, the methods and the techniques used in the characterization are presented, as well as the reaction system where catalytic tests were carried out.

Chapter 3 covers the preparation and characterization of the different supports.

In Chapter 4 the study of nickel catalysts supported on single metal oxides is shown. The preparation and characterization of fresh Ni/Me_xO_y catalysts is presented, as well as their catalytic behaviour in CDESR and substoichiometric ethanol steam reforming reactions. This part also reports about the application of carbon dioxide for regeneration of partially deactivated nickel catalysts and the characterization of spent catalysts.

Chapter 5 presents the preparation and characterization of nickel catalysts supported on binary and ternary systems and their catalytic behaviour under ESR. This chapter is also focused on the regeneration of catalysts by CO_2-treatments. The final part describes the characterisation of spent catalysts.

The most relevant conclusions are summarized in Chapter 6.

1.5. References

[1] European Commission E. EU Transport in Figures. Statistical Pocketbook 2014. 2014. doi:10.2832/63317.

[2] International Energy Agency. Energy and Air Pollution. World Energy Outlook - Spec Rep 2016:266. doi:10.1021/ac00256a010.

[3] International Energy Agency. Key World Energy Statistics 2015 2015:81. doi:10.1787/9789264039537-en.

[4] Ji C, Wang S. Combustion and emissions performance of a hydrogen engine at idle and lean conditions. Int J Energy Res 2013;37:468–74. doi:10.1002/er.

[5] Ball M, Weeda M. The hydrogen economy - Vision or reality? Int J Hydrogen Energy 2015;40:7903–19. doi:10.1016/j.ijhydene.2015.04.032.

[6] International Energy Agency. Hydrogen Production and Storage. vol. 13. 2006. doi:10.1016/0360-3199(88)90106-1.

[7] Worley M, Yale J. Biomass Gasification Technology Assessment - Consolidated Report; NREL/SR-5100-57085 2012. http://www.nrel.gov/docs/fy13osti/57085.pdf (accessed September 20, 2016).

[8] Peres APG, Lunelli BH, Filho RM. Application of biomass to hydrogen and syngas production. Chem Eng Trans 2013;32:589–94. doi:10.3303/CET1332099.

[9] Navarro RM, Peña MA, Fierro JLG. Hydrogen production reactions from carbon feedstocks: Fossil fuels and biomass. Chem Rev 2007;107:3952–91. doi:10.1021/cr0501994.

[10] Wang D, Czernik S, Montane D, Mann M, Chornet E. Biomass to Hydrogen via Fast Pyrolysis and Catalytic Steam Reforming of the Pyrolysis Oil or Its Fractions. Ind Eng Chem Res 1997;36:1507–18. doi:10.1021/ie960396g.

[11] Departament of Energy US, FreedomCAR&FuelPartenrship. HYDROGEN PRODUCTION Overview of Technology Options 2009. https://www.hydrogen.energy.gov/pdfs/fc_fuel_partnership_plan.pdf (accessed September 20, 2016).

[12] Pimentel D, Patzek T, Cecil G. Ethanol Production: Energy, Economic, and Environmental Losses. Rev. Environ. Contam. Toxicol., vol. 189, 2007, p. 25–41.

[13] Bhatia L, Johri S, Ahmad R. An economic and ecological perspective of ethanol production from renewable agro waste: a review. AMB Express 2012;2:65. doi:10.1186/2191-0855-2-65.

[14] Ramírez de la Piscina P, Homs N. Use of biofuels to produce hydrogen (reformation processes). Chem Soc Rev 2008;37:2459–67. doi:10.1039/b712181b.

[15] Kumar A, Prasad R, Sharma YC. Steam Reforming of Ethanol: Production of Renewable Hydrogen. Int J Environ Res Dev 2014;4:203–12.

[16] Contreras JL, Salmones J, Colín-Luna JA, Nuño L, Quintana B, Córdova I, et al. Catalysts for H_2 production using the ethanol steam reforming (a review). Int J Hydrogen Energy 2014;39:18835–53. doi:10.1016/j.ijhydene.2014.08.072.

[17] Padilla R, Benito M, Rodríguez L, Serrano A, Muñoz G, Daza L. Nickel and cobalt as active phase on supported zirconia catalysts for bio-ethanol reforming: Influence of the reaction mechanism on catalysts performance. Int J Hydrogen Energy 2010;35:8921–8. doi:10.1016/j.ijhydene.2010.06.021.

[18] Fatsikostas AN, Verykios XE. Reaction network of steam reforming of ethanol over Ni-based catalysts. J Catal 2004;225:439–52. doi:10.1016/j.jcat.2004.04.034.

[19] Alberton AL, Souza MMVM, Schmal M. Carbon formation and its influence on ethanol steam reforming over Ni/Al_2O_3 catalysts. Catal Today 2007;123:257–64. doi:10.1016/j.cattod.2007.01.062.

[20] Mattos L V, Jacobs G, Davis BH, Noronha FB. Production of hydrogen from ethanol: Review of reaction mechanism and catalyst deactivation. Chem Rev 2012;112:4094–123. doi:10.1021/cr2000114.

[21] Pereira EB, Ramírez de la Piscina P, Martí S, Homs N. H_2 production by oxidative steam reforming of ethanol over K promoted Co-Rh/CeO_2-ZrO_2 catalysts. Energy Environ Sci 2010;3:487. doi:10.1039/b924624j.

[22] Osorio-Vargas P, Campos CH, Navarro RM, Fierro JLG, Reyes P. Improved ethanol steam reforming on Rh/Al_2O_3 catalysts doped with CeO_2 or/and La_2O_3: Influence in reaction pathways including coke formation. Appl Catal A Gen 2015;505:159–72. doi:10.1016/j.apcata.2015.07.037.

[23] Carbajal-Ramos IA, Gomez MF, Condó AM, Bengió S, Andrade-Gamboa JJ, Abello MC, et al. Catalytic behavior of Ru supported on $Ce_{0.8}Zr_{0.2}O_2$ for hydrogen production. Appl Catal B Environ 2016;181:58–70. doi:10.1016/j.apcatb.2015.07.025.

[24] Pereira EB, Homs N, Martí S, Fierro JLG, Ramírez de la Piscina P. Oxidative steam-reforming of ethanol over Co/SiO_2, Co-Rh/SiO_2 and Co-Ru/SiO_2 catalysts: Catalytic behavior and deactivation/regeneration processes. J Catal 2008;257:206–14. doi:10.1016/j.jcat.2008.05.001.

[25] Ananikov VP. Nickel: The “spirited horse” of transition metal catalysis. ACS Catal 2015;5:1964–71. doi:10.1021/acscatal.5b00072.

[26] Dan M, Mihet M, Biris AR, Marginean P, Almasan V, Borodi G, et al. Supported nickel catalysts for low temperature methane steam reforming: Comparison between metal additives and support modification. React Kinet Mech Catal 2012;105:173–93. doi:10.1007/s11144-011-0406-0.

[27] Nguyen LQ, Abella L, Gallardo S, Hinode H. Effect of Nickel Loading on The Activity of Ni/ZrO_2 for Methane Steam Reforming at Low Temperature. React Kinet Catal Lett 2008;93:227–32.

[28] Hou T, Zhang S, Chen Y, Wang D, Cai W. Hydrogen production from

ethanol reforming: Catalysts and reaction mechanism. Renew Sustain Energy Rev 2015;44:132–48. doi:10.1016/j.rser.2014.12.023.

[29] Llorca J, Ramírez de la Piscina P, Sales J, Homs N. Direct production of hydrogen from ethanolic aqueous solutions over oxide catalysts. Chem Commun 2001:641–2. doi:10.1039/b100334h.

[30] Osorio-Vargas P, Flores-González NA, Navarro RM, Fierro JLG, Campos CH, Reyes P. Improved stability of Ni/Al_2O_3 catalysts by effect of promoters (La_2O_3, CeO_2) for ethanol steam-reforming reaction. Catal Today 2015;259:27–38. doi:10.1016/j.cattod.2015.04.037.

[31] Alipour Z, Rezaei M, Meshkani F. Effects of support modifiers on the catalytic performance of Ni/Al_2O_3 catalyst in CO_2 reforming of methane. Fuel 2014;129:197–203. doi:10.1016/j.fuel.2014.03.045.

[32] Gálvez ME, Ascaso S, Stelmachowski P, Legutko P, Kotarba A, Moliner R, et al. Influence of the surface potassium species in $Fe\text{-}K/Al_2O_3$ catalysts on the soot oxidation activity in the presence of NOx. Appl Catal B Environ 2014;152-153:88–98. doi:10.1016/j.apcatb.2014.01.041.

[33] Shi C, Zhang P. Effect of a second metal (Y, K, Ca, Mn or Cu) addition on the carbon dioxide reforming of methane over nanostructured palladium catalysts. Appl Catal B Environ 2012;115-116:190–200. doi:10.1016/j.apcatb.2011.12.002.

[34] Llera I, Mas V, Bergamini ML, Laborde M, Amadeo N. Bio-ethanol steam reforming on Ni based catalyst. Kinetic study. Chem Eng Sci 2012;71:356–66. doi:10.1016/j.ces.2011.12.018.

[35] Song YQ, He DH, Xu BQ. Effects of preparation methods of ZrO_2 support on catalytic performances of Ni/ZrO_2 catalysts in methane partial oxidation to syngas. Appl Catal A Gen 2008;337:19–28. doi:10.1016/j.apcata.2007.11.032.

[36] Chen J, Ma Q, Rufford TE, Li Y, Zhu Z. Influence of calcination temperatures of Feitknecht compound precursor on the structure of $Ni\text{-}Al_2O_3$ catalyst and the corresponding catalytic activity in methane

decomposition to hydrogen and carbon nanofibers. Appl Catal A Gen 2009;362:1–7. doi:10.1016/j.apcata.2009.04.025.

[37] Hadian N, Rezaei M, Mosayebi Z, Meshkani F. CO_2 reforming of methane over nickel catalysts supported on nanocrystalline $MgAl_2O_4$ with high surface area. J Nat Gas Chem 2012;21:200–6. doi:10.1016/S1003-9953(11)60355-1.

[38] Zou J, Yu B, Zhang S, Zhang J, Chen Y, Cui L, et al. Hydrogen production from ethanol over Ir/CeO_2 catalyst: Effect of the calcination temperature. Fuel 2015;159:741–50. doi:10.1016/j.fuel.2015.07.040.

[39] Fu L, Xie W, Lü S, Qiu F. Influence of support on resistance to carbon-deposition of catalyst for CH_4, CO_2 with O_2 to synthesis gas. Sci China Ser B Chem 2000;43:154–61. doi:10.1007/BF03027305.

[40] Bellido JDA, Assaf EM. Effect of the Y_2O_3-ZrO_2 support composition on nickel catalyst evaluated in dry reforming of methane. Appl Catal A Gen 2009;352:179–87. doi:10.1016/j.apcata.2008.10.002.

[41] Youn MH, Seo JG, Lee H, Bang Y, Chung JS, Song IK. Hydrogen production by auto-thermal reforming of ethanol over nickel catalysts supported on metal oxides: Effect of support acidity. Appl Catal B Environ 2010;98:57–64. doi:10.1016/j.apcatb.2010.05.002.

[42] Penkova A, Bobadilla L, Ivanova S, Domínguez MI, Romero-Sarria F, Roger AC, et al. Hydrogen production by methanol steam reforming on NiSn/MgO–Al_2O_3 catalysts: The role of MgO addition. Appl Catal A Gen 2011;392:184–91. doi:10.1016/j.apcata.2010.11.016.

[43] García V, Fernández JJ, Ruíz W, Mondragón F, Moreno A. Effect of MgO addition on the basicity of Ni/ZrO_2 and on its catalytic activity in carbon dioxide reforming of methane. Catal Commun 2009;11:240–6. doi:10.1016/j.catcom.2009.10.003.

[44] Hu X, Lu G. Syngas production by CO_2 reforming of ethanol over Ni/Al_2O_3 catalyst. Catal Commun 2009;10:1633–7. doi:10.1016/j.catcom.2009.04.030.

[45] Roh HS, Jun KW. Carbon dioxide reforming of methane over Ni catalysts supported on Al_2O_3 modified with La_2O_3, MgO, and CaO. Catal Surv from Asia 2008;12:239–52. doi:10.1007/s10563-008-9058-0.

[46] Yermán L, Homs N, Pereira EB, Ramírez de la Piscina P. H_2 production from oxidative steam reforming of 1-propanol and propylene glycol over yttria-stabilized supported bimetallic Ni–M (M = Pt, Ru, Ir) catalysts. Int J Hydrogen Energy 2014;39:5225–33. doi:10.1016/j.ijhydene.2013.12.163.

[47] Bellido JDA, Tanabe EY, Assaf EM. Carbon dioxide reforming of ethanol over Ni/Y_2O_3–ZrO_2 catalysts. Appl Catal B Environ 2009;90:485–8. doi:10.1016/j.apcatb.2009.04.009.

[48] Li JF, Xia C, Au CT, Liu BS. Y_2O_3-promoted NiO/SBA-15 catalysts highly active for CO_2/CH_4 reforming. Int J Hydrogen Energy 2014;39:10927–40. doi:10.1016/j.ijhydene.2014.05.021.

[49] Fatsikostas AN, Kondarides DI, Verykios XE. Production of hydrogen for fuel cells by reformation of biomass-derived ethanol. Catal Today 2002;75:145–55. doi:10.1016/S0920-5861(02)00057-3.

[50] Bespalko N, Roger A-C, Bussi J. Comparative study of NiLaZr and CoLaZr catalysts for hydrogen production by ethanol steam reforming: Effect of CO_2 injection to the gas reactants. Evidence of Rh role as a promoter. Appl Catal A Gen 2011;407:204–10. doi:10.1016/j.apcata.2011.08.042.

[51] Roh HS, Jun KW, Dong WS, Chang JS, Park SE, Joe Y Il. Highly active and stable Ni/Ce-ZrO_2 catalyst for H_2 production from methane. J Mol Catal A Chem 2002;181:137–42. doi:10.1016/S1381-1169(01)00358-2.

[52] Akande AJ, Idem RO, Dalai AK. Synthesis, characterization and performance evaluation of Ni/Al_2O_3 catalysts for reforming of crude ethanol for hydrogen production. Appl Catal A Gen 2005;287:159–75. doi:10.1016/j.apcata.2005.03.046.

[53] Cai W, Wang F, Daniel C, van Veen AC, Schuurman Y, Descorme C, et al. Oxidative steam reforming of ethanol over Ir/CeO_2 catalysts: A structure sensitivity analysis. J Catal 2012;286:137–52. doi:10.1016/j.jcat.2011.10.021.

[54] de Lima SM, da Silva AM, Jacobs G, Davis BH, Mattos L V., Noronha FB. New approaches to improving catalyst stability over Pt/ceria during ethanol steam reforming: Sn addition and CO_2 co-feeding. Appl Catal B Environ 2010;96:387–98. doi:10.1016/j.apcatb.2010.02.036.

[55] da Silva AM, de Souza KR, Jacobs G, Graham UM, Davis BH, Mattos L V., et al. Steam and CO_2 reforming of ethanol over Rh/CeO_2 catalyst. Appl Catal B Environ 2011;102:94–109. doi:10.1016/j.apcatb.2010.11.030.

[56] Zawadzki A, Bellido JDA, Lucrédio AF, Assaf EM. Dry reforming of ethanol over supported Ni catalysts prepared by impregnation with methanolic solution. Fuel Process Technol 2014;128:432–40. doi:10.1016/j.fuproc.2014.08.006.

[57] Bahari MB, Phuc NHH, Abdullah B, Alenazey F, Vo DVN. Ethanol dry reforming for syngas production over Ce-promoted Ni/Al2O3 catalyst. J Environ Chem Eng 2015:1–9. doi:10.1016/j.jece.2016.01.038.

[58] Koubaissy B, Pietraszek A, Roger AC, Kiennemann A. CO_2 reforming of methane over Ce-Zr-Ni-Me mixed catalysts. Catal Today 2010;157:436–9. doi:10.1016/j.cattod.2010.01.050.

2. Experimental

The first part of this chapter presents the description of methods and techniques used for the characterization of catalysts. In the second part, the experimental setup employed in catalytic tests is shown and the reaction conditions are specified.

2.1. Characterization techniques

The methods and techniques used for the characterization of the supports and fresh and spent catalysts are listed below:

1) Chemical analysis by inductively-coupled plasma atomic emission spectroscopy (ICP-AES)
2) Physisorption of nitrogen (BET)
3) Powder X-ray diffraction (XRD)
4) Temperature-programmed reduction with H_2 (H_2-TPR)
5) Temperature-programmed desorption of CO_2 (CO_2-TPD)
6) CO_2 adsorption calorimetry
7) X-ray photoelectron spectroscopy (XPS)
8) Raman spectroscopy
9) Temperature-programmed oxidation coupled with mass spectrometry (TPO-MS)
10) Diffuse reflectance infrared Fourier transform spectroscopy (DRIFTS)

Detailed descriptions of above presented methods and techniques are showed as follows.

2.1.1. Chemical analysis by inductively-coupled plasma atomic emission spectroscopy (ICP-AES)

The chemical analysis of catalysts was determined by inductively-coupled plasma atomic emission spectroscopy using a Perkin Elmer Optima 3200Rl ICP-AES equipment.

This technique measures electromagnetic radiation, emitted by excited atoms and ions and produced under the influence of inductively-coupled plasma [1]. For catalysts containing MgO, about 50 mg of sample was treated with 8 cm^3 of nitric acid hydrochloride (molar ratio of nitric acid to hydrochloric acid is 1:3) and heated for 20 min at 180 ^oC (heating rate 10 ^oC/min). For the rest of materials, about 50 mg of sample was treated with 50 mg of ammonium chloride, 4 cm^3 of hydrochloric acid and 3 cm^3 of sulphuric acid. Then, the solution was kept at 210 ^oC for 20 min (heating rate 10 ^oC/min). Afterward, prepared solutions were diluted with HPLC grade water up to 50 cm^3 volume and measured by ICP-AES. Additionally, water solutions of adequate standards were prepared. The results were presented in the form of weight percent of each metal (Ni, Mg, Al, Y, La and Zr).

The measurements were performed in the Scientific and Technological Centres of the University of Barcelona.

2.1.2. Physisorption of nitrogen (BET)

The specific surface area of catalysts, as well as pore size, pore volume and distribution of pores were determined from isotherms of adsorption/desorption of nitrogen at -196 °C.

The method was described by Brunauer, Emmet and Teller, commonly known as the B.E.T. method, and it is an accredited way of analysis [2,3]. The specific area is obtained basing on the quantity of nitrogen adsorbed when a monolayer is formed (V_m), using the B.E.T. equation:

$$\frac{p}{V(p^0-p)} = \frac{1}{V_m C} + \frac{C-1}{V_m C} \cdot \frac{p}{p^0} \qquad (2.1)$$

where V is the volume of adsorbed gas, measured under standard conditions, V_m is the volume of the gas adsorbed when a monolayer is formed, p/p^0 is the relative pressure, p is the pressure of gas in equilibrium when the volume (V) of gas is adsorbed, and C is a constant that depends on the heat of adsorption of the adsorbed gas over the surface.

Therefore, B.E.T. surface area can be expressed as:

$$A_{BET} = a_m \cdot n_m \cdot N_A \qquad n_m = \frac{V_m \cdot \rho}{M_m \cdot m} \qquad (2.2)$$

where a_m is the area effectively occupied by one molecule of adsorbed gas, n_m is the number of moles of the gas adsorbed in monolayer per gram of catalyst, N_A is the Avogadro constant, ρ is the

density of adsorbed gas, M_m is the molecular mass, and m is the weight of adsorbent.

Porosity characteristics were obtained using the information provided by desorption isotherms, using the method of Barret, Joyner and Halenda [4].

In this work, N_2 adsorption-desorption isotherms were recorded at -196 ^oC using a Micromeritics Tristar-II. Prior to the measurements, the samples were outgassed at 150 ^oC for 2 h, under a nitrogen flow (20 cm^3/min).

The analyses were carried out in the Catalonia Institute for Energy Research (IREC).

The analyses were carried out with fresh supports and catalysts.

2.1.3. Powder X-ray diffraction (XRD)

X-ray diffraction is a method of characterization of materials that allows determining crystalline phases and crystallite size. In this technique, the X-rays are collimated and directed onto the sample that can be a powder. When the geometry of the incident X-rays impinging the sample satisfies the Bragg Equation (Eq. 2.3), constructive interference occurs as well as a peak in the recorded scattered radiation is observed. A detector registers and processes this X-ray signal and converts it to a count rate [5].

$$n \cdot \lambda = 2d_{hkl}\sin\theta \qquad (2.3)$$

where *n* is a natural number, λ is the wavelength of the beam, d_{hkl} is the interplanar spacing of the crystal, and θ is the incident angle.

Crystallite size (d) can be estimated from XRD patterns, using the Debye-Scherrer equation:

$$d = \frac{K \cdot \lambda}{b \cdot \cos\theta} \quad (2.4)$$

$$b = \sqrt{(B^2 - \beta^2)} \quad (2.5)$$

where *K* is a constant which depends on the structure, λ is the X-Ray wavelength, θ is the angle of Bragg diffraction expressed in radians. The *b* value is corrected full width at half maximum (FWHM) of peak of desired phase.

In the equation 2.5, B is FWHM of peak of corresponding phase, and β is FWHM of standard compound and is calculated from below presented equation.

$$\beta = 1.354 \cdot 10^{-6}(2\theta)^2 + 1.524 \cdot 10^{-4}(2\theta) + 7.737 \cdot 10^{-4} \quad (2.6)$$

where 2θ is the angle of diffraction of the main peak. In performed analyses, γ-Al_2O_3 was used as a standard (2θ = 0.16°).

In this work, supports, fresh and post-reaction catalysts were characterized by XRD. During the preparation of the catalysts and their posterior use in the catalytic tests also other materials were in contact with the mentioned materials, such as quartz wool (SiO_2) and silicon carbide (SiC); in some cases, peaks attributed to SiC and SiO_2 were detected.

The XRD analyses were performed using a PANalytical X'Pert PRO MPD Alpha1 powder diffractometer in Bragg-Brentano θ/2θ geometry of 240 millimetres of radius. The analyser was equipped in Cu $K\alpha_1$ radiation lamp (λ = 1.5406 Å) and focalizing Ge (111) primary monochromator. The measurements were registered at room temperature, in the range 2θ = 4° - 100°, with a step size of 0.017° and time of measuring of 50 seconds per step.

The analyses were carried out in the Scientific and Technological Centres of the University of Barcelona.

2.1.4. Temperature-programmed reduction with H_2 (H_2-TPR)

The temperature-programmed reduction is a technique, which gives information about the reducibility of the materials. In order to carry out the measurements, about 40 mg of sample was placed on quartz wool, in a U-shape quartz reactor. First, the sample was pre-treated at 100 ^oC for 1 h under flowing He. After cooling to room temperature, the sample was exposed to a flow of H_2/Ar (12% vol/vol), and the temperature was linearly increased with a rate of 10 ^oC/min up to 800 ^oC. The analysis of TCD signal allows obtaining the profile of H_2 consumption and determining its consumption (area under the graph), and the temperature at which the material is reduced.

The H_2-TPR profiles were additionally treated by OriginPro software in order to perform deconvolution in several peaks of the curves obtained.

The H_2-TPR analyses were performed using a Micromeritics AutoChem II chemisorption analyser. Furthermore, in chosen cases, the outflow was analysed by mass spectrometry to check if other gases than water were formed.

2.1.5. Temperature-programmed desorption of CO_2 (CO_2-TPD)

The CO_2 adsorption and temperature-programmed desorption of CO_2 allow determining basicity of the catalysts. The CO_2-TPD experiments were carried out with approximately 100 mg of catalyst. Prior each run, the catalyst was treated at 400 ^oC for 15 min under He, then cooled to room temperature and reduced under flowing H_2/Ar (12% vol/vol) for 45 min at 600 ^oC and then cooled to 20 ^oC under flowing He. The adsorption of CO_2 was carried out using a feed of CO_2/Ar (10% vol/vol) for 1 h. The reactor was then purged with He and then, the temperature was increased to 800 ^oC with a heating rate 10 ^oC/min, under a He flow. During desorption, the TCD signal was registered. Resulting profiles indicate at which temperature CO_2 desorbs and the overall CO_2 desorbed (area under the graph). The temperature of CO_2 desorption can be related with the strength of basic centres. The analyses were performed using a Micromeritics AutoChem II chemisorptions analyser.

The analyses were carried out in the Catalonia Institute for Energy Research (IREC).

2.1.6. CO_2 adsorption calorimetry

The heat of CO_2 adsorption was analysed by calorimetry. The amount of the heat released during CO_2 adsorption depends on the strength and the number of the basic sites [6,7].

The mean adsorption enthalpy of CO_2 was calorimetrically measured using a Sensys evo TG-DSC instrument (Setaram) equipped with a 3D thermal flow sensor. The sample was firstly reduced in H_2/Ar (12% vol/vol) for 1 h at 600 ^oC, cooled to 35 ^oC under an Ar flow and then contacted with a CO_2/Ar (10% vol/vol) mixture. The exothermic peak corresponding to CO_2 adsorption was integrated to provide the total enthalpy of adsorption and the mean heat of adsorption per mole of adsorbed CO_2.

This study was done in the Catalonia Institute for Energy Research (IREC).

2.1.7. X-ray photoelectron spectroscopy (XPS)

XPS is a technique used for chemical characterization of the surface of the solids. It gives information about elemental composition and the electronic state of the elements. The base of the technique is the photoelectric effect.

The kinetic energy of the emitted electrons depends on the energy of the X-ray used and the level of the electrons emitted:

$$h\nu = E_k + E_b + \phi_{sp} \quad (2.7)$$

where $h\nu$ is the energy of the incident X-ray, E_k is the kinetic energy of the electron emitted and analysed with an appropriate detector, E_b is the binding energy of the electron, and ϕ_{sp} is the work function of the spectrometer [5].

XPS analyses were performed using a VG Escalab 200R spectrometer with Al Kα ($h\nu$ = 1486.6 eV) at a pressure of $4 \cdot 10^{-9}$ mbar during data acquisition. The binding energy (BE) values were referred to the BE of environmental carbon C 1s at 284.8 eV. Appropriate sensitivity factors were used for determining the surface atomic ratios of the corresponding elements.

The measurements were performed in the Scientific and Technological Centres of the University of Barcelona.

2.1.8. Raman spectroscopy

Raman spectroscopy was used for the analysis of carbon deposits in the post-reaction catalysts. Raman spectroscopy analyses were performed using a Jobin-Yvon LabRam HR 800, fitted to an optical microscope Olympus BXFM with a CCD detector cooled at -70 ^{o}C and a 532 nm laser. The laser power was limited to 0.5 mW to minimize laser-heating effects. Each

obtained spectrum was the result of three accumulations, during 10 s each. Due to the possibility of not homogenized distribution of carbon species, the DuoScan® technique was applied. The DuoScan® analyses an area instead of a point, in order to have more representative results. In this work during each analysis a surface of 400 μm^2 was analysed, the magnification of the lens was 50x.

The measurements were performed in the Scientific and Technological Centres of the University of Barcelona.

2.1.9. Temperature-programmed oxidation coupled with mass spectrometry (TPO-MS)

TPO-MS analyses were performed with spent catalysts to quantify the amount of carbon deposits and to determine the temperature at which deposited carbon reacted with oxygen. The TPO-MS experiments were carried out using thermogravimetric analysis and differential scanning calorimetry (DSC) coupled with mass spectrometry.

For each analysis, about 50 mg of the spent catalyst, previously sieved to separate out the SiC, was treated under air flow up to 800 ^oC with a heating rate of 10 °C/min. The heat flow and mass change were continuously registered and the outgoing gases were analysed on-line by an Omnistar (Pfeiffer) mass-spectrometer equipment.

This study was done in the Catalonia Institute for Energy Research (IREC).

2.1.10. Diffuse reflectance infrared Fourier transform spectroscopy (DRIFTS)

DRIFTS measurements were performed with spent catalysts to investigate the nature of the deposited hydrogenated carbon species.

DRIFTS analyses were carried out using a Nicolet Magna-IR 750 FTIR spectrometer equipped with a liquid nitrogen-cooled MCT detector. The spectra were recorded at room temperature and consisted of 128 scans at a spectral resolution of 4 cm^{-1}. The sample was placed on a supporting mirror, previously dried to avoid signal coming from water, and maintained under nitrogen flow to avoid influence of humidity.

2.2. Reaction system and experimental procedures for ethanol steam reforming (ESR) and CO_2-assisted ethanol steam reforming (CDESR)

In this work, three different experiments were carried out for the evaluation of catalytic properties: substoichiometric ethanol steam reforming (ESR), CO_2-assisted substoichiometric ethanol steam reforming (CDESR), and the use of CO_2 for the regeneration of catalysts.

The ESR experiments were carried out with molar ratio ethanol/water 1.0/1.6. The reactant mixture was diluted with argon and nitrogen (internal standard) and the final molar ratio was 1.0 ethanol/1.6 water/22.8 ($Ar+N_2$).

For CDESR tests, the ESR reactant mixture was modified; the flow of argon was substituted by a mixture of 10% vol/vol CO_2 diluted in argon, and the final molar ratio was 1.0 ethanol/1.6 water/1.6 CO_2/21.2 (Ar+N_2).

The regeneration of partially deactivated catalysts was done by CO_2-treatment, carried out with a flow of 7% vol/vol CO_2 diluted in argon and nitrogen, at the reaction temperature.

All catalytic tests were carried out at atmospheric pressure and at 600 °C. The experiments were performed in a custom-built continuous-flow reaction system, with a tubular fixed-bed stainless steel reactor and with on-line analysis of products. The total GHSV (inlet gas volumetric flow/catalyst bed volume) was always approximately 8100 h^{-1}. Figure 2.1 presents a scheme of the reaction system, and Figure 2.2 shows a general view of the system.

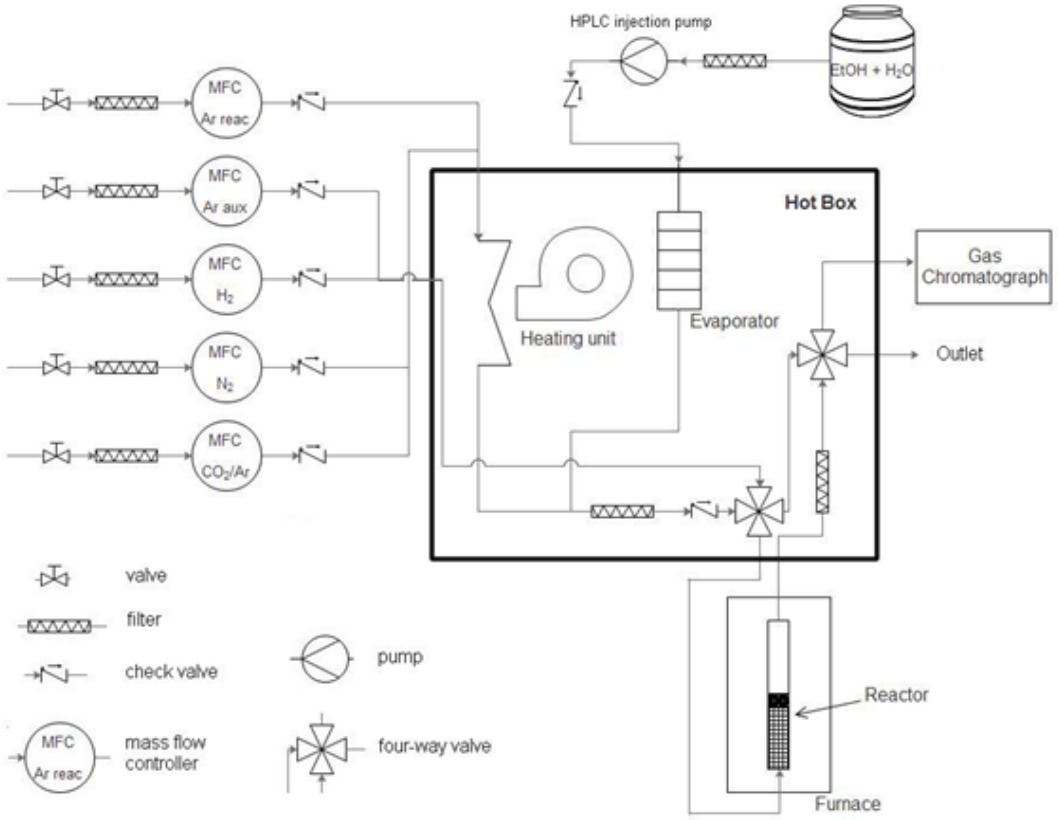

Figure 2.1. Scheme of the reaction system

The mixture of gases (N_2 and Ar or 10% vol/vol CO_2/Ar), after passing through mass flow controllers, enters in the hot-box. The hot-box is an integrated set of devices and connections, consisted of an evaporator of liquids, a heating unit, two 4-way valves, filters and check valves. The temperature inside the hot-box was 180 °C. Figure 2.1 shows the location of the hot box in the system, and Figure 2.3 presents its image with marked main elements, and also shows the reactor used in the experiments. Afterwards, the gases are mixed with evaporated liquid mixture and

directed to the reactor, entering by the bottom part. The reactor (332 mm long, inner diameter 10 mm) was placed inside the tubular furnace; the temperature control was achieved through a K-type thermocouple. The effluent leaves the reactor by the superior vent and continues, through a heated line, to the analysis unit – a gas chromatograph BRUKER 450-GC. The effluent was analysed on-line using the gas chromatograph equipped with a thermal conductivity detector (TCD), two flame ionization detectors (FID) and a methanizer. After passing of reaction products through a separation column Hayesep Q and a molecular sieve 13X, the TCD was used for detection of H_2 and N_2; afterward, the rear FID detected hydrocarbons, CO and CO_2. The middle FID, followed by capillary column CP-Sil 8 CB, detected liquid products and non-converted ethanol. In the methanizer takes place the transformation of CO and CO_2 to CH_4, in order to convert the reaction products into CH_4 well detectable by FID, according following reactions:

$$CO + 3H_2 \rightarrow CH_4 + H_2O \quad (2.8)$$

$$CO_2 + 4H_2 \rightarrow CH_4 + 2H_2O \quad (2.9)$$

A calibrated mixture of gases was used for calibration of the GC and afterwards for quantification of the reaction products. Before and after each test, the reaction mixture was analysed twice. During these analyses, the reaction system presented high repeatability, expressed as similar chromatography peak areas of nitrogen and ethanol.

Figure 2.2. General view of the reaction system (1-liquid pump, 2-gas connections, 3-control devices, 4-tubural furnace, 5-gas chromatograph, 6-hot box)

In each run, 200 mg of the catalyst was diluted in inactive SiC, up to a volume of 1 cm^3. Before each test, the catalysts were reduced *in-situ* with a flow of 10% vol/vol H_2/Ar. A liquid mixture of ethanol/water (0.022 cm^3/min, molar ratio = 1.0/1.6) was injected using the liquid pump (GILSON 307), evaporated at 200 ^oC and mixed with a flow of N_2 (30% vol/vol, internal standard) and Ar (for the substoichiometric ethanol steam reforming tests) or Ar/CO_2 (for the CO_2-assisted substoichiometric ethanol

steam reforming tests molar ratio of mixture ethanol/H_2O/CO_2 was 1.0/1.6/1.6), and then directed to the reactor.

For regeneration experiments under ESR conditions, the liquid flow of the reactant mixture was stopped and instead a flow of 7% vol/vol CO_2/(Ar+N_2) was admitted until CO was no longer detected in the reactor outlet.

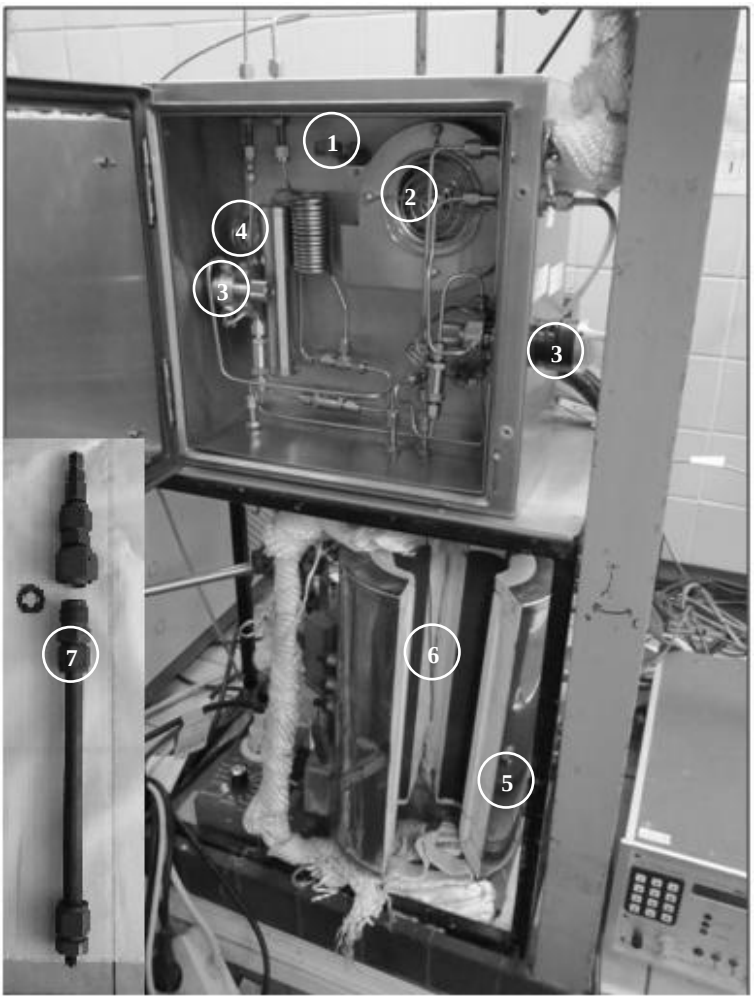

Figure 2.3. Photography of the hot box, electric furnace and reactor (1-hot box thermocouple, 2-hot box heating unit, 3-4-way valve, 4-evaporator thermocouple, 5-tubular furnace, 6-reactor thermocouple, 7-reactor)

Ethanol conversion and product distribution were calculated as follows:

$$\textit{Ethanol conversion (\%)} = \left(1 - \frac{\text{mol } ethanol\ out}{mol\ ethanol\ in}\right) \cdot 100$$

$$\textit{Molar concentration of a given product (\%)} = \frac{ni}{n\ total} \cdot 100$$

where *ni* is the number of moles of the *i* product (H_2, CO, CH_4, CO_2, CH_3CHO, C_2H_4 or C_2H_6), *n total* is the total number of moles of products (H_2, CO, CH_4, CO_2, CH_3CHO, C_2H_4 and C_2H_6), excluding water.

Hydrogen yield was calculated based on the H_2 determined in the outlet gas ($H_{2_{out}}$) referred to the maximum H_2 attainable ($H_{2_{max}}$: 4.6 mol H_2/ 1 mol ethanol), according to the below presented reactions:

$$H_2\textit{-yield (\%)} = \frac{H_{2_{out}}}{H_{2_{max}}} \cdot 100$$

$C_2H_5OH + H_2O \rightarrow 4H_2 + 2CO$

$0.6H_2O + 0.6CO \rightarrow 0.6H_2 + 0.6CO_2$

$C_2H_5OH + 1.6H_2O \rightarrow 4.6H_2 + 1.4CO + 0.6CO_2$

2.3. References

[1] Mermet JM. Is it still possible, necessary and beneficial to perform research in ICP-atomic emission spectrometry? J Anal At Spectrom 2005;20:11. doi:10.1039/b416511j.

[2] Brunauer S, Emmett PH, Teller E. Adsorption of Gases in Multimolecular Layers. J Am Chem Soc 1938;60:309–19. doi:citeulike-article-id:4074706\rdoi: 10.1021/ja01269a023.

[3] Thommes M, Kaneko K, Neimark A V., Olivier JP, Rodriguez-Reinoso F, Rouquerol J, et al. Physisorption of gases, with special reference to the evaluation of surface area and pore size distribution (IUPAC Technical Report). Pure Appl Chem 2015;87:1051–69. doi:10.1515/pac-2014-1117.

[4] Barrett EP, Joyner LG, Halenda PP. The Determination of Pore Volume and Area Distributions in Porous Substances. I. Computations from Nitrogen Isotherms. J Am Chem Soc 1951;73:373–80. doi:10.1021/ja01145a126.

[5] Imelik B, Vedrine JC. Catalyst Characterization, Physical Techniques for Solid Materials. Springer; 1994.

[6] Liu Z-S, Peng Y-H, Huang C-Y, Hung M-J. Application of thermogravimetry and differential scanning calorimetry for the evaluation of CO_2 adsorption on chemically modified adsorbents. Thermochim Acta 2015;602:8–14. doi:10.1016/j.tca.2015.01.002.

[7] Vargas DP, Giraldo L, Moreno-Piraján JC. Calorimetric study of the CO_2 adsorption on carbon materials. J Therm Anal Calorim 2014;117:1299–309. doi:10.1007/s10973-014-3909-x.

3. Preparation and characterization of supports

Three series of metal oxide supports were prepared: single metal oxide, and oxides systems containing two or three different metals. Supports were labelled as Me_xO_y (single metal oxide), aMbM' (binary systems) and aMbM'cM'' (ternary systems), where a, b and c represent metal content (weight percentage) of M, M' and M'' in the corresponding catalysts.

The following supports were prepared:

- five single metal oxides: MgO, Al_2O_3, Y_2O_3, La_2O_3 and ZrO_2,
- four ZrO_2-Y_2O_3 and ZrO_2-La_2O_3 binary systems: 35Zr14La, 36Zr14Y, 8Zr45Y and 8Zr50La,
- two ZrO_2-Y_2O_3-La_2O_3 ternary systems: 12Zr29Y13La and 12Zr12Y31La.

The supports were prepared using a pseudo sol-gel method with urea as precipitation agent, and active carbon to tailor the morphological properties, according to a nanocasting procedure [1–4].

All the supports were prepared using adequate nitrate salts ($Mg(NO_3)_2{\cdot}6H_2O$ (Fluka 99.0%), $Al(NO_3)_3{\cdot}9H_2O$ (Alfa Aesar 98%), $Y(NO_3)_3{\cdot}6H_2O$ (Alfa Aesar 99.9%), $La(NO_3)_3{\cdot}6H_2O$ (Panreac 99.0%) and $ZrO(NO_3)_2{\cdot}H_2O$ (Aldrich 99%)), urea (Sigma), active carbon (Sigma Aldrich 20-40 mesh) and distilled water. The exact amounts of compounds used for the preparations are presented in the Annex (Table A.1 and Table A.2).

In the first step, a water solution of urea was mixed with adequate nitrate (or nitrates) and active carbon. This mixture was heated up to 90 ^oC in an oil bath system (Fig. 3.1.), and maintained at this temperature for 50 h, with

vigorous magnetic stirring. Produced vapour was condensed in a Dimroth condenser and returned to the boiling flask. Afterwards, the suspension was filtered, washed with ethanol and dried overnight at 100 ^{o}C. In order to eliminate the carbon, the solid was treated under air flow (40 cm^3/min) at 600 °C (heating rate: 2.5 °C/min) for 4 h, in a tubular quartz reactor between quartz wool (Fig. 3.2.).

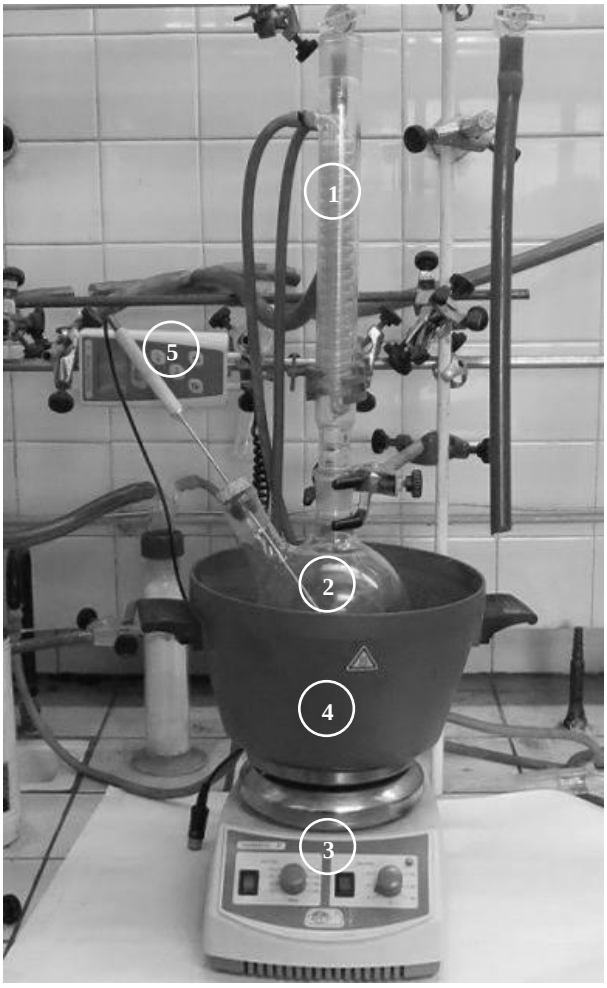

Figure 3.1. System used for the preparation of the supports (1-Dimroth condenser, 2-boiling flask, 3-electric heater with magnetic stirring, 4-silicon oil bath, 5-thermocouple with programmer)

The supports were characterized by physisorption of nitrogen (BET) and temperature-programmed reduction with H_2 (H_2-TPR). In all cases, the crystalline phases corresponding to the support were determined by XRD analysis of the corresponding catalysts (Chapters 4 and 5). For 35Zr14La, 8Zr50La and 12Zr12Y31La supports, additional XRD analyses were preformed separately.

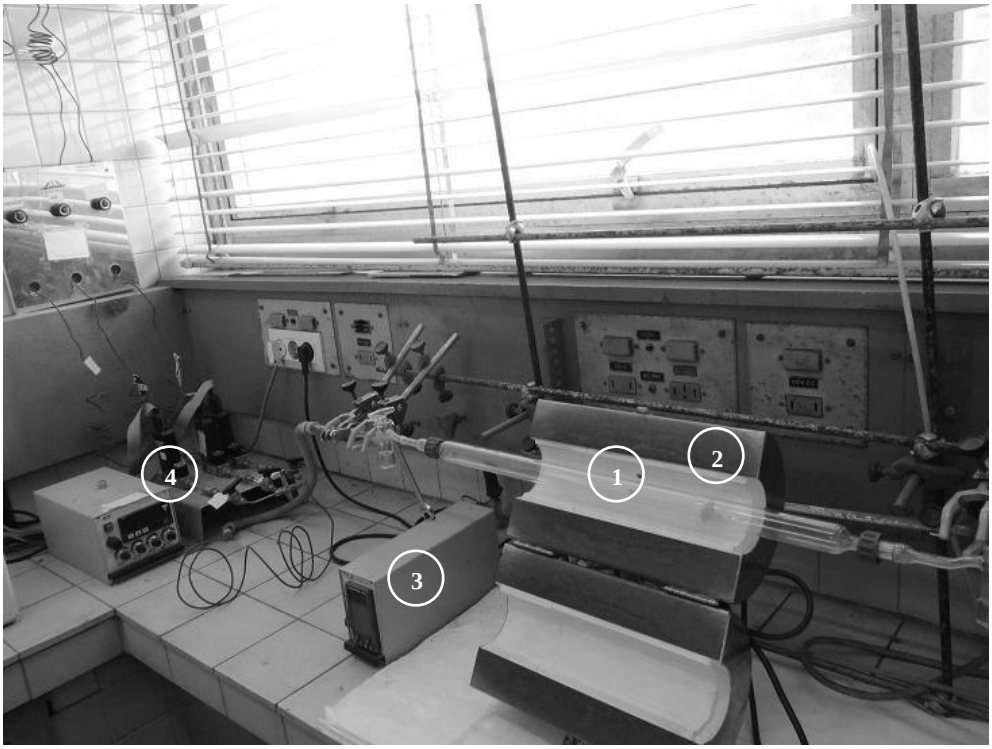

Figure 3.2. Electric tubular oven with quartz reactor and gas connection used for the preparation of the supports (1-quartz tubular reactor, 2-electric tubular oven, 3-overn programmer, 4-gas connections with mass flow controls)

Specific areas of the supports are presented in Table 3.1. For single oxide supports, a wide distribution of specific areas values was obtained; the

highest was determined for Al_2O_3 (193 m^2/g) and the lowest for Y_2O_3 (29 m^2/g). For binary systems, ZrO_2-La_2O_3 supports had smaller area than ZrO_2-Y_2O_3. The 36Zr14Y support showed the highest area (203 m^2/g) among all the supports prepared. For ZrO_2-Y_2O_3-La_2O_3 ternary systems, 12Zr12Y31La with a higher lanthanum content than 12Zr29Y13La showed a lower surface area.

Table 3.1. Specific area determined by physisorption of nitrogen, and apparent consumption of hydrogen during H_2-TPR analysis of prepared supports; the results into brackets are probably overestimated because of the presence of $La_2O_2CO_3$

Support	BET area (m^2/g)	Apparent consumption of H_2 (mmol H_2/g)
MgO	100	1.34
Al_2O_3	193	1.39
Y_2O_3	29	2.01
La_2O_3	50	(3.04)
ZrO_2	146	0.54
35Zr14La	49	(2.20)
36Zr14Y	203	1.04
8Zr45Y	76	1.51
8Zr50La	50	(2.28)
12Zr29Y13La	131	(2.18)
12Zr12Y31La	94	(2.92)

H_2-TPR profiles obtained for all prepared supports are presented in Figure 3.3. Table 3.1 shows the total apparent consumption of hydrogen during the H_2-TPR analyses of the supports, if the variation of the TCD signal is related only with the H_2 consumed. The supports containing lanthanum showed values of apparent consumption of hydrogen higher than for

corresponding supports containing Y_2O_3. This is related with the presence of $La_2O_2CO_3$ in these samples which could react with H_2 [5–8]:

$$La_2O_2CO_3 + H_2 \rightarrow La_2O_3 + H_2O + CO \quad (3.1)$$

And could decompose at temperature below 500 ^oC [9]:

$$La_2O_2CO_3 \rightarrow La_2O_3 + CO_2 \quad (3.2)$$

In Chapter 4, the results of a H_2-TPR experiment coupled with mass-spectrometry analysis of Ni/La_2O_3 catalyst account for this (p.65).

In fact, the XRD analyses of 35Zr14La, 8Zr50La and 12Zr12Y31La supports show the presence of crystalline $La_2O_2CO_3$ (Fig. 3.4). Lanthanum carbonate oxide can be formed during the preparation of the support, according to the following reaction:

$$La_2O_3 + CO_2 \rightarrow La_2O_2CO_3 \quad (3.3)$$

The small values of H_2 consumption obtained for the rest of the supports may partially be related to the presence of residual carbon, which was estimated lower than 1 %wt.

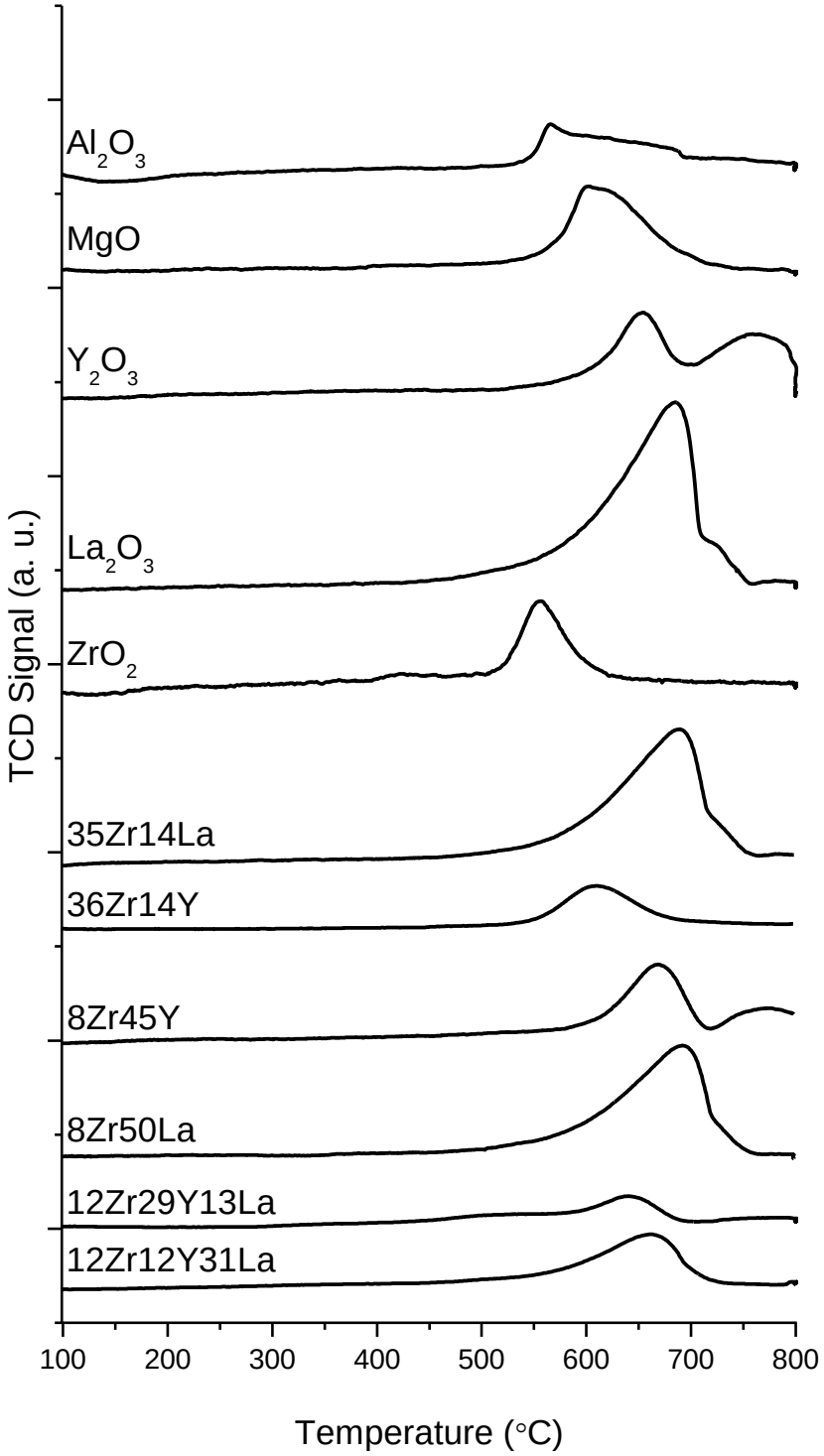

Figure 3.3 H_2-TPR profiles of the supports

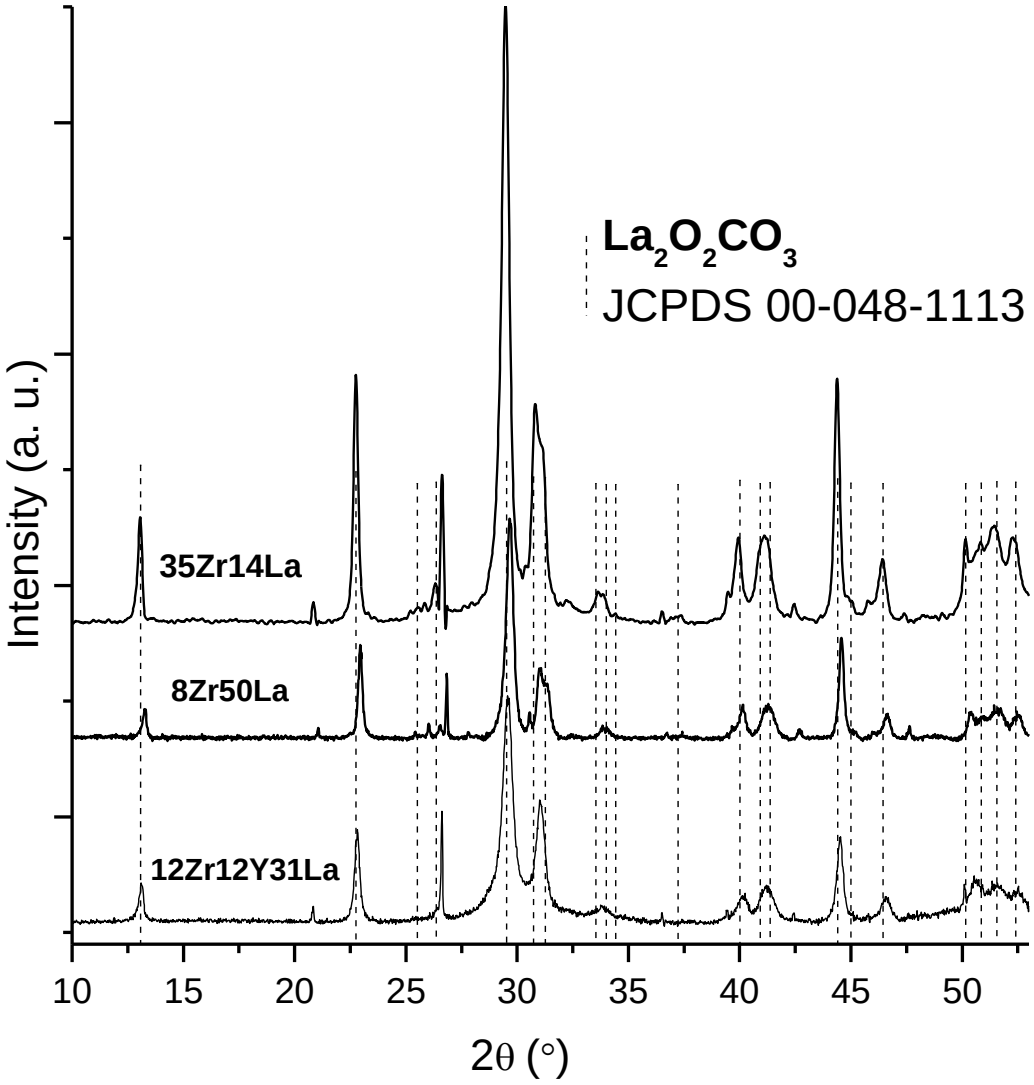

Figure 3.4 XRD patterns of 35Zr14La, 8Zr50La and 12Zr12Y31La supports with pattern of monoclinic lanthanum carbonate oxide

3.1. References

[1] Fulvio P, Vinu A, Jaroniec M. Nanocasting Synthesis of Iron-Doped Mesoporous Al - Ti Mixed Oxides Using Ordered Mesoporous Carbon Templates. J Phys Chem C 2009;16:13565–73.

[2] Haffer S, Weinberger C, Tiemann M. Mesoporous Al_2O_3 by nanocasting: Relationship between crystallinity and mesoscopic order. Eur J Inorg Chem 2012;i:3283–8. doi:10.1002/ejic.201200131.

[3] Półrolniczak P, Kowalak S. Ordered mesoporous tin oxide and tin phosphate synthesized by nanocasting strategy. J Porous Mater 2011;18:703–6. doi:10.1007/s10934-010-9429-6.

[4] Soler-Illia G, Jobbágy M. Synthesis of nickel hydroxide by homogeneous alkalinization. Precipitation mechanism. Chem Mater 1999;11:3140–6. doi:10.1021/cm9902220.

[5] Lin KH, Wang C Bin, Chien SH. Catalytic performance of steam reforming of ethanol at low temperature over $LaNiO_3$ perovskite. Int J Hydrogen Energy 2013;38:3226–32. doi:10.1016/j.ijhydene.2013.01.005.

[6] Chen H, Yu H, Peng F, Wang H, Yang J, Pan M. Efficient and stable oxidative steam reforming of ethanol for hydrogen production: Effect of in situ dispersion of Ir over Ir/La_2O_3. J Catal 2010;269:281–90. doi:10.1016/j.jcat.2009.11.010.

[7] Liu JY, Lee CC, Wang CH, Yeh CT, Wang CB. Application of nickel-lanthanum composite oxide on the steam reforming of ethanol to produce hydrogen. Int J Hydrogen Energy 2010;35:4069–75. doi:10.1016/j.ijhydene.2010.01.141.

[8] Liu SW, Liu JY, Liu YH, Huang YH, Yeh CT, Wang C Bin. Ultrasonic-assisted fabrication of $LaNiO_x$ composite oxide nanotubes and application to the steam reforming of ethanol. Catal Today 2011;164:246–50. doi:10.1016/j.cattod.2010.10.017.

[9] Shirsat AN, Ali M, Kaimal KNG, Bharadwaj SR, Das D. Thermochemistry of $La_2O_2CO_3$ decomposition. Thermochim Acta 2003;399:167–70. doi:10.1016/S0040-6031(02)00459-8.

4. Study of Ni/Me_xO_y (Me = Mg, Al, Y, La, Zr) catalysts under CO_2-assisted substoichiometric ethanol steam reforming (CDESR); Regeneration of catalysts by CO_2-treatment

In this chapter the preparation of nickel-based catalysts supported on single metal oxides Ni/Me_xO_y is presented, as well as their characterization by means of chemical analysis (ICP-AES), physisorption of N_2, XRD, XPS, H_2-TPR, CO_2-TPD and CO_2 adsorption calorimetry. The catalytic behaviour was studied under substoichiometric ethanol steam reforming (ESR) and CO_2-assisted substoichiometric ethanol steam reforming (CDESR). Moreover, the use of CO_2 was applied in regeneration of partially deactivated catalysts after ESR. Spent catalysts were characterized by means of the following techniques: XRD, XPS, TPO-MS and Raman spectroscopy.

4.1. Preparation and characterization of Ni/Me_xO_y (Me = Mg, Al, Y, La, Zr) catalysts

Ni/Me_xO_y catalysts were prepared by incipient wetness impregnation using nickel (II) nitrate (Panreac 99%), and potassium nitrate (Panreac 99.0%) in the corresponding cases. After impregnation, samples were dried overnight at 100 °C and then calcined in air at 450 °C (heating rate: 2.5 °C/min) for 5 h. Calcined catalysts were reduced *in-situ*, at 600 °C, in the reactor before each catalytic test.

Table 4.1 shows the chemical composition of Ni/Me_xO_y catalysts prepared in this work and compares the surface area and the pore volume of the catalysts with those of related supports.

Table 4.1. Results of chemical analysis, specific area and pore volume of Ni/Me_xO_y

Catalyst	Ni content (wt%)	K content (wt%)	BET area support (m^2/g)	BET area catalyst (m^2/g)	Pore volume support (cm^3/g)	Pore volume catalyst (cm^3/g)
Ni/MgO	7.5		100	83	0.492	0.446
Ni/Al_2O_3	7.7		193	125	0.343	0.224
Ni/Y_2O_3	9.6		29	16	0.229	0.052
Ni/La_2O_3	10.4		50	10	0.034	0.057
Ni/ZrO_2	8.3		146	63	0.251	0.119
Ni(K)/MgO	8.5	0.34	100	36	0.492	0.275
$Ni(K)/Al_2O_3$	9.3	0.39	193	86	0.343	0.215
$Ni(K)/Y_2O_3$	8.5	0.34	29	21	0.229	0.078

As expected, all the catalysts presented lower BET area than their corresponding supports. Potassium containing catalysts, $Ni(K)/Al_2O_3$ and Ni(K)/MgO, showed lower surface area than Ni/Al_2O_3 and Ni/MgO, respectively. Except for Ni/La_2O_3, the pore volume of catalysts was lower than that of the corresponding support. Figure 4.1 shows the pore diameter distribution of the catalysts; in all cases, the catalysts were mesoporous (pore diameter between 2 nm and 50 nm). The introduction of K changed only the pore distribution for $Ni(K)/Al_2O_3$ with respect to Ni/Al_2O_3.

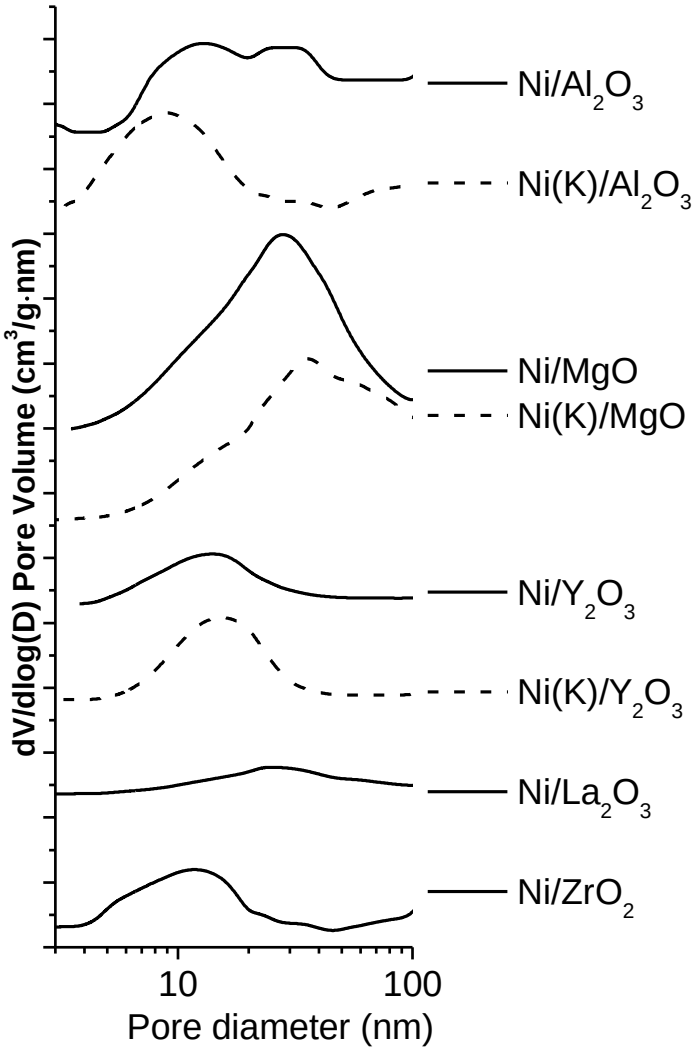

Figure 4.1. Pore diameter distribution of Ni/Me_xO_y catalysts

The XRD patterns of the catalysts are presented in Figure 4.2. For Ni/MgO and Ni(K)/MgO, Ni/Al_2O_3 and Ni(K)/Al_2O_3, and Ni/Y_2O_3 and Ni(K)/Y_2O_3 catalysts, peaks of expected crystalline support phases were found: MgO (JCPDS 00-043-1022, cubic), Al_2O_3 (JCPDS 00-001-1303, cubic) and Y_2O_3

(JCPDS 03-065-3178, cubic), respectively. From the Ni/ZrO_2 pattern, it was not possible to discern between the presence of tetragonal ZrO_2 (JCPDS 00-050-1089) and cubic ZrO_2 (JCPDS 03-065-0461) phases due to the close proximity of their characteristic diffraction lines.

The presence of crystalline $La_2O_2CO_3$ (JCPDS 00-048-1113, monoclinic) was identified from the Ni/La_2O_3 XRD pattern. $La_2O_2CO_3$ can be easily formed by reaction of La_2O_3 with CO_2 [1,2]. In this work, the $La_2O_2CO_3$ formation may occur during the burning elimination of the active carbon.

Only in the XRD pattern of Ni/ZrO_2 it was possible clearly identify the peaks corresponding to NiO (JCPDS 01-075-0197, cubic). A NiO crystallite size of 27 nm was determined for Ni/ZrO_2, using the (200) NiO diffraction peak at $2\theta = 43.3°$ and the Debye-Scherrer equation [3]. In the rest of the patterns, the NiO peaks were not detected or were overlapped with the peaks coming from the support.

XRD patterns of potassium-doped catalysts were similar to the corresponding non-doped. Potassium oxide was not detected by XRD probably due to its low content or amorphous nature. As it can be deduced from inspection of the X-ray diffraction patterns of doped and non-doped catalysts in Figure 4.2, neither influence of potassium oxide on the crystallinity of the support phases was found.

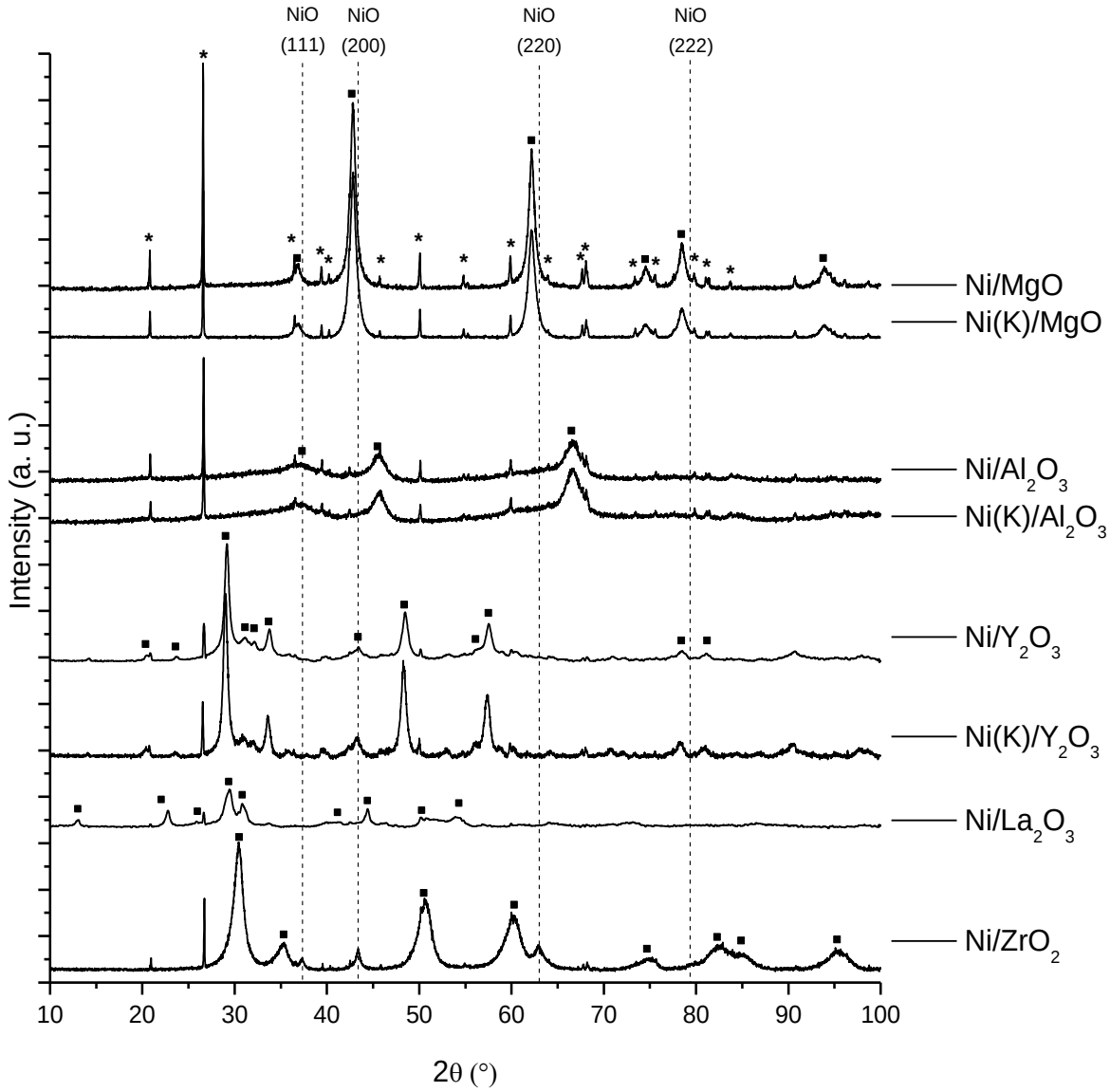

Figure 4.2. XRD patterns of calcined Ni/Me$_x$O$_y$ catalysts. The dashed vertical lines indicate the characteristics peaks of the cubic NiO (JCPDS 01-075-0197). The squares above the patterns indicate the corresponding support peaks; the asterisks indicate quartz wool SiO_2 peaks

XPS was used to analyse core level spectra of the main elements on the surface of reduced catalysts: Ni 2p, Mg 2s, Al 2p, Y 3d, La 3d, and Zr 3d. For Ni/La_2O_3, it was not possible to analyse the Ni 2p level due to its overlapping with La $3d_{3/2}$ level. The absence of XPS characteristic peaks of potassium levels did not allow determine the presence of potassium species on the surface of the catalysts. Figure 4.3 presents XPS spectra in the Ni 2p region of Ni/Me_xO_y catalysts (*ex-situ* reduced). Ni $2p_{3/2}$ core level peaks were located at approximately 855.5 eV. This value, together with the satellite peak around 861.8 eV, indicates the presence of surface Ni^{2+} species [4].

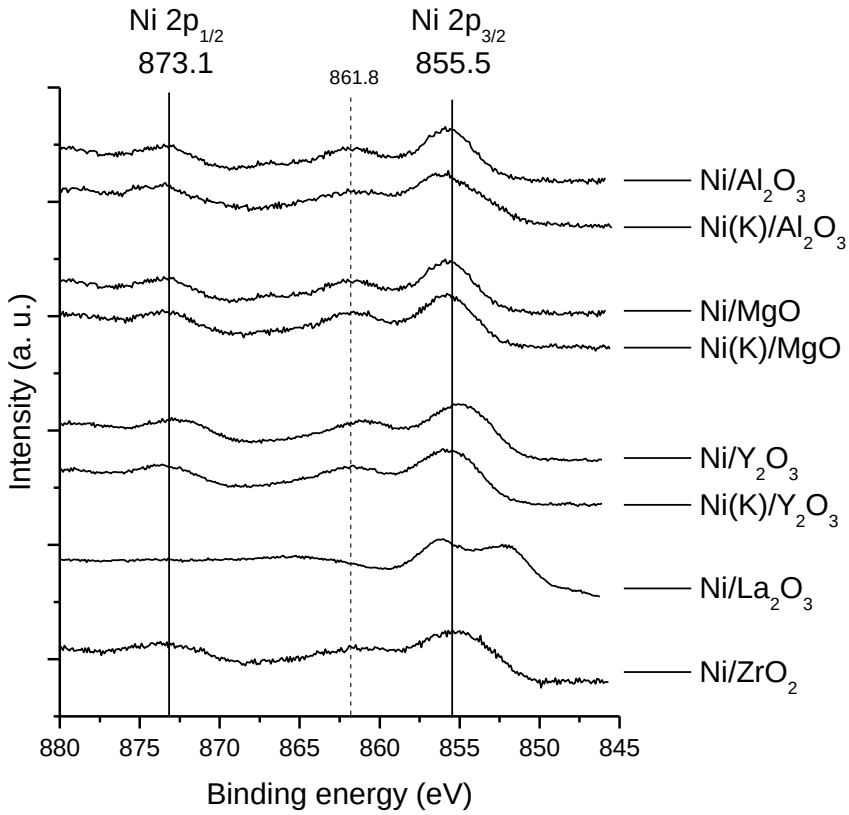

Figure 4.3. Nickel 2p core level XPS spectra of *ex-situ* reduced Ni/Me_xO_y catalysts

Using the XPS spectra and sensitivity factors (with help of PHI MultiPak® software), the Ni/Me surface atomic ratio on Ni/Me_xO_y catalysts was determined and compared to the Ni/Me bulk atomic ratio determined by chemical analysis (Tab. 4.2).

Table 4.2. Ni/Me atomic ratios determined by XPS and ICP-AES of Ni/Me_xO_y catalysts

Catalyst	Ni/Me atomic ratio	
	XPS	Chemical analysis (ICP-AES)
Ni/MgO	0.225	0.056
Ni/Al_2O_3	0.111	0.074
Ni/Y_2O_3	0.585	0.210
Ni/La_2O_3	-	-
Ni/ZrO_2	0.176	0.192
Ni(K)/MgO	0.134	0.118
Ni(K)/Al_2O_3	0.059	0.123
Ni(K)/Y_2O_3	0.314	0.261

Except for Ni/ZrO_2 and Ni(K)/Al_2O_3, higher surface atomic Ni/Me ratios than those corresponding to the bulk were found, indicating a segregation of nickel species on the surface of the catalysts. In all cases, the potassium-doped catalysts had lower Ni/Me surface atomic ratio than non-doped analogues.

Reducibility of the catalysts was determined by H_2-TPR analysis. Figure 4.4 shows the corresponding hydrogen consumption profiles, while the apparent H_2 consumption appears in Table 4.3. According to the following reaction, for complete reduction of NiO, a molar ratio H_2/Ni = 1 is expected:

$$NiO + H_2 \rightarrow Ni + H_2O \qquad (4.1)$$

Consumption of H_2 in the range 375-425 °C is usually associated to the reduction of NiO which does not interact with the support [5]. Often, an increase in the strength of interaction of Ni^{2+} species with the support produces an increase in the temperature of reduction of these species.

H_2-TPR profile of Ni/ZrO_2 accords with the presence of NiO particles that do not interact with the support. For Al_2O_3-supported catalysts, a weak interaction between most of Ni^{2+} species and Al_2O_3 can be proposed. The broad band of hydrogen consumption obtained for MgO-supported catalysts can be related with the presence of heterogeneous Ni^{2+} species.

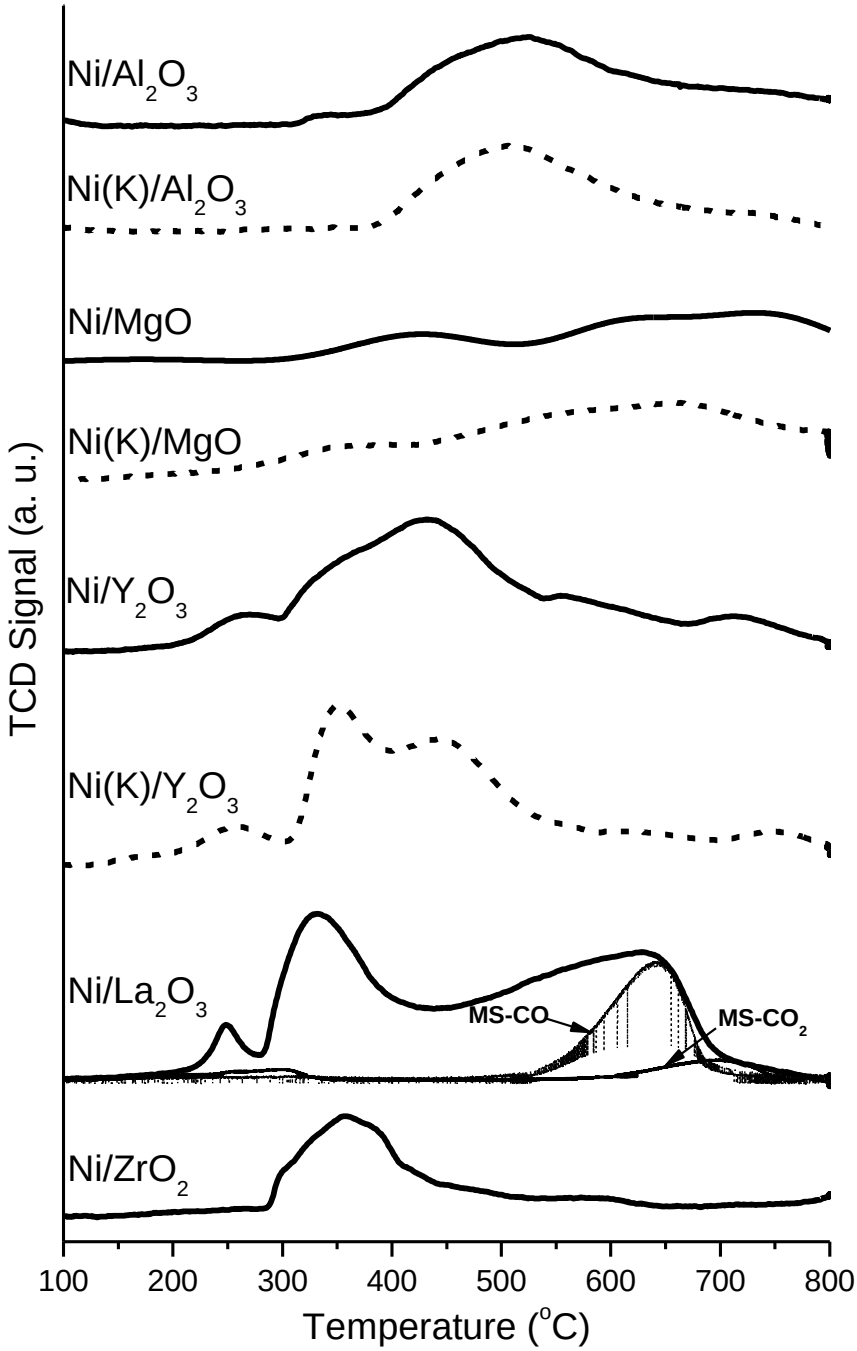

Figure 4.4. H_2-TPR profiles of the Ni/Me_xO_y catalysts. For Ni/La_2O_3, the profiles of CO and CO_2 evolution, determined from coupled mass-spectrometry analysis, are presented

Table 4.3. Apparent consumption of hydrogen and its relation to the amount of nickel; results from H_2-TPR analyses of the Ni/Me_xO_y catalysts

Catalyst	mmol H_2/g	mol H_2/mol Ni
Ni/MgO	1.69	1.32
Ni(K)/MgO	2.26	1.55
Ni/Al_2O_3	1.94	1.21
Ni(K)/Al_2O_3	1.45	1.00
Ni/Y_2O_3	5.13	3.13
Ni(K)/Y_2O_3	4.14	2.87
Ni/La_2O_3	7.58	(4.27)
Ni/ZrO_2	2.00	1.41

Y_2O_3-supported catalysts also showed a broad band of H_2 consumption and a much greater amount of H_2 consumed than that necessary for the total reduction of NiO (Tab. 4.3). For these catalysts, the peak at 260 °C can be related with the reduction of NiO particles favoured by the presence of oxygen vacancies in Y_2O_3 [6,7]. The excess of H_2 consumption could be related with the reduction of oxide species which could take place at temperatures higher than 500 °C. The presence of Ni could enhance the surface oxygen mobility and favour the reduction of Y_2O_3 [8]. Ni/La_2O_3 catalyst showed a very broad H_2-TPR profile, with an intense peak with maximum at 650 °C (Fig.4.4), and a high value of apparent H_2 consumption (Tab. 4.3).

As stated before, the presence of crystalline $La_2O_2CO_3$ was found by XRD. As discussed in Chapter 3, $La_2O_2CO_3$ can react with H_2 and contribute to the enhanced H_2 consumption [9–12]:

$$La_2O_2CO_3 + H_2 \rightarrow La_2O_3 + H_2O + CO \quad (4.2)$$

Moreover, $La_2O_2CO_3$ can decompose:

$$La_2O_2CO_3 \rightarrow La_2O_3 + CO_2 \quad (4.3)$$

To clarify these possible reactions, for Ni/La_2O_3, a H_2-TPR experiment with coupled mass-spectrometry (MS) analysis was performed. The results showed that, above 550 ^oC, CO was detected in the outlet gas (see Fig.4.4). Moreover, CO_2 was also detected above 630 ^oC. For the Ni/La_2O_3 catalyst, the apparent consumption of H_2 above 550 ^oC and the excess of consumption of H_2 (Tab. 4.3) can be attributed to the above discussed processes. The TCD detector signal can be perturbed by the evolved gases.

The CO_2 adsorption and desorption onto the reduced catalysts was studied by CO_2-TPD and calorimetry experiments. The experiments of CO_2-TPD were carried out after CO_2 adsorption at 20 °C; Figure 4.5 shows the corresponding CO_2-TPD profiles. The values of the total and mean enthalpies of CO_2 adsorption and the density of basic sites, obtained from CO_2 adsorption experiment with calorimetric measurements, are reported in Table 4.4. The temperature of CO_2 desorption reflects the strength of basic sites, while the areas under desorption peaks can be related to the number of basic sites on the surface of catalysts. CO_2-TPD peaks at

temperature lower that 225 °C are related with the presence of low strength basic sites; these in the range 225-425 °C with medium-strength basic sites, and CO_2-TPD peaks at temperatures higher than 425 °C correspond to basic centres to which CO_2 is strongly bonded [13].

The TPD-CO_2 profiles of Al_2O_3-supported catalysts mainly exhibited a low intensity desorption peak at low temperature due to the presence of weak basic centres; these catalysts showed, as expected, the lowest CO_2 adsorption enthalpy.

Ni/ZrO_2 and MgO-supported catalysts presented more intense and broader desorption peaks than Al_2O_3-supported catalysts. Desorption extended from low up to medium temperatures (400 °C); these profiles can be related to the presence of low- and medium-strength basic sites [14]. Y_2O_3-supported catalysts showed CO_2 desorption at a wide range of temperatures, indicating heterogeneity of the strength of the basic sites [15].

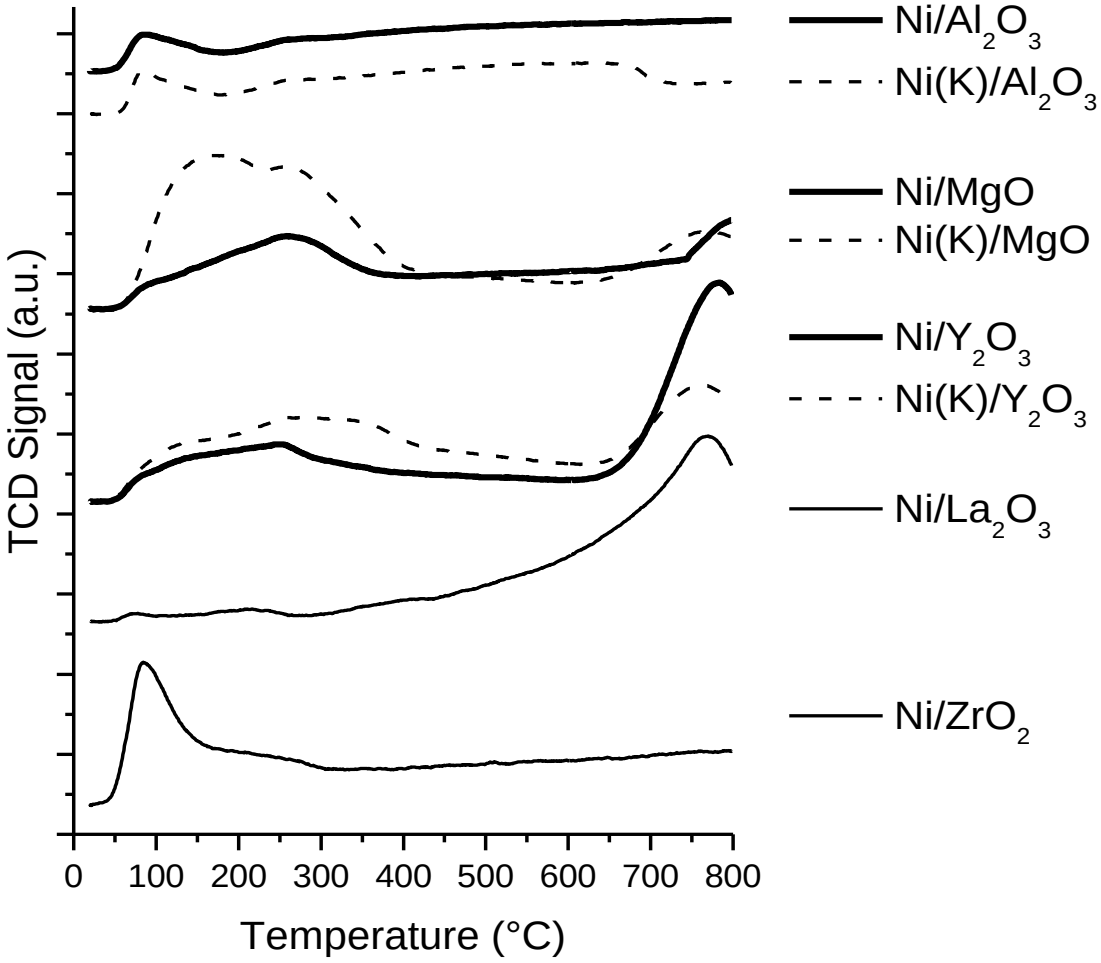

Figure 4.5. CO_2-TPD profiles of Ni/Me_xO_y catalysts

The desorption peaks of CO_2 at high temperatures found for Y_2O_3- and La_2O_3-supported catalysts (Fig. 4.5) are indicative of the presence of strongly bonded CO_2. Moreover, these catalysts show a higher surface density of basic sites than the remaining catalysts (Tab. 4.4). The higher relative abundance of strong basic sites on Ni/La_2O_3 accords with its mean CO_2 adsorption heat (Tab. 4.4).

For MgO- and Al_2O_3-supported catalysts, addition of potassium resulted in a higher surface density of basic sites. In the case of Y_2O_3-supported catalysts, a higher CO_2 total adsorption heat was found for the catalyst containing potassium.

Table 4.4. Total and mean CO_2 adsorption enthalpies and surface density of basic sites determinate by CO_2 adsorption calorimetry

Catalyst	ΔH_{ads} (J/g)	ΔH_{ads} (J/mmol)	Surface density of basic sites ($\mu mol/m^2$)
Ni/Al_2O_3	-4.352	-37.4	1.1
$Ni(K)/Al_2O_3$	-4.833	-34.5	1.8
Ni/MgO	-5.650	-42.6	1.6
Ni(K)/MgO	-6.377	-42.8	4.3
Ni/Y_2O_3	-8.684	-59.9	9.1
$Ni(K)/Y_2O_3$	-12.383	-63.2	9.3
Ni/La_2O_3	-5.994	-75.1	8.0
Ni/ZrO_2	-13.127	-61.3	3.4

4.2. Catalytic behaviour under CO_2-assisted substoichiometric ethanol steam reforming (CDESR); Characterization of spent catalysts and carbon deposits

Ni/Me_xO_y catalysts were tested under substoichiometric ethanol steam reforming (ESR), followed by CO_2-assisted substoichiometric ethanol steam reforming (CDESR), as it has been presented in the experimental section. Instead of stoichiometric ethanol/water molar ratio 1.0/3.0, a lower ratio 1.0/1.6, was chosen. Under these unfavourable conditions, deactivation of catalysts due to the carbon deposits formation was studied. In CDESR, CO_2 was applied as a reactant using a reaction mixture: ethanol/water/CO_2 = 1.0/1.6/1.6, molar ratios.

All the catalytic tests were carried out at 600 °C, under atmospheric pressure and with GHSV = 8100 h^{-1}, with 200 mg of calcined catalyst. The catalysts were *in-situ* reduced before launching the reaction.

The variation of ethanol conversion along time, during the ESR/CDESR catalytic tests is presented in Figure 4.6. In all cases, under substoichiometric ethanol steam reforming, the ethanol conversion decreased along time. Then, during the next 18 h under CDESR conditions, except for MgO-supported catalysts, the ethanol conversion values showed smaller changes; Ni/MgO showed a continuous decrease of ethanol conversion under CDESR condition, meanwhile the ethanol conversion slightly increased for Ni(K)/MgO.

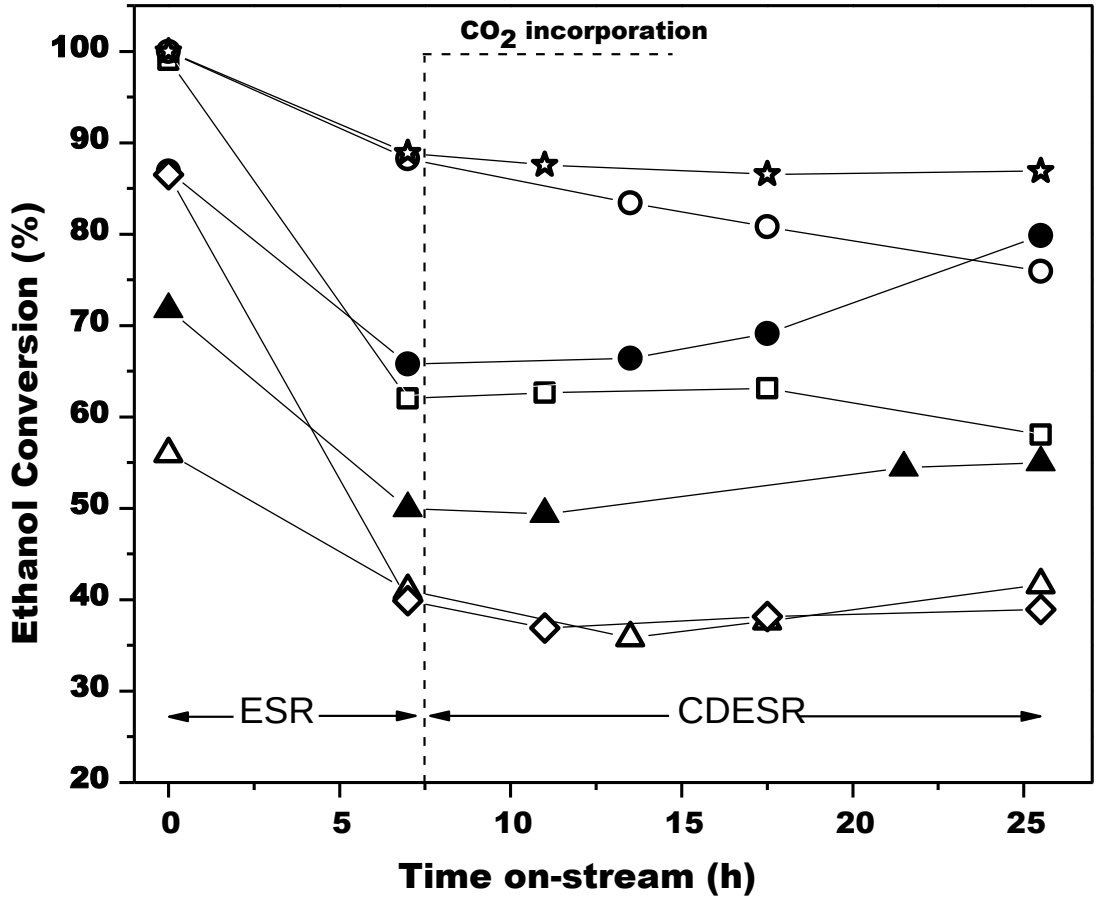

Figure 4.6. Ethanol conversion along time under ESR (ethanol/H_2O=1.0/1.6, molar ratio) and after CO_2 introduction, CDESR (ethanol/H_2O/CO_2=1.0/1.6/1.6, molar ratios) over the catalysts: (□) Ni/Al_2O_3; (○) Ni/MgO; (●) Ni(K)/MgO; (Δ) Ni/Y_2O_3; (▲) Ni(K)/Y_2O_3; (◊) Ni/La_2O_3; (☆) Ni/ZrO_2. T = 600 °C, GHSV = 8100 h^{-1}

Figures 4.7a, 4.7b and 4.7c show the product distribution along time under ESR and CDESR conditions. In all cases, H_2 was the main product obtained (molar concentration 40-60 %) and only in the case of Ni/La_2O_3 its concentration significantly changed along time. Although an exhaustive analysis of the distribution of carbon-containing products is complex, in

general acetaldehyde and CO were the most abundant. Acetaldehyde can be formed under reaction conditions through:

$C_2H_5OH \rightarrow CH_3CHO + H_2$ (4.4)

And then CH_3CHO could react producing CO:

$CH_3CHO + H_2O \rightarrow 2CO + 3H_2$ (4.5)

These processes could justify the variation of acetaldehyde and CO concentration along time due to the ethanol conversion change. This effect is clearly visible for: Ni/Al_2O_3, Ni/La_2O_3 and Ni/ZrO_2 catalysts.
Besides CH_3CHO and CO, in general, smaller amounts of CH_4 and C_2H_4 were produced. The following reactions could account for this behaviour:

$C_2H_5OH \rightarrow C_2H_4 + H_2O$ (4.6)

$C_2H_5OH \rightarrow CH_4 + CO + H_2$ (4.7)

$CH_3CHO \rightarrow CH_4 + CO$ (4.8)

The production of ethene was more significant for Ni(K)/Y_2O_3 and Ni/ZrO_2 catalysts at the first stage of the ESR reaction, achieving molar concentration of about 20 %.

Formation of small amount (up to 5% mol/mol) of CO_2 was observed during the ESR stage. Under the CDESR conditions, the evaluation of CO_2 production was not possible to determine, thus its concentration is not presented in Figures 4.7a-c.

In general, the catalytic behaviour of K-dopped catalysts did not show large difference comparing with those of corresponding catalysts without K.

As it can be seen (Fig. 4.7a-c), the product distribution was not strongly affected by the CO_2 incorporation; except for Ni/La_2O_3, no major changes during CDESR were found. For Ni/La_2O_3 catalyst, the possible formation of $La_2O_2CO_3$ species under CDESR conditions could contribute to the observed variation of H_2 and CH_3CHO distribution. However, in general, the stabilization of the ethanol conversion values during CDESR could be related with the small variation of reaction product concentrations found along time.

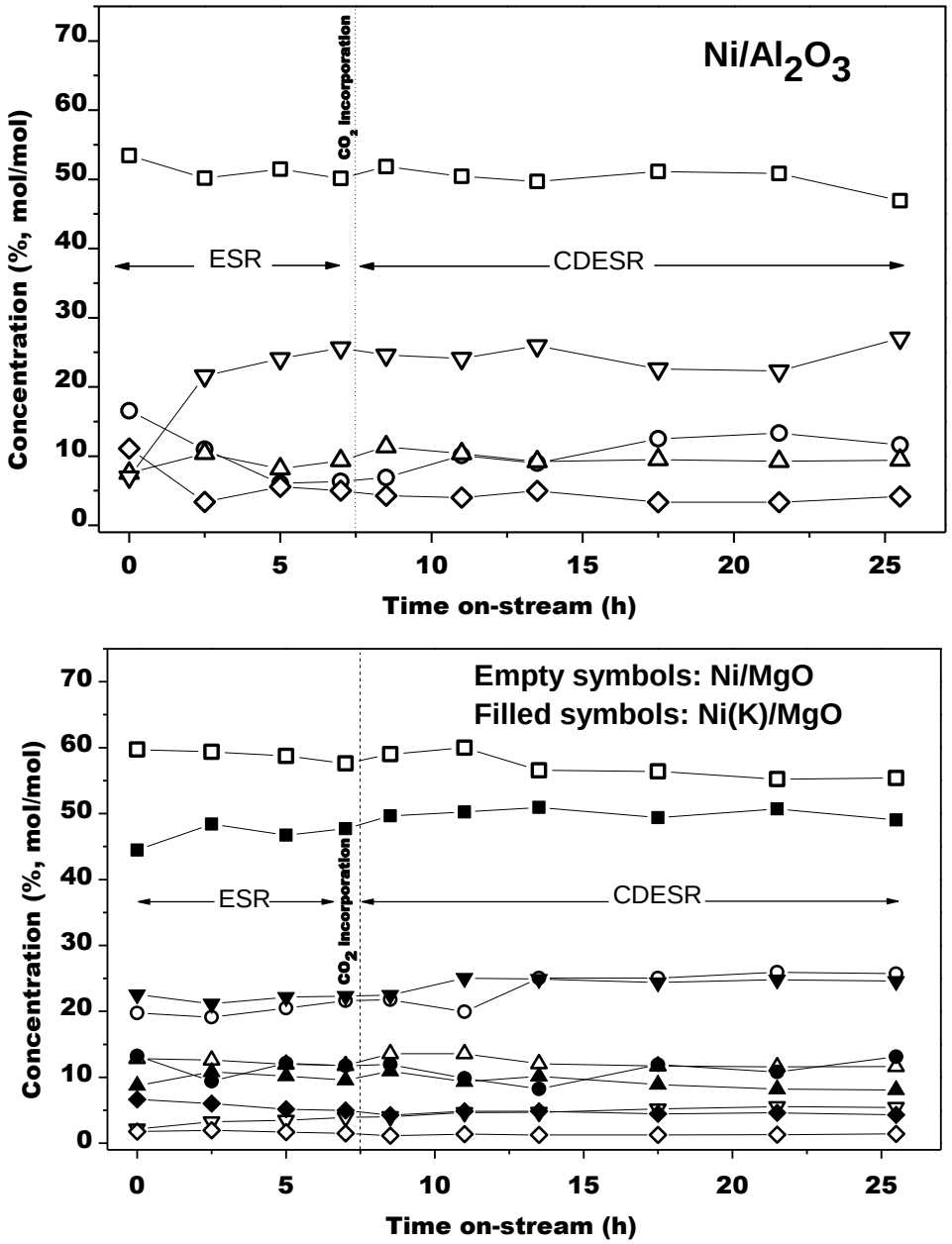

Figure 4.7a. Catalytic behaviour under ESR and CDESR over different catalysts. Molar concentration of (□) H_2, (○) CO, (△) CH_4, (▽) CH_3CHO and (◇) C_2H_4 in the outlet gas is shown. Reaction conditions: GHSV = 8100 h^{-1}, m_{cat} = 200 mg, T = 600 °C; 1.0 EtOH/1.6 H_2O/22.8 (Ar+N_2) molar ratios for first 7.5 hours, and 1.0 EtOH/1.6 H_2O/1.6 CO_2/21.2 (Ar+N_2) molar ratios for 18 hours

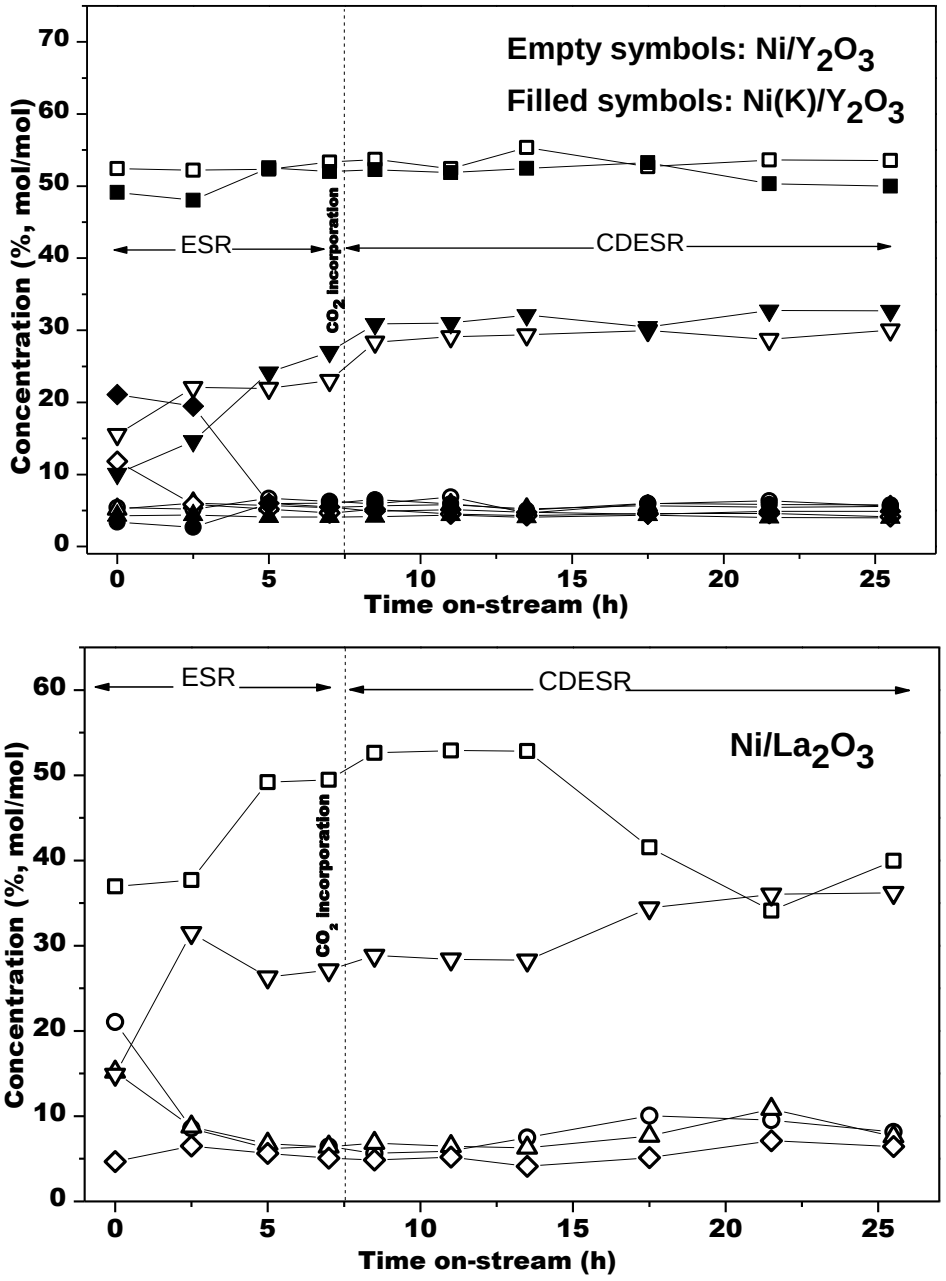

Figure 4.7b. Catalytic behaviour under ESR and CDESR over different catalysts. Molar concentration of (□) H_2, (○) CO, (△) CH_4, (▽) CH_3CHO and (◊) C_2H_4 in the outlet gas is shown. Reaction conditions: GHSV = 8100 h^{-1}, m_{cat} = 200 mg, T = 600 °C; 1.0 EtOH/1.6 H_2O/22.8 (Ar+N_2) molar ratios for first 7.5 hours, and 1.0 EtOH/1.6 H_2O/1.6 CO_2/21.2 (Ar+N_2) molar ratios for 18 hours

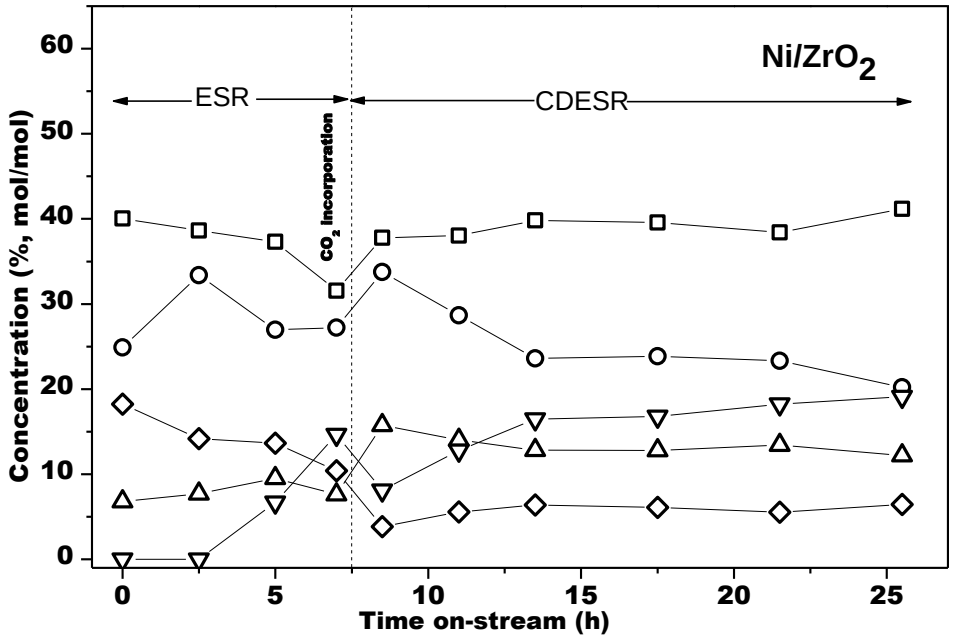

Figure 4.7c. Catalytic behaviour under ESR and CDESR over Ni/ZrO_2. Molar concentration of (□) H_2, (○) CO, (△) CH_4, (▽) CH_3CHO and (◊) C_2H_4 in the outlet gas is shown. Reaction conditions: GHSV = 8100 h^{-1}, m_{cat} = 200 mg, T = 600 °C; 1.0 EtOH/1.6 H_2O/22.8 (Ar+N_2) molar ratios for first 7.5 hours, and 1.0 EtOH/1.6 H_2O/1.6 CO_2/21.2 (Ar+N_2) molar ratios for 18 hours

The post-reaction catalysts were characterized by XRD, XPS and Raman spectroscopy, and with TPO-MS determining the heat flow and mass changes, with coupled MS analysis.

XRD patterns of post-reaction catalysts used in the ESR/CDESR experiments are shown in Figure 4.8. Main peaks of the support phase maintained their shape and position with respect to fresh calcined catalysts (Fig. 4.2). The presence of Ni^0 was determined in all samples, except for Ni/La_2O_3 due to the overlapping with $La_2O_2CO_3$ peaks. For Ni/Al_2O_3 and Ni/ZrO_2 it was

possible to determine Ni^0 (JCDPS 03-065-2865 cubic) with crystallite sizes of ca. 10 nm and 14 nm, respectively, using the Ni^0 (200) (Ni/Al_2O_3) and the Ni^0 (111) (Ni/ZrO_2) diffraction peaks and the Debye-Scherrer method [3].

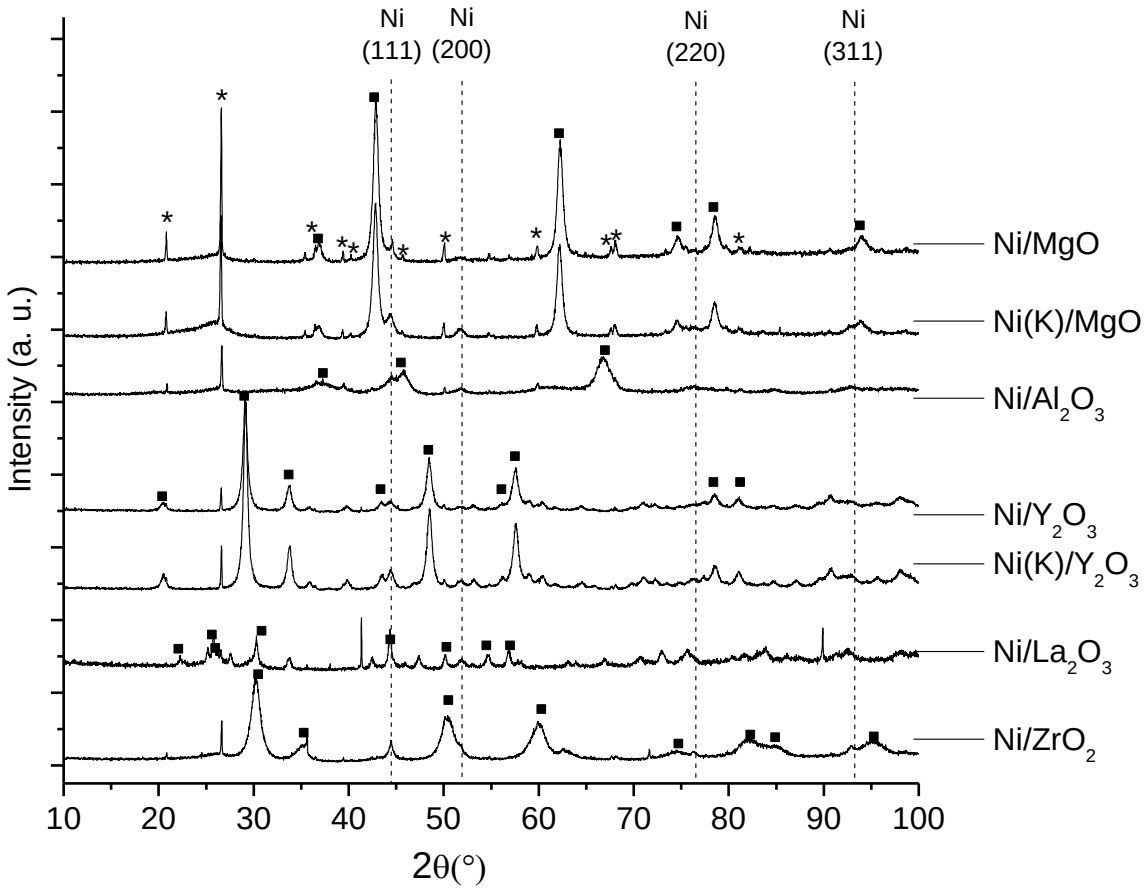

Figure 4.8. XRD patterns of post-reaction Ni/Me_xO_y catalysts used in ESR/CDESR. The dashed vertical lines indicate the position of the cubic phase of Ni^0 peaks (JCPDS 03-065-2865). The squares above the patterns indicate the corresponding support peaks; the asterisks indicate quartz wool SiO_2 peaks

XPS analysis of the post-reaction catalysts was carried out. After ESR/CDESR test, it was only possible to determine the presence of nickel surface species from the analysis of Ni/Al_2O_3 and Y_2O_3-supported samples. For the post-reaction Ni/ZrO_2 and MgO-supported samples, it was not possible to analyse the Ni 2p core level because of the very weak signal; this is possibly due to a high surface carbon deposition.

A special emphasis was placed on characterization of carbon deposits. For this purpose, XPS, Raman spectroscopy and TPO-MS analyses were carried out to evaluate the amount and characteristics of the carbon deposits.

From XPS results, the corresponding BE region of the C1s level resulted of complex analysis; besides a peak located at around 285 eV (Fig. 4.9), a broad contribution to the spectra at higher BE can be observed. This could be ascribed to the presence of amorphous carbonaceous species containing C=O groups [16,17]. For Ni/Y_2O_3 the broad component at higher BE (286 - 289 eV) would be indicative of the presence of chemisorbed CO_2 [16].

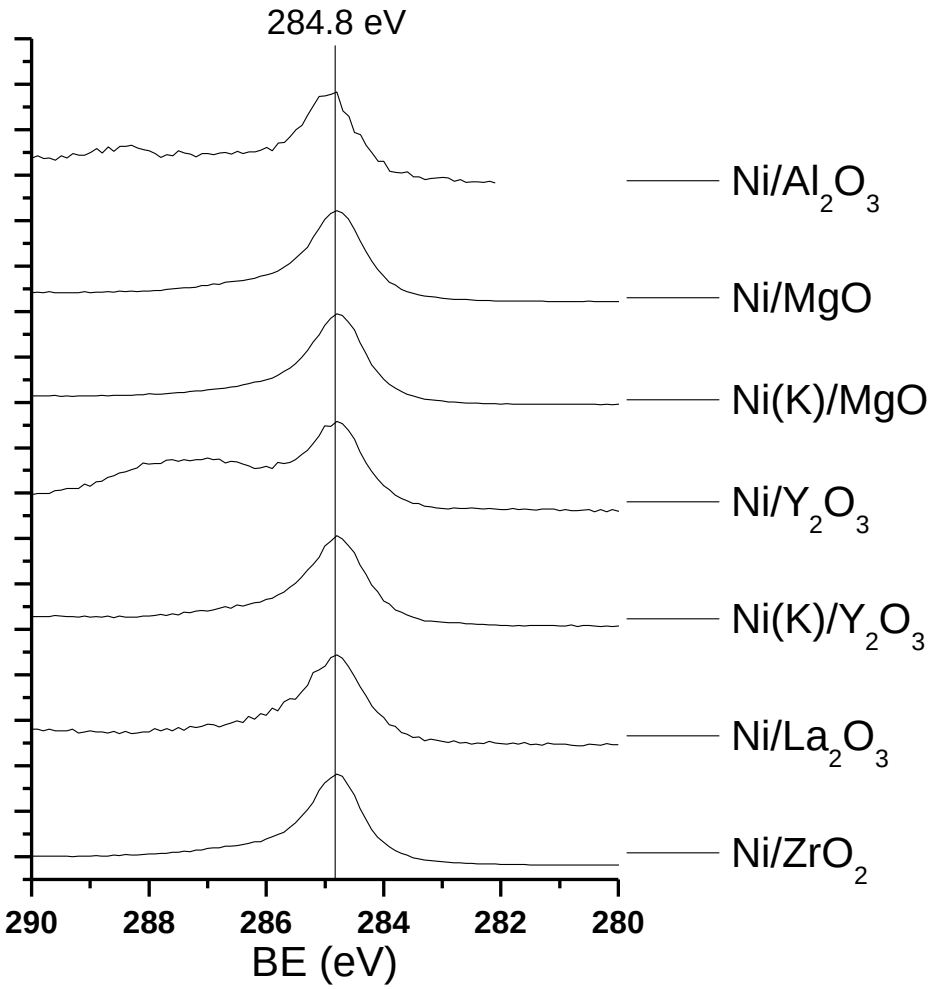

Figure 4.9. XPS spectra of C1s region of post-reaction Ni/Me_xO_y catalysts after ESR/CDESR

The analysis by Raman spectroscopy of the catalysts after ESR/CDESR reaction was used in order to characterize the carbon deposits. Raman spectroscopy was applied to determine the distribution between amorphous and graphitic carbons as this technique is commonly used for this purpose. Carbon deposits generally present Raman shift bands

between 1300 cm^{-1} and 1610 cm^{-1}; two specific bands may be distinguished at about 1340 cm^{-1}, named D band, and at about 1580 cm^{-1}, named G band. The D band is characteristic for poorly structured carbonaceous deposits; while the G band is assigned to the in-plane sp^2 C=C stretching vibrations of well-structured carbon deposits; the ratio of the corresponding intensities, I_G/I_D, may be related to the order of the carbon deposits [18–21]. Figure 4.10 shows the spectra registered for all catalysts, while Table 4.5 presents the corresponding I_G/I_D values. All determined values resulted in narrow range (0.56-0.67) not revealing big differences between the catalysts.

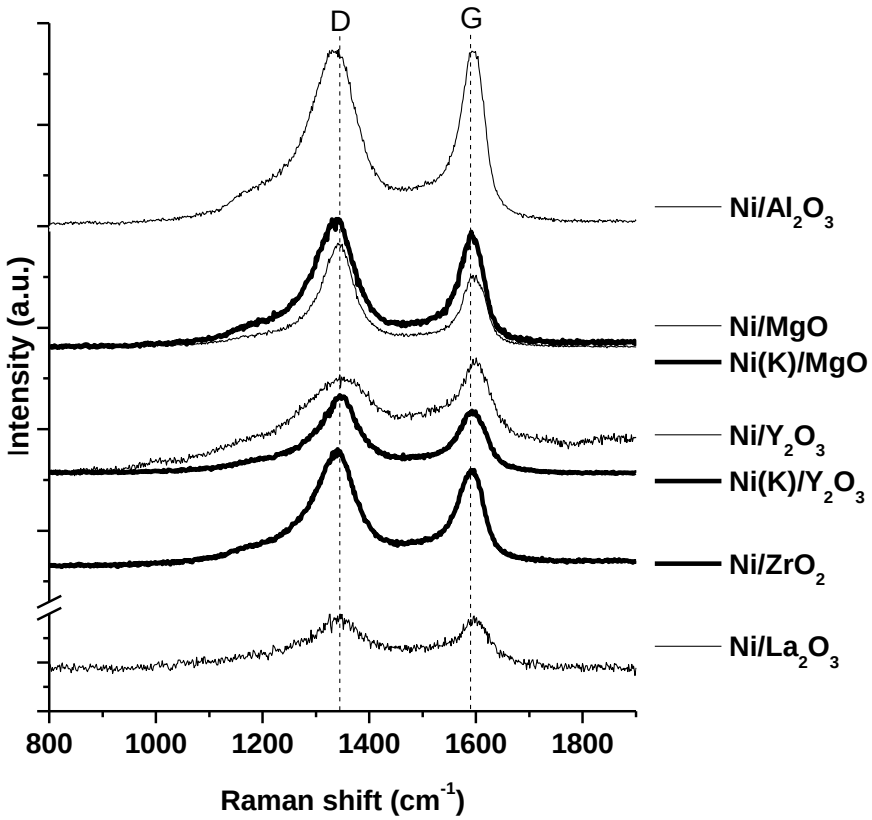

Figure 4.10. Carbon region of Raman spectra of post-reaction Ni/Me_xO_y catalysts after ESR/CDESR

Table 4.5. I_G/I_D Raman ratio for post-reaction Ni/Me_xO_y catalysts after ESR/CDESR

Catalyst	CDESR
Ni/Al_2O_3	0.59
Ni/MgO	0.59
Ni(K)/MgO	0.61
Ni/Y_2O_3	0.56
$Ni(K)/Y_2O_3$	0.64
Ni/La_2O_3	0.67
Ni/ZrO_2	0.56

The quantification of the carbonaceous deposits after the ESR/CDESR catalytic tests was carried by using TPO-MS experiments, as indicated before.

The characteristics of carbonaceous species, formed during the reaction, are expected to depend on experimental conditions and the nature of the catalysts [22]. TPO-MS results provide information about the carbon oxidation temperature, the heat flow produced during the analysis, and the loss of weight during the experiment. These parameters can allow quantifying the amount of deposited carbon and can be related with the carbon deposits characteristics. Combustion temperatures below 450 °C can be attributed to the presence of low ordered carbon deposits. Peaks in the TPO profile above this temperature are related with the oxidation of carbon deposits with higher graphitization degree. The exothermic combustion of carbonaceous deposits was observed in all cases above 300 °C. TPO-MS analysis was performed after ESR/CDESR tests over Ni/Al_2O_3,

Ni(K)/MgO, Ni(K)/Y_2O_3, Ni/La_2O_3 and Ni/ZrO_2. Figure 4.11 shows the TPO profile for the Ni/La_2O_3 catalyst after the ESR/CDESR test. For this catalyst, a main peak about 370 °C is observed; the main part of the carbonaceous deposits corresponds to poorly ordered species. The TPO profiles for the other post-reaction catalysts analysed are given in the Annex (Figures A.3-A.8). In all cases, the presence of main peaks at temperatures higher than 600 °C indicated the predominance of the more ordered carbon deposits.

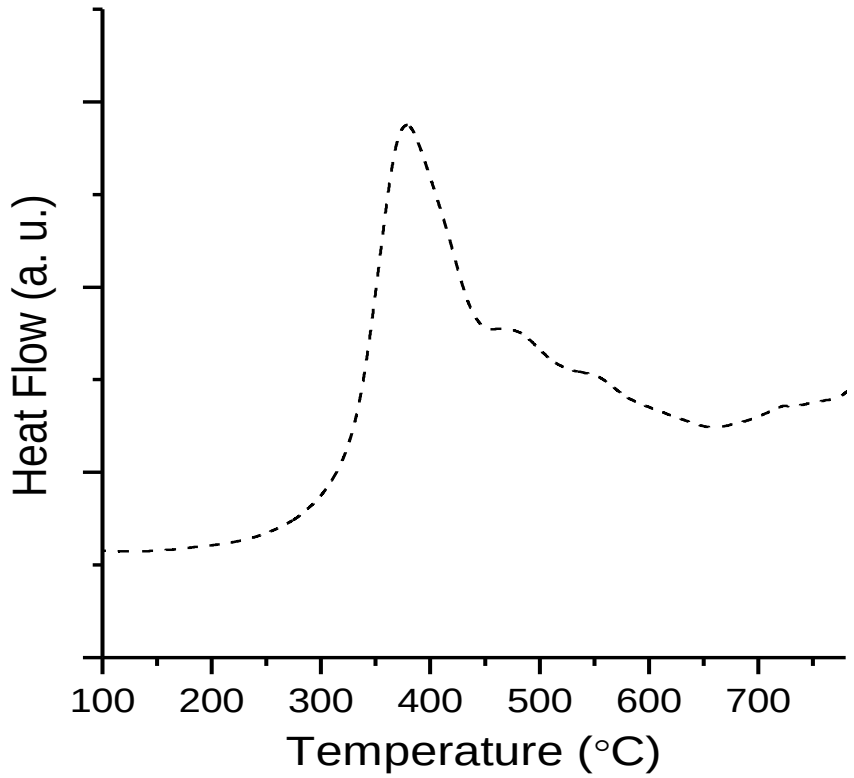

Figure 4.11. Heat flow profile obtained during TPO-MS analysis of Ni/La_2O_3 catalyst after ESR/CDESR

On the other hand, this experiment allowed quantifying the amount of deposited carbon after the ESR/CDESR test. Table 4.6 compiles the determined carbon formation rates for several catalysts. The Ni/La_2O_3 resulted in the lowest carbon formation rate.

Table 4.6. Carbon formation rate determined from TPO-MS analysis of Ni/Me_xO_y catalysts after ESR/CDESR experiments

Catalyst	Carbon deposited (mmol C/h·g_{cat})
Ni/Al_2O_3	0.720
Ni/MgO	-
Ni(K)/MgO	1.138
Ni/Y_2O_3	-
$Ni(K)/Y_2O_3$	0.230
Ni/La_2O_3	0.060
Ni/ZrO_2	1.047

For a better evaluation of the effect of introduction of CO_2 in the ESR/CDESR catalytic test in relation to the carbon formation, a separate ESR catalytic test for 17.5 h was carried out. The spent catalysts from this ESR test were also analysed by XPS, Raman spectroscopy and TPO-MS experiments.

In all cases, the XPS spectra in the region corresponding to C1s core level exhibited asymmetric peaks centred at 284.8 eV, with a tail at higher BE. The corresponding XPS spectra are given in the Annex (Figure A.1)

The Raman spectra of the catalysts used in the ESR catalytic test appear in Figure 4.12, and the corresponding I_G/I_D ratios are presented in Table 4.7. For Y_2O_3-supported catalysts poorly resolved Raman spectra were obtained which could not be properly analysed. Values of I_G/I_D in the range 0.52-0.64 were obtained; these values did not allow establish large difference between the natures of carbon deposits generated on the different catalysts neither after the ESR catalytic tests.

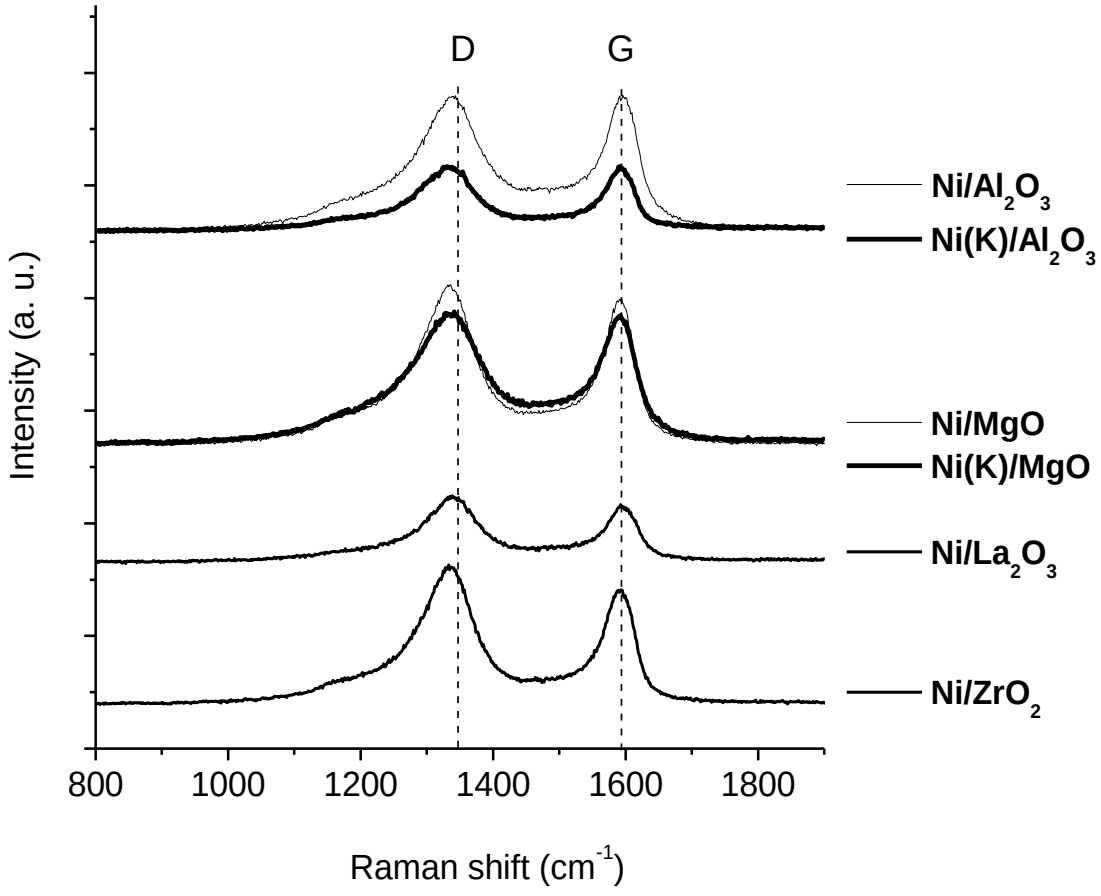

Figure 4.12. Carbon region of Raman spectra of post-reaction Ni/Me_xO_y catalysts after ESR/CDESR

Table 4.7. I_G/I_D Raman ratio for post-reaction Ni/Me_xO_y catalysts after ESR/CDESR

Catalyst	ESR
Ni/Al_2O_3	0.64
$Ni(K)/Al_2O_3$	0.64
Ni/MgO	0.59
Ni(K)/MgO	0.54
Ni/La_2O_3	0.64
Ni/ZrO_2	0.52

The carbon formation rate determined after the ESR catalytic test is presented in the Table 4.8. Y_2O_3-supported catalysts and the Ni/La_2O_3 showed the lowest values of carbon formation rate under the ESR conditions used. Only the Ni/La_2O_3 catalyst showed a significantly lower carbon formation rate under ESR/CDESR (0.060 mmol C/h·g_{cat}) than during ESR (0.191 mmol C/h·g_{cat}). The role of CO_2 in elimination of the graphitic carbon deposits in Ni/La_2O_3 could be related with the formation of $La_2O_2CO_3$ under CDESR conditions, which could further react via:

$$La_2O_2CO_3 + C \rightarrow La_2O_3 + 2CO \qquad (4.9)$$

Table 4.8. Carbon formation rate determined from TPO-MS analysis of Ni/Me_xO_y catalysts after ESR experiments

Catalyst	Carbon deposited (mmol C/h·g_{cat})
Ni/Al_2O_3	0.554
Ni(K)/Al_2O_3	0.583
Ni/MgO	0.971
Ni(K)/MgO	1.078
Ni/Y_2O_3	0.078
Ni(K)/Y_2O_3	0.074
Ni/La_2O_3	0.191
Ni/ZrO_2	1.157

The Figure 4.13 shows the TPO profiles obtained from the Ni/La_2O_3 catalyst after the separate ESR and ESR/CDESR tests. As can be seen, after the ESR catalytic test, the TPO profile shows combustion peaks corresponding to the presence of both poorly and highly ordered carbonaceous deposits. The oxidation is extended above 500 °C; relative maxima about 550 °C and 600 °C are observed, which reasonably points to the presence of abundant ordered deposits.

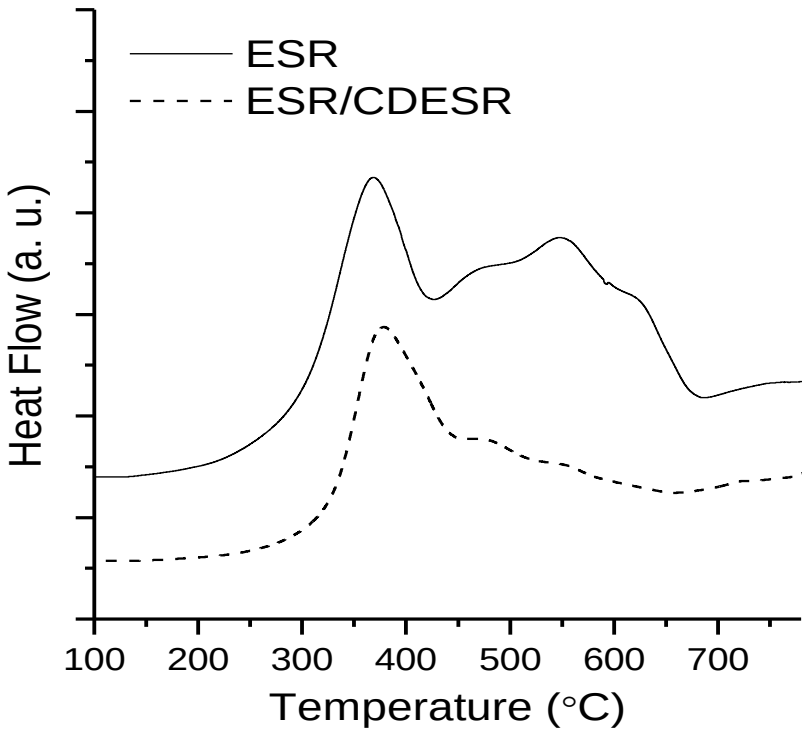

Figure 4.13. Heat flow profiles obtained during TPO-MS analysis of post-reaction Ni/La_2O_3 catalysts after ESR and ESR/CDESR

The presence of CO_2 under the CDESR conditions could prevent in some way the formation of ordered carbon deposits in this catalyst.

On the other hand, Ni(K)/Y_2O_3 showed a higher amount of carbon deposits after ESR/CDESR (0.230 mmol C/h·g_{cat}) than after ESR (0.074 mmol C/h·g_{cat}). This catalyst showed the highest surface density of basic sites which adsorbed CO_2 (Tab. 4.4). In this catalyst, a competition between CO_2 and H_2O for the adsorption sites during CDESR could exist. The low amount of carbon deposits formed during ESR over Y_2O_3-supported catalysts (Tab. 4.8)

can be related with the presence of active surface oxygen species that could help to oxidize carbon deposits [23].

TPO profiles of Y_2O_3-supported catalysts, after ESR (Fig. 4.14) showed a main peak with maximum around 400 °C and a less intensive peak at higher temperatures, indicating the main presence of poorly ordered carbon deposits in this case.

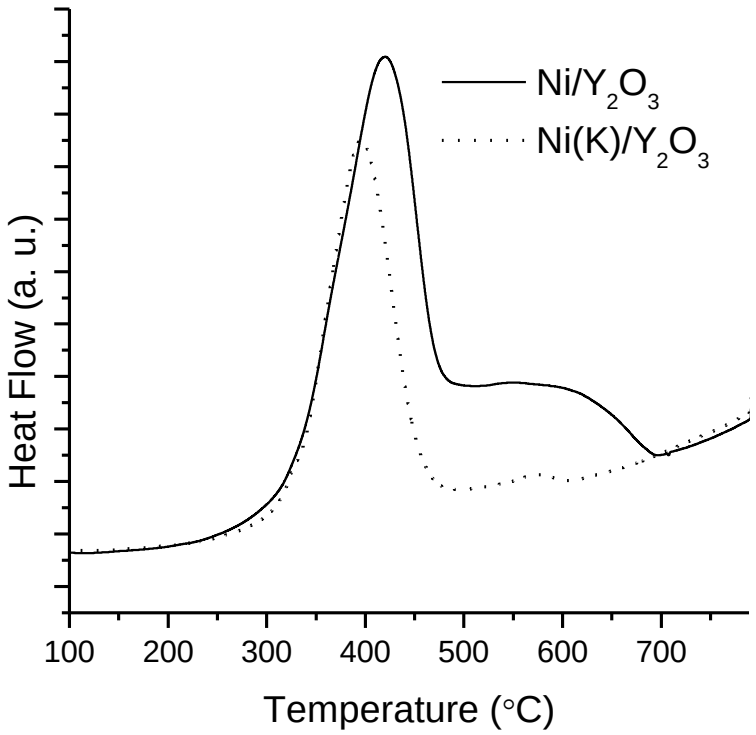

Figure 4.14. Heat flow profiles obtained during TPO-MS analysis of post-reaction Ni/Y_2O_3 and $Ni(K)/Y_2O_3$ catalysts after ESR

On the other hand, TPO profiles of Al_2O_3-, MgO- and ZrO_2-supported catalysts after ESR showed main peaks with maxima about 600-700 °C,

indicating the formation of relatively ordered carbon deposits under ESR conditions. The corresponding TPO profiles are given in the Annex (Figures A.3-A.8).

4.3. Studies of regeneration of Ni/Me_xO_y catalysts by CO_2-treatment after ESR

As stated above, CO_2-treatments were used in an attempt of regeneration of deactivated catalysts after substoichiometric ESR.

Under substoichiometric ESR conditions, the catalysts suffered deactivation which could be related to formation of carbon deposits. Removing of carbon by its gasification through reverse Boudouard reaction would help in reactivation of the catalysts, and with this aim CO_2-treatment was applied as a separate actuation. In this way, CO_2 would be valorised and would be used as a source of CO.

For the regeneration experiments, after substoichiometric ESR, the liquid flow of the reactant mixture was stopped and a flow of 7% vol/vol CO_2/(Ar+N_2) was admitted. During the treatment, CO was produced. The reverse Boudouard reaction could take place and carbon deposits could be eliminated with CO evolution:

$$CO_2 + C \rightarrow 2CO \qquad (4.10)$$

The CO_2-treatment was extended until CO was no longer detected in the reactor outlet. Afterwards, the reactor was flushed with argon and ESR was continued.

Effect of the CO_2-treatment on the ethanol conversion under ESR conditions before and after treatment is presented in Figure 4.15. As can be seen, the performed CO_2-treatment had, in all cases, a positive influence on ethanol conversion. Except for Ni(K)/Al_2O_3, the deactivation of catalysts under ESR conditions was evidenced. Then, after the CO_2-treatment an increase of the ethanol conversion was found. Ni/La_2O_3 suffered serious deactivation under ESR conditions; however, after the CO_2-treatment, this catalyst exhibited a high increase in ethanol conversion, from 27% to 70%. For Ni/ZrO_2, after the CO_2-treatment, a higher ethanol conversion than the initial one was achieved. Complete results of the ethanol conversion, along all reaction time, are presented in the Annex (Figure A.12).

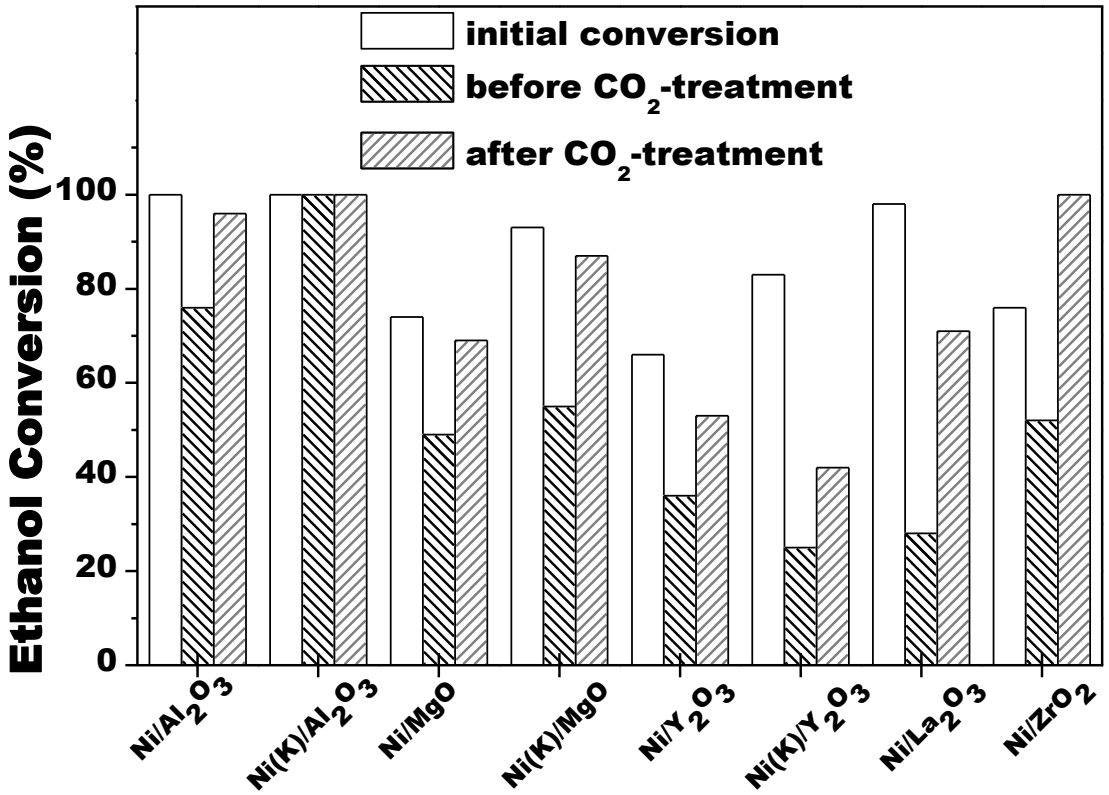

Figure 4.15. Effect of CO_2-treatment on the ethanol conversion. Reaction cycle: ESR 14 h / CO_2-treatment / ESR 4 h. T = 600 °C, GHSV = 8100 h^{-1}, ethanol/H_2O/(Ar+N_2) = 1.0/1.6/22.8, molar ratios

After the CO_2-treatment, in general, a variation in the concentration of products can be related with the change of ethanol conversion. Figure 4.16 illustrates the product distribution for Ni/La_2O_3 and Ni/ZrO_2 catalysts before and after the CO_2-treatment. The complete results for all catalysts are presented in the Annex (Figures A.9-A.11).

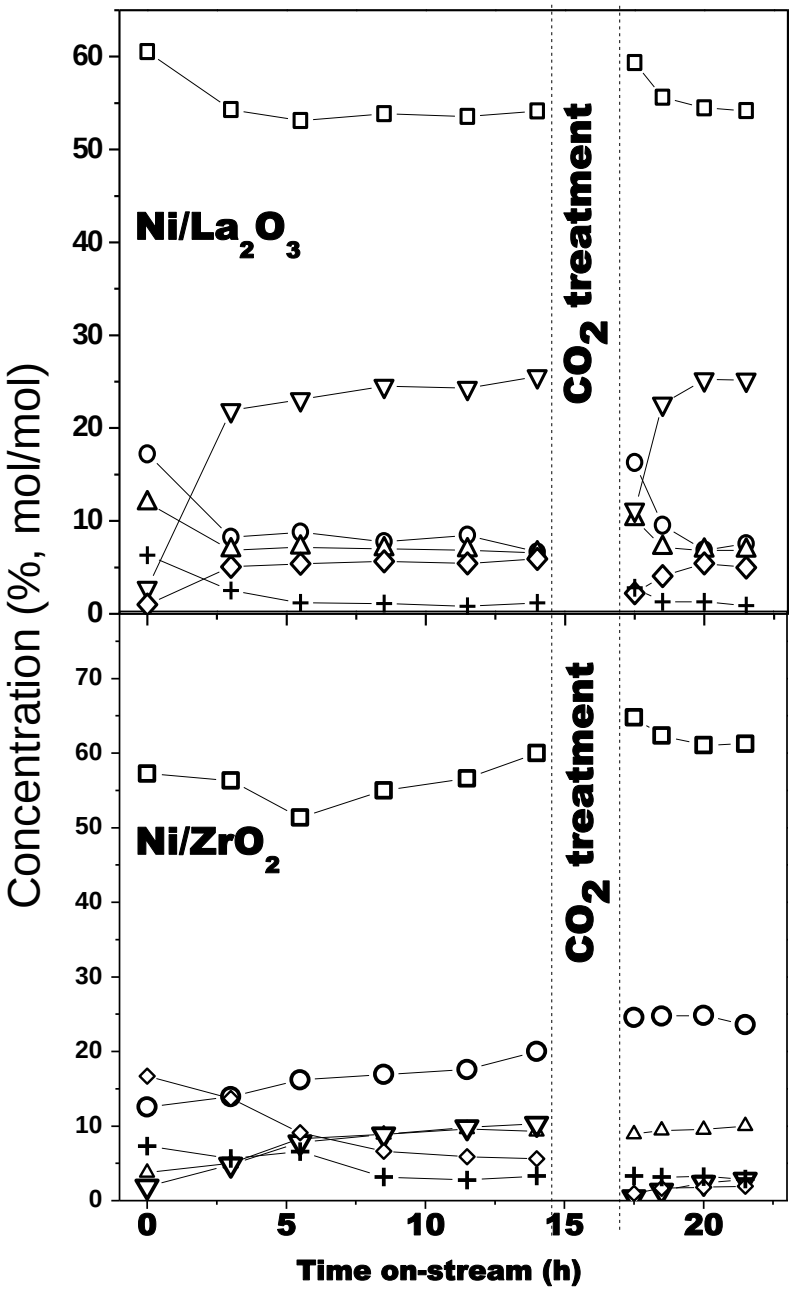

Figure 4.16. Effect of the CO_2-treatment on the product distribution obtained over Ni/La_2O_3 and Ni/ZrO_2 catalysts. Molar concentrations of (□) H_2, (○) CO, (△) CH_4, (▽) CH_3CHO, (**+**) CO_2 and (◊) C_2H_4 in the outlet gas are shown. Reaction conditions: GHSV = 8100 h^{-1}, m_{cat} = 200 mg, T = 600 °C; 1.0 EtOH/1.6 H_2O/22.8 ($Ar+N_2$), molar ratios

The catalysts, after use in ESR with regenerating CO_2-treatment, were analysed by XPS, Raman spectroscopy and TPO-MS experiments in order to evaluate the amount and characteristics of the carbon deposits.

In general, the XPS analysis showed slightly broader C1s peaks than those registered after ESR. The asymmetry of the peaks at high BE is indicative of the presence of amorphous carbon deposits with C=O bonds [16,17]. All the XPS spectra are given in the Annex (Figure A.2).

Figure 4.17 shows the carbon region of Raman spectra and Table 4.10 the corresponding I_G/I_D values. For $Ni(K)/Al_2O_3$ poorly resolved Raman spectra was obtained.

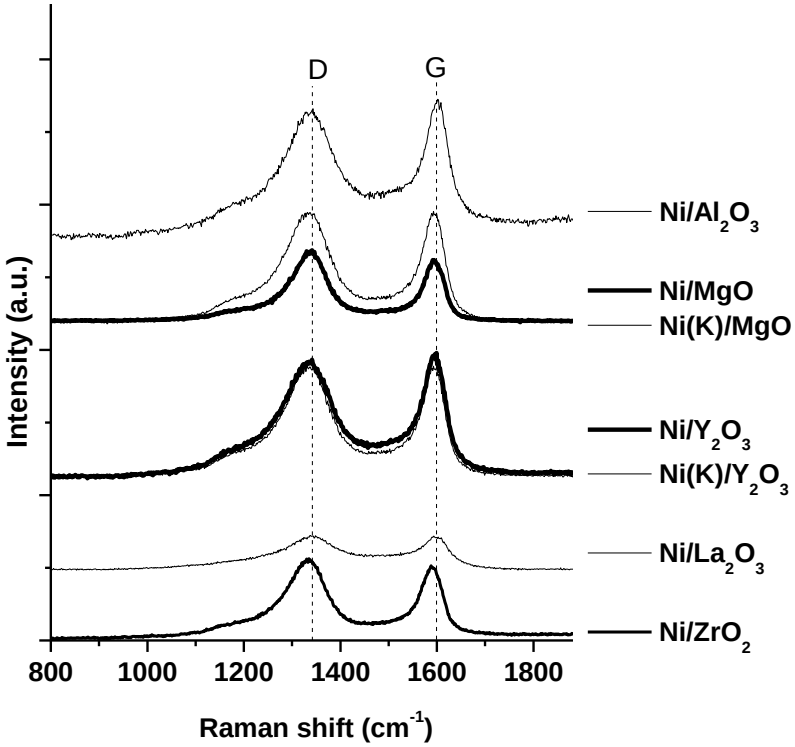

Figure 4.17. Carbon region of Raman spectra of post-reaction Ni/Me_xO_y catalysts after ESR with CO_2-treatment

Except for Ni/ZrO_2, the I_G/I_D ratio was slightly smaller after ESR with CO_2-treatment than after ESR (Tab. 4.7).

Table 4.10. I_G/I_D Raman ratio for post-reaction Ni/Me_xO_y catalysts after ESR with CO_2-treatment

Catalyst	ESR with CO_2-treatment
Ni/Al_2O_3	0.52
Ni/MgO	0.52
Ni(K)/MgO	0.49
Ni/Y_2O_3	0.52
$Ni(K)/Y_2O_3$	0.52
Ni/La_2O_3	0.54
Ni/ZrO_2	0.59

During the TPO-MS analysis, the catalysts exhibited heat flow between 300 °C and 800 °C, which is indicative of the presence of amorphous and graphitic carbons [22].

Figures 4.18 and 4.19 compare the TPO profiles of Ni/La_2O_3 and Ni/Y_2O_3 after ESR with and without the CO_2-treatment. In both cases, after ESR with CO_2-treatment a less intense combustion peak at high temperatures was found. Moreover, the low temperature TPO peak, associated to poorly ordered carbonaceous deposits, was shifted toward lower temperatures when the CO_2-treatment was applied. The CO_2-treament could help to remove the more ordered carbon deposits formed under ESR.

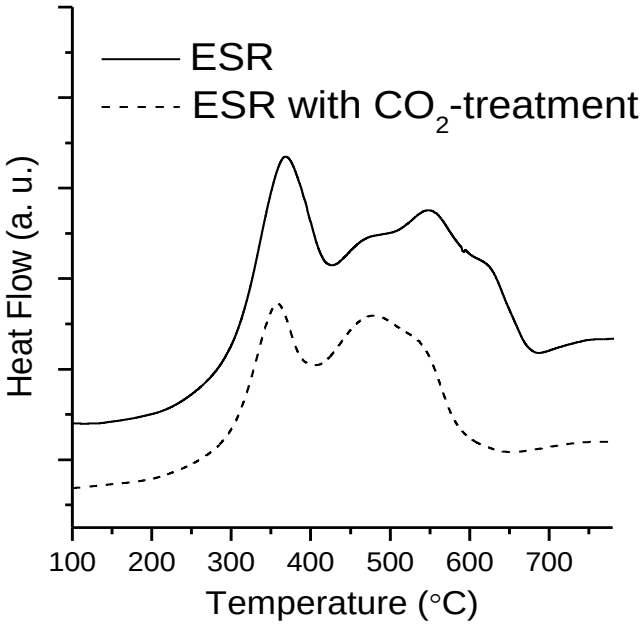

Figure 4.18. Heat flow profiles obtained during TPO-MS analysis of post-reaction Ni/La_2O_3 catalysts, after ESR and ESR with CO_2-treatment

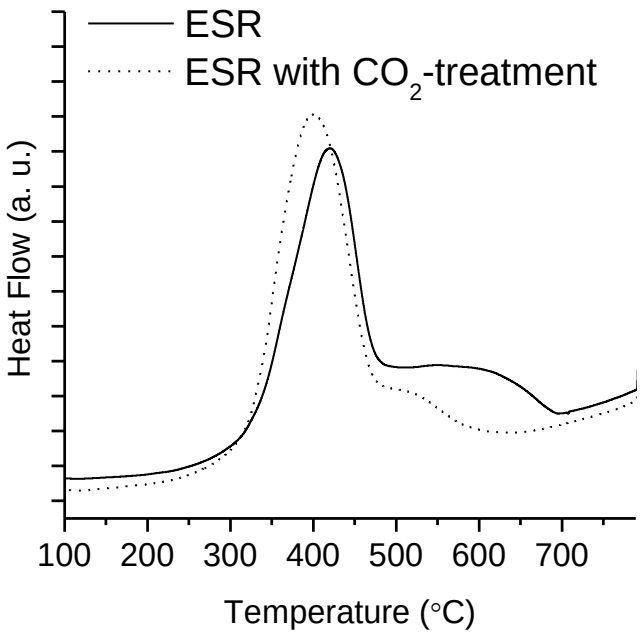

Figure 4.19. Heat flow profiles obtained during TPO-MS analysis of post-reaction Ni/Y_2O_3 catalysts, after ESR and ESR with CO_2-treatment

Table 4.11 compares the carbon deposition rates obtained from TPO-MS analysis of catalysts after ESR with CO_2-treatment with those obtained after ESR.

It can be seen that, except for Ni/Al_2O_3, the application of a CO_2-treatment produces a diminution of the total carbonaceous deposits.

The effect of CO_2-treatment on carbon deposits was more significant for Ni/Y_2O_3 and Ni/La_2O_3 catalysts. These catalysts showed high densities of CO_2 adsorption sites and high values of mean enthalpy of CO_2 adsorption (Tab. 4.4).

Table 4.11. Carbon formation rate determined from TPO-MS analysis of Ni/Me_xO_y catalysts after ESR with CO_2-treatment and after ESR

Catalyst	Carbon deposited (mmol C/h·g_{cat})	
	ESR with CO_2-treatment	ESR
Ni/Al_2O_3	0.611	0.554
Ni(K)/Al_2O_3	0.541	0.583
Ni/MgO	0.796	0.971
Ni(K)/MgO	0.911	1.078
Ni/Y_2O_3	0.030	0.078
Ni(K)/Y_2O_3	0.056	0.074
Ni/La_2O_3	0.119	0.191
Ni/ZrO_2	1.111	1.157

4.4. References

[1] Panchula ML, Akinc M. Morphology of Lanthanum Carbonate Particles Prepared by Homogeneous Precipitation. J Eur Ceram Soc 1996;16:833–41. doi:10.1016/0955-2219(95)00211-1.

[2] Bakiz B, Guinneton F, Arab M, Benlhachemi A, Villain S, Satre P, et al. Carbonatation and Decarbonatation Kinetics in the La_2O_3-$La_2O_2CO_3$ System under CO_2 Gas Flows. Adv Mater Sci Eng 2010;2010:1–6. doi:10.1155/2010/360597.

[3] Debye P, Scherrer P. Interferences in irregularly oriented particles in Reontgen light. Phys Zeitschrift 1916;17:227–83.

[4] Biesinger MC, Payne BP, Lau LWM, Gerson A, Smart RSC. X-ray photoelectron spectroscopic chemical state Quantification of mixed nickel metal, oxide and hydroxide systems. Surf Interface Anal 2009;41:324–32. doi:10.1002/sia.3026.

[5] Chary KVR, Ramana Rao PV, Venkat Rao V. Catalytic functionalities of nickel supported on different polymorphs of alumina. Catal Commun 2008;9:886–93. doi:10.1016/j.catcom.2007.09.016.

[6] Yermán L, Homs N, Ramírez de la Piscina P. Hydrogen production from oxidative steam-reforming of n-propanol over Ni/Y_2O_3–ZrO_2 catalysts. Int J Hydrogen Energy 2012;37:7094–100. doi:10.1016/j.ijhydene.2011.11.045.

[7] Liu H, He D. Properties of Ni/Y_2O_3 and its catalytic performance in methane conversion to syngas. Int J Hydrogen Energy 2011;36:14447–54. doi:10.1016/j.ijhydene.2011.08.025.

[8] Sun GB, Hidajat K, Wu XS, Kawi S. A crucial role of surface oxygen mobility on nanocrystalline Y_2O_3 support for oxidative steam reforming of ethanol to hydrogen over Ni/Y_2O_3 catalysts. Appl Catal B Environ 2008;81:303–12. doi:10.1016/j.apcatb.2007.12.021.

[9] Chen H, Yu H, Peng F, Wang H, Yang J, Pan M. Efficient and stable

oxidative steam reforming of ethanol for hydrogen production: Effect of in situ dispersion of Ir over Ir/La_2O_3. J Catal 2010;269:281–90. doi:10.1016/j.jcat.2009.11.010.

[10] Liu JY, Lee CC, Wang CH, Yeh CT, Wang CB. Application of nickel-lanthanum composite oxide on the steam reforming of ethanol to produce hydrogen. Int J Hydrogen Energy 2010;35:4069–75. doi:10.1016/j.ijhydene.2010.01.141.

[11] Liu SW, Liu JY, Liu YH, Huang YH, Yeh CT, Wang C Bin. Ultrasonic-assisted fabrication of $LaNiO_x$ composite oxide nanotubes and application to the steam reforming of ethanol. Catal Today 2011;164:246–50. doi:10.1016/j.cattod.2010.10.017.

[12] Lin KH, Wang C Bin, Chien SH. Catalytic performance of steam reforming of ethanol at low temperature over $LaNiO_3$ perovskite. Int J Hydrogen Energy 2013;38:3226–32. doi:10.1016/j.ijhydene.2013.01.005.

[13] Zhu J, Peng X, Yao L, Tong D, Hu C. CO_2 reforming of methane over Mg-promoted Ni/SiO_2 catalysts: the influence of Mg precursors and impregnation sequences. Catal Sci Technol 2012;2:529. doi:10.1039/c1cy00333j.

[14] Roh HS, Jun KW, Dong WS, Chang JS, Park SE, Joe Y Il. Highly active and stable Ni/Ce-ZrO_2 catalyst for H_2 production from methane. J Mol Catal A Chem 2002;181:137–42. doi:10.1016/S1381-1169(01)00358-2.

[15] Arena F, Parmaliana A, Mondello N, Frusteri F, Giordano N. Influence of the Calcination Treatment on the Surface Chemical Properties of Ni/MgO Catalyst: A CO_2 Temperature Programmed Desorption Approach. Langmuir 1991;7:1555–7.

[16] Liu BS, Jiang L, Sun H, Au CT. XPS, XAES, and TG/DTA characterization of deposited carbon in methane dehydroaromatization over Ga-Mo/ZSM-5 catalyst. Appl Surf Sci 2007;253:5092–100. doi:10.1016/j.apsusc.2006.11.031.

[17] Albers P, Seibold K, Prescher G, Müller H. XPS and SIMS studies of carbon deposits on Pt/Al_2O_3 and Pd/SiO_2 catalysts applied in the synthesis of hydrogen cyanide and selective hydrogenation of acetylene. Appl Catal A Gen 1999;176:135–46. doi:10.1016/S0926-860X(98)00325-1.

[18] da Silva AM, de Souza KR, Jacobs G, Graham UM, Davis BH, Mattos L V., et al. Steam and CO_2 reforming of ethanol over Rh/CeO_2 catalyst. Appl Catal B Environ 2011;102:94–109. doi:10.1016/j.apcatb.2010.11.030.

[19] Ferrari A, Robertson J. Interpretation of Raman spectra of disordered and amorphous carbon. Phys Rev B 2000;61:14095–107. doi:10.1103/PhysRevB.61.14095.

[20] Lespade Piere; Marchand A. Caracterisation de materiaux carbones par microspectrometrie Raman. Carbon N Y 1984;4-5:375–85. doi:10.1016/0008-6223(84)90009-5.

[21] Cai W, Homs N, Ramirez de la Piscina P. Renewable hydrogen production from oxidative steam reforming of bio-butanol over $CoIr/CeZrO_2$ catalysts: Relationship between catalytic behaviour and catalyst structure. Appl Catal B Environ 2014;150-151:47–56. doi:10.1016/j.apcatb.2013.11.032.

[22] Padilla R, Benito M, Rodríguez L, Serrano A, Muñoz G, Daza L. Nickel and cobalt as active phase on supported zirconia catalysts for bio-ethanol reforming: Influence of the reaction mechanism on catalysts performance. Int J Hydrogen Energy 2010;35:8921–8. doi:10.1016/j.ijhydene.2010.06.021.

[23] Edwards ER, Antunes EF, Botelho EC, Baldan MR, Corat EJ. Evaluation of residual iron in carbon nanotubes purified by acid treatments. Appl Surf Sci 2011;258:641–8. doi:10.1016/j.apsusc.2011.07.032.

[24] Bednarczuk L, Ramírez de la Piscina P, Homs N. H_2-production from CO_2-assisted ethanol steam reforming: The regeneration of Ni-based catalysts. Int J Hydrogen Energy 2015;40:5256–63.

doi:10.1016/j.ijhydene.2015.01.061.

5. Study of Ni/ZrY, Ni/ZrLa and Ni/ZrYLa catalysts under substoichiometric ethanol steam reforming (ESR); Regeneration of catalysts by CO_2-treatment

This chapter contains the preparation of nickel catalysts supported on binary (Ni/ZrY and Ni/ZrLa) and ternary (Ni/ZrYLa) systems, and their characterization by means of chemical analysis (ICP-AES), physisorption of N_2, XRD, XPS, H_2-TPR, CO_2-TPD and CO_2 adsorption calorimetry. Thereafter, the catalytic behaviour under substoichiometric ethanol steam reforming (ESR) reaction is presented, with special emphasis on regeneration of the catalysts by CO_2-treatment. The last part shows the results of the XRD characterization of post-reaction catalysts, and the characteristics of carbon deposits determined from TPO-MS, Raman and DRIFT spectroscopy.

5.1. Preparation and characterization of Ni/ZrY, Ni/ZrLa and Ni/ZrYLa catalysts

The Ni/ZrY, Ni/ZrLa and Ni/ZrYLa catalysts were prepared in a similar way to that previously presented for Ni/Me_xO_y catalysts. Nickel was incorporated to the carbon-free supports by incipient wetness impregnation using aqueous solutions of nickel (II) nitrate (Panreac 99%), to obtain catalysts with a Ni content of approximately 9 wt%. After the impregnation, the samples were dried overnight at 100 °C and then calcined in air at 450 °C (heating rate: 2.5 °C/min) for 5 h. Calcined catalysts were reduced *in-situ*, at 600 °C, in the reactor before each catalytic test.

The catalysts supported on binary and ternary systems were labelled as: Ni/35Zr14La, Ni/36Zr14Y, Ni/8Zr45Y, Ni/8Zr50La, Ni/12Zr29Y13La and

Ni/12Zr12Y31La, where the number before the element indicates its content (weight percentage) determined by chemical analysis.

Table 5.1 shows the nickel content of the catalysts and compares the values of surface area and pore volume of the catalysts with those of the supports.

Table 5.1. Results of chemical analysis, specific area and pore volume of Ni/ZrY, Ni/ZrLa and Ni/ZrYLa

Catalyst	Ni content (wt%)	BET area support (m^2/g)	BET area catalyst (m^2/g)	Pore volume support (cm^3/g)	Pore volume catalyst (cm^3/g)
Ni/35Zr14La	8.5	49	117	0.142	0.236
Ni/36Zr14Y	8.5	203	152	0.336	0.260
Ni/8Zr45Y	8.8	76	26	0.390	0.061
Ni/8Zr50La	9.3	50	21	0.148	0.065
Ni/12Zr29Y13La	8.6	131	53	0.675	0.089
Ni/12Zr12Y31La	8.7	94	42	0.277	0.098

Except Ni/35Zr14La, catalysts showed lower values of surface area than the corresponding supports. All catalysts showed values of surface area higher than those of Ni/La_2O_3 (10 m^2/g) and Ni/Y_2O_3 (16 m^2/g), and catalysts with higher zirconium content showed higher values of surface area, independently of the components of the support. This relationship is illustrated in Figure 5.1. The small ZrO_2 particles contributed to the surface area and additionally could prevent the crystallization and sintering of yttrium oxide and lanthanum species in the catalysts.

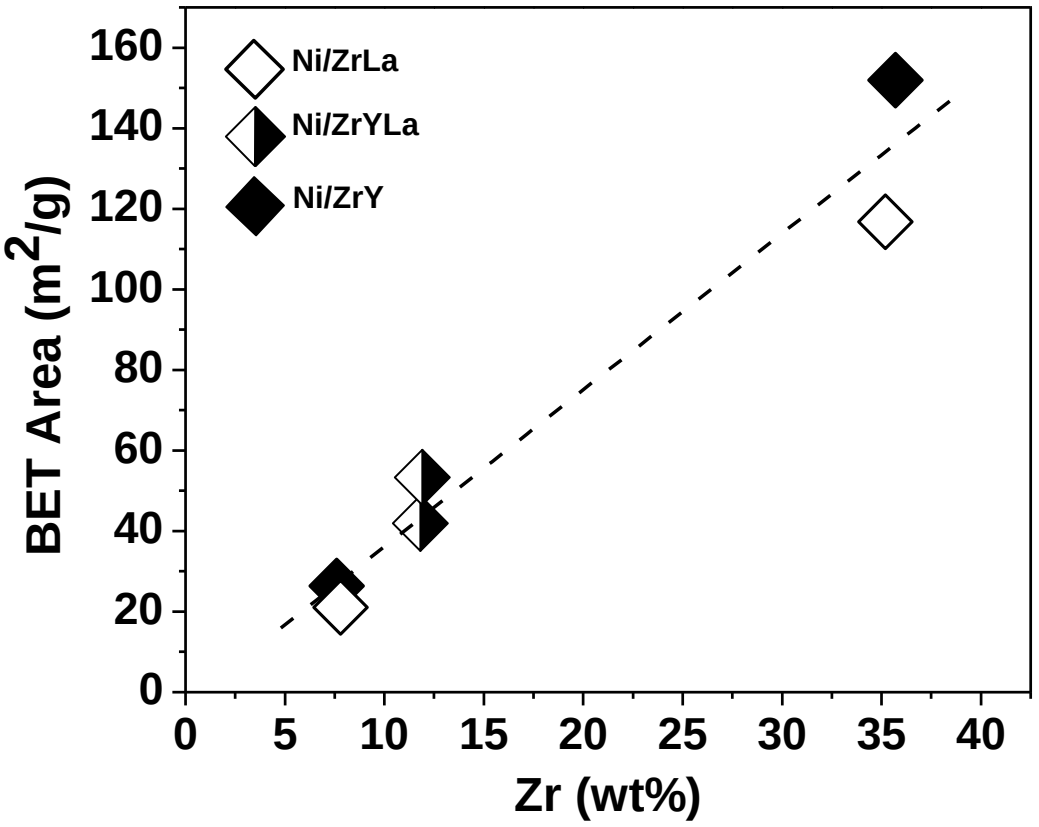

Figure 5.1. Relationship between Zr content in catalysts and their BET surface area

Analysis of the results of the pore volume of the catalysts (Tab. 5.1) shows that this depends on the content of zirconium, as above mentioned for BET area. The highest value was found for Ni/36Zr14Y with the highest weight percentage of Zr; while Ni/8Zr45Y and Ni/8Zr50La, with the lowest zirconium content, had the lowest pore volume.

The pore size distribution of the catalysts is shown in Figure 5.2. All catalysts were mesoporous. The pore size distribution suggests a strong influence of Zr content on the textural properties of the catalysts.

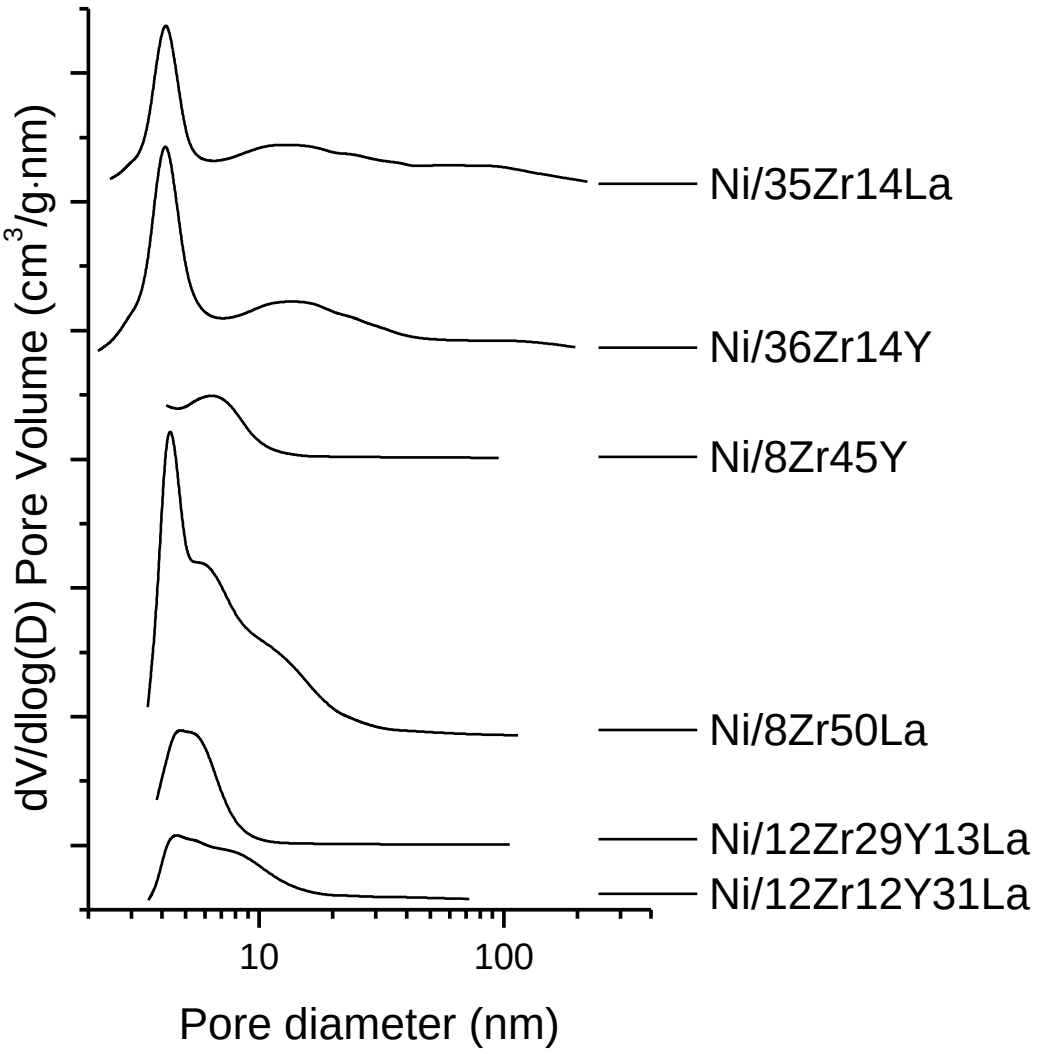

Figure 5.2. Pore diameter distribution of Ni/ZrY, Ni/ZrLa and Ni/ZrYLa catalysts

The X-ray diffraction patterns of calcined catalysts are shown in Figures 5.3a and 5.3b. Figure 5.3a shows the 2θ = 27-33° and 2θ = 42-45° zones corresponding to the most intense peaks of the supports and NiO, respectively. The catalysts with high zirconium content (Ni/35Zr14La and Ni/36Zr14Y) were more crystalline than the remaining catalysts. XRD patterns of Ni/35Zr14La and Ni/36Zr14Y showed peaks characteristics of crystalline ZrO_2 (tetragonal or cubic). However, the most intense peak corresponding to the (111) diffraction line for ZrO_2 appeared at lower θ values (30.209° for Ni/36Zr14Y and 29.975° for Ni/35Zr14La) when compared with Ni/ZrO_2 catalysts (2θ = 30.436°) [1]. This suggests the formation of ZrO_2-Y_2O_3 and ZrO_2-La_2O_3 solid solutions, according to published results [2].

For Ni/35Zr14La and Ni/36Zr14Y clear peaks of cubic NiO phase (JCPDS 01-073-1523) were found; using the (200) diffraction peaks centred at approximately 2θ = 43.2° and the Debye-Scherrer equation [3] crystallite sizes of 27 nm (Ni/35Zr14La) and 57 nm (Ni/36Zr14Y) were calculated for NiO.

From XRD patterns of Ni/8Zr45Y and Ni/12Zr29Y13La, the presence of cubic Y_2O_3 (JCPDS 03-065-3178) and crystalline ZrO_2 (tetragonal and cubic) can be deduced. For these catalysts, a low intensity peak at about 2θ = 43.5° was found; this peak corresponds well with the most intense of NiO. However, the contribution to this peak of others coming from the support cannot be discarded. For Ni/8Zr50La and Ni/12Zr12Y31La, besides the presence of

tetragonal ZrO_2, that of La_2O_3 and/or $La_2O_2CO_3$ with a poor crystalinity cannot be ruled out. For these catalysts, the high dispersion of NiO into $La_2O_2CO_3$ and/or La_2O_3 could be the responsible of the absence of characteristics NiO peaks. The XRD patterns for the Ni/8Zr50La and Ni/12Zr12Y31La catalysts, largely differed from those of the corresponding supports which indicated the presence of crystalline $La_2O_2CO_3$ (Fig. 5.4).

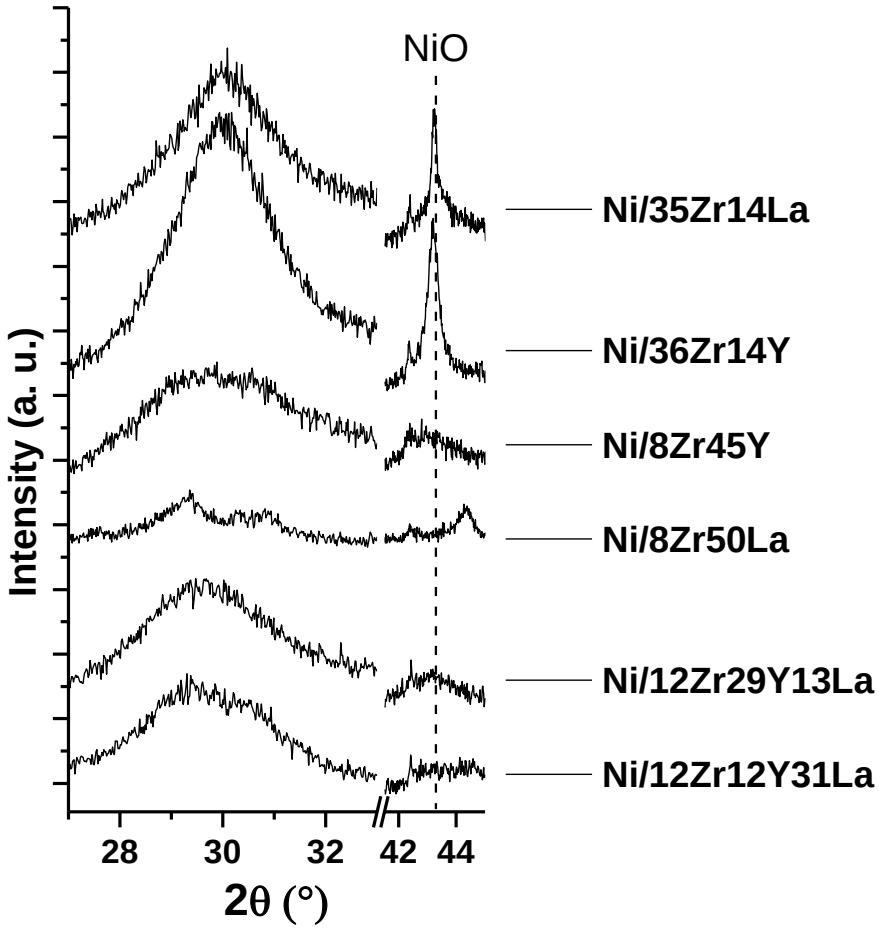

Figure 5.3a. XRD patterns of calcined Ni/ZrY, Ni/ZrLa and Ni/ZrYLa catalysts in the zones corresponding to the most intensive peaks of the supports (2θ = 27-33°) and NiO (2θ = 42-45°)

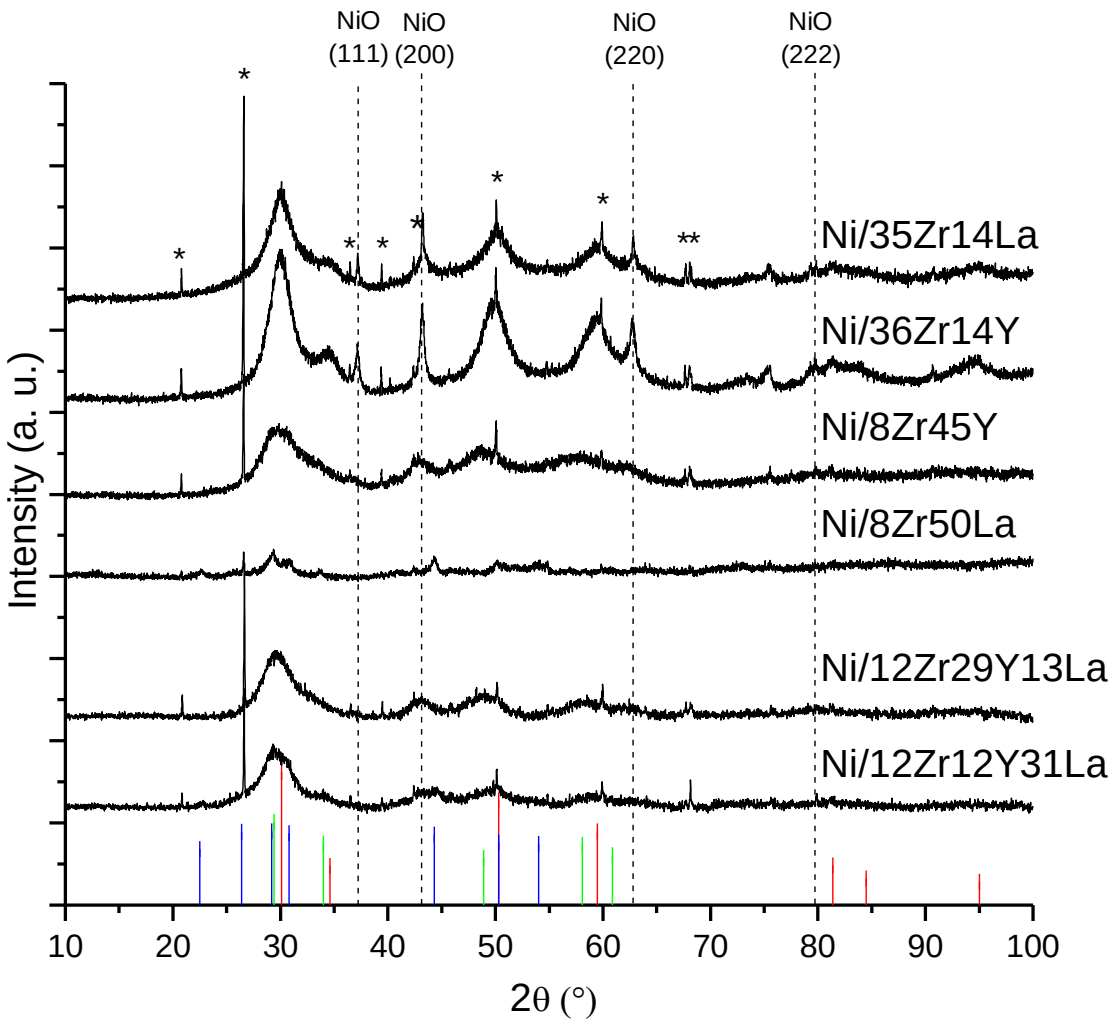

Figure 5.3b. XRD patterns of calcined Ni/ZrY, Ni/ZrLa and Ni/ZrYLa catalysts. Dashed vertical lines indicate the position of NiO cubic phase (JCPDS 01-073-1523). In the bottom part, XRD patterns of recognized phases: |-ZrO_2 tetragonal (JCPDS 00-024-1164), |-Y_2O_3 cubic (JCPDS 00-043-0661), |-$La_2O_2CO_3$ monoclinic (JCPDS 00-048-1113). Asterisks indicate quartz wool SiO_2 peaks

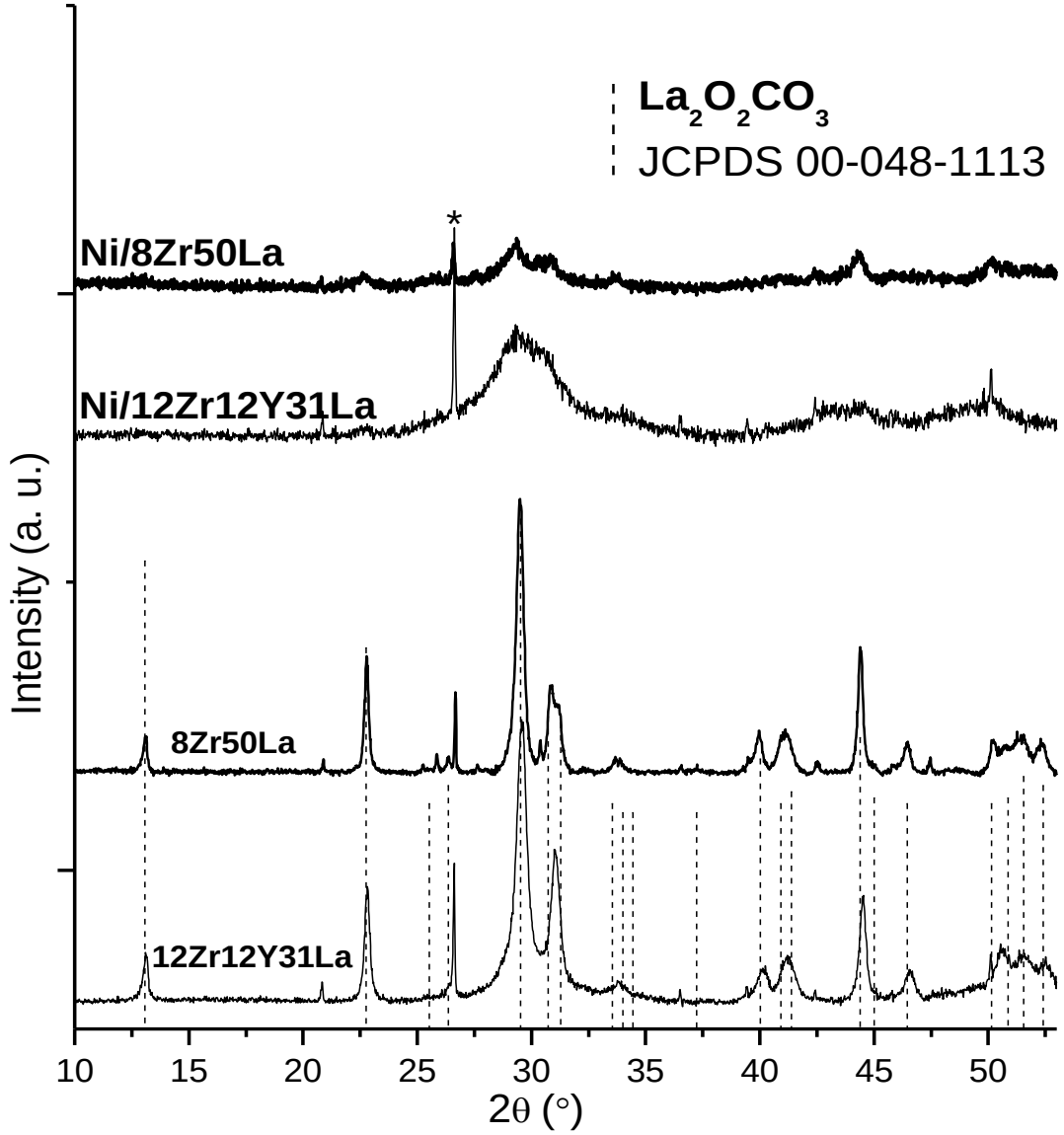

Figure 5.4. XRD patterns of calcined Ni/8Zr50La and Ni/12Zr12Y31La catalysts and corresponding supports, compared with XRD pattern of monoclinic $La_2O_2CO_3$ (JCPDS 00-048-1113). The asterisk indicates quartz wool SiO_2 peak

XPS was used to analyse core levels of the main elements (Ni 2p, Zr 3d and Y 3d) on the reduced catalysts. Due to the overlapping of the Ni $2p_{3/2}$ band with the band corresponding to La $3d_{3/2}$, Ni 2p levels were analysed only for Ni/ZrY catalysts. For Ni/ZrY catalysts, the Ni $2p_{3/2}$ core level peaks were located at approximately 855 eV. This position, and the observation of a satellite peak around 862 eV, indicates the presence of Ni^{2+} surface species [4].

XPS analysis of C1s level of Ni/35Zr14La and Ni/8Zr50La catalysts shows a prominent shoulder at 288-290 eV (Fig. 5.5). This shoulder could be ascribed to the presence of surface carbonate species such as $La_2O_2CO_3$ [5,6].

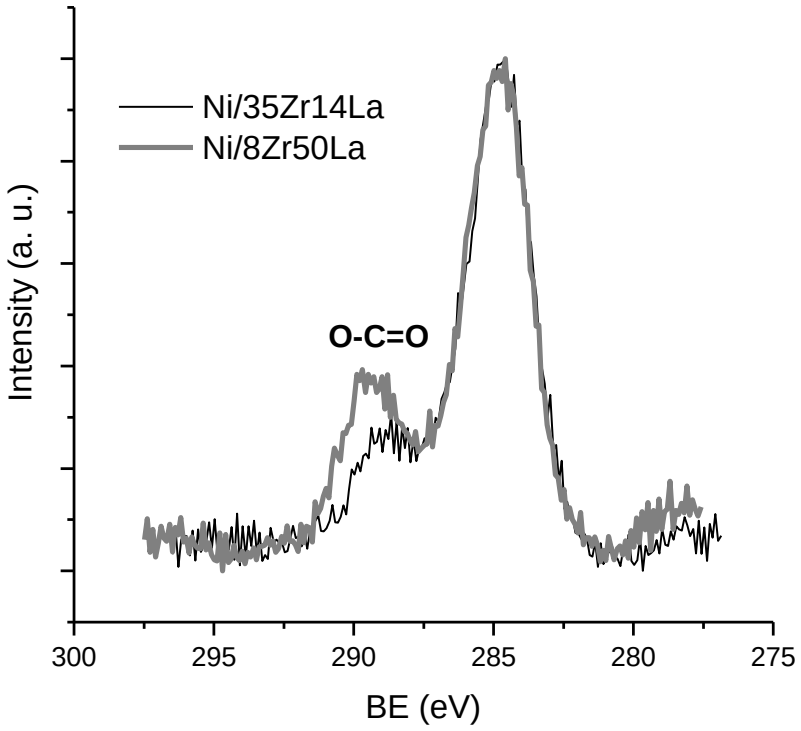

Figure 5.5. C 1s XPS region of reduced Ni/35Zr14La and Ni/8Zr50La catalysts

Table 5.2 compares surface Ni/(Zr+Y) atomic ratios determined for reduced Ni/ZrY catalysts and Ni/(Zr+Y) atomic ratio determined by chemical analysis of calcined Ni/ZrY samples. For both, Ni/36Zr14Y and Ni/8Zr45Y catalysts, a segregation of nickel on the surface occurs, higher for Ni/8Zr45Y.

Table 5.2. Ni/(Zr+Y) atomic ratio determined by XPS and ICP-AES of Ni/ZrY catalysts

Catalyst	Ni/(Zr+Y) atomic ratio	
	XPS	Chemical analysis (ICP-AES)
Ni/36Zr14Y	0.327	0.267
Ni/8Zr45Y	0.579	0.251

Figure 5.6 presents the H_2-TPR profiles of the catalysts. The most important part of the hydrogen consumption took place between 300 and 500 ^oC. Peaks in the range 370-425 ^oC are usually assigned to the reduction of NiO which does not interact with the support; an increase of the strength in the interaction between Ni^{2+} species and support produces an increase in the reduction temperature [7–9].

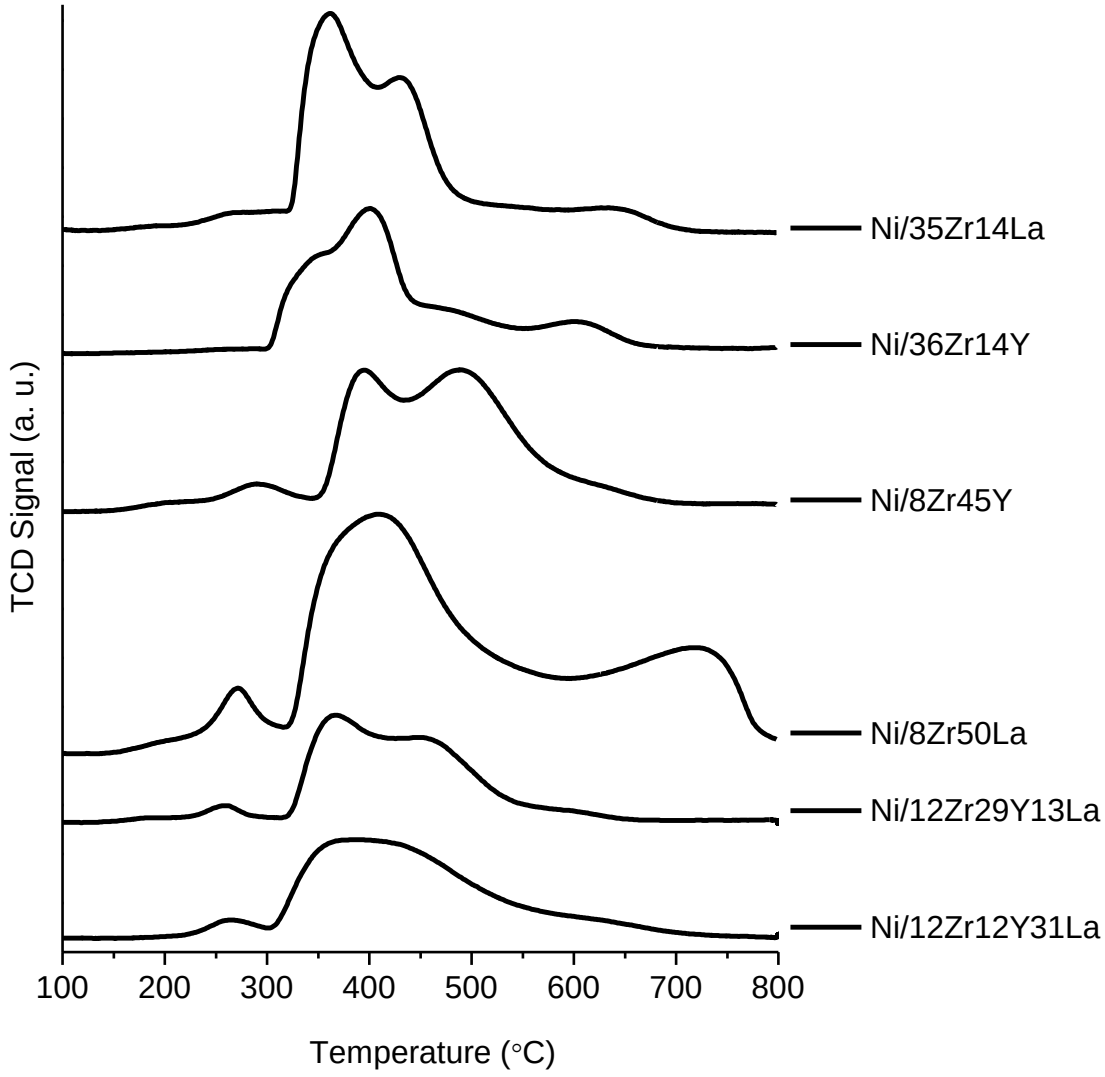

Figure 5.6. H_2-TPR profiles of Ni/ZrY, Ni/ZrLa and Ni/ZrYLa catalysts

Moreover, high concentration of oxygen vacancies on the surface may result in a decrease of the reduction temperature of Ni^{2+}. Small peaks of hydrogen consumption, at around 270 ^{o}C, found in the H_2-TPR profiles of Ni/8Zr45Y, Ni/8Zr50La, Ni/12Zr29Y13La and Ni/12Zr12Y31La can be related

with the reduction of well dispersed NiO promoted by oxygen vacancies of the support [10].

As stated above, an increase in the interaction between nickel species and the support can produce an increase in the temperature of reduction of Ni^{2+} [7]. Hydrogen consumption above 500 ^{o}C suggests this phenomenon. Moreover, for the Ni/8Zr50La, the peak centred at about 730 ^{o}C is probably related with the reduction and/or decomposition of $La_2O_2CO_3$, as it has been explained in the previous chapter (p. 65) [11].

Table 5.3 presents the apparent consumption of hydrogen and the consumption related to the nickel content. For all catalysts, an excess of H_2 consumption with respect to that necessary for the reduction of Ni^{2+} to Ni^0 (1 mol H_2/1 mol Ni) was found. This excess was especially high for catalysts supported on ternary systems. In general, the excess of consumption of H_2 can be related with the Y_2O_3 reduction, which is favoured by the presence of surface oxygen vacancies, and with the presence of $La_2O_2CO_3$ [1,2,12,13].

Table 5.3. Apparent consumption of hydrogen obtained from H_2-TPR analyses of Ni/ZrY, Ni/ZrLa and Ni/ZrYLa catalysts

Catalyst	mmol H_2/g	mol H_2/mol Ni
Ni/35Zr14La	2.99	2.06
Ni/36Zr14Y	1.67	1.15
Ni/8Zr45Y	2.79	1.87
Ni/8Zr50La	2.89	1.83
Ni/12Zr29Y13La	4.65	3.19
Ni/12Zr12Y31La	5.38	3.63

A study of the distribution of basic sites was done by means of CO_2-TPD technique. Figure 5.7 presents the CO_2-TPD profiles of Ni/ZrY, Ni/ZrLa and Ni/ZrYLa catalysts. The results show that the distribution of the basic sites depends on the composition of the support; the temperature of CO_2 desorption reflects the strength of basic sites, while the areas under desorption peaks can be related to the amount of basic sites on the surface of catalysts [14]. For Ni/35Zr14La and Ni/36Zr14Y, desorption of CO_2 took place at temperature below 400 °C, indicating majority presence of low-strength basic sites. These results are similar to that of Ni/ZrO_2, presented in Chapter 4 (p.67). This suggests that basic properties of these catalysts were strongly determined by the presence of ZrO_2.

CO_2-TPD profiles of Ni/8Zr45Y and Ni/8Zr50La indicate the presence of medium- and high-strength basic sites, as deduced from the observed desorption of CO_2 at temperatures up to 800 °C [15]. For these catalysts, the highest value of surface density of basic sites was determined (Table 5.4). This accords with the lower surface density of basic sites found for Ni/ZrO_2 when compared with Ni/Y_2O_3 and Ni/La_2O_3 catalysts (Chapter 4).

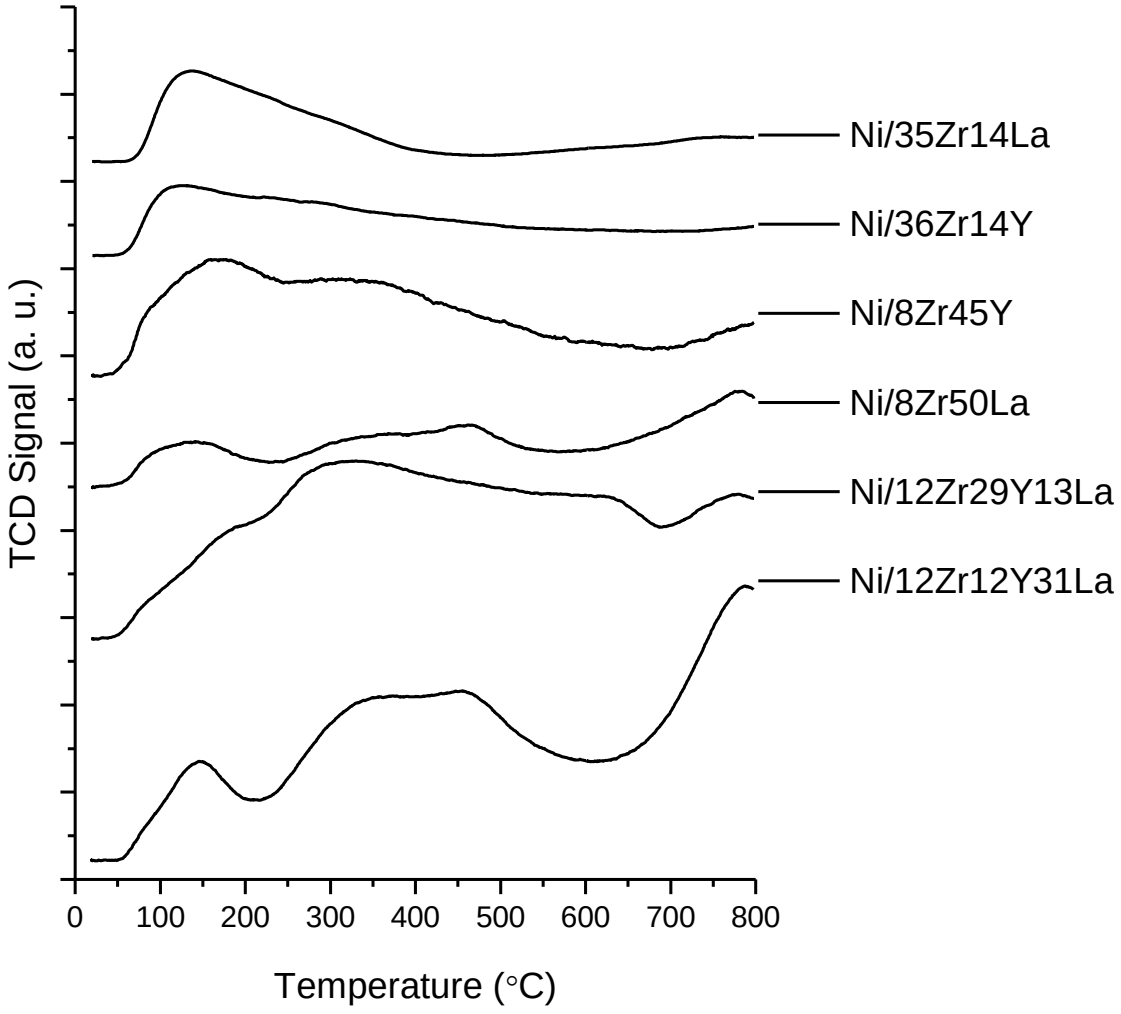

Figure 5.7. CO_2-TPD profiles of Ni/ZrY, Ni/ZrLa and Ni/ZrYLa catalysts

The desorption peaks at high temperatures found for Ni/12Zr29Y13La and Ni/12Zr12Y31La catalysts are indicative of the presence of CO_2 bonded to strong basic centres. For Ni/12Zr29Y13La, the highest mean enthalpy of CO_2 adsorption was determined: -100.3 J/mmol CO_2.

Table 5.4. Total and mean CO_2 adsorption enthalpies and surface density of basic sites determinate by experiments of CO_2 adsorption calorimetry

Catalyst	ΔH_{ads} (J/g)	ΔH_{ads} (J/mmol)	Surface density of basic sites (μmol/m^2)
Ni/35Zr14La	-33.18	-74.1	3.84
Ni/36Zr14Y	-25.52	-63.0	2.67
Ni/8Zr45Y	-26.14	-82.2	12.05
Ni/8Zr50La	-14.23	-70.4	10.32
Ni/12Zr29Y13La	-37.14	-100.3	7.00
Ni/12Zr12Y31La	-22.49	-75.6	7.10

5.2. Catalytic behaviour under substoichiometric ethanol steam reforming (ESR); the effect of CO_2-treatment regeneration

Ni/ZrY, Ni/ZrLa and Ni/ZrYLa catalysts were tested under ESR conditions, at the same temperature (600 °C), GHSV (8100 h^{-1}) and using the same reaction mixture (1.0 EtOH/1.6 H_2O/22.8 ($Ar+N_2$), molar ratios), as previously described for Ni/Me_xO_y catalysts.

Figures 5.8a-c present results of the catalytic behaviour of the catalysts under ESR, during the first part (3.5 h) of the 10.5 h experiment. Under these conditions, Ni/35Zr14La, Ni/8Zr50La, and Ni/12Zr12Y31La catalysts achieved high ethanol conversion; meanwhile Ni/12Zr29Y13La, Ni/36Zr14Y and Ni/8Zr45Y suffered a clear deactivation.

For all the catalysts, H_2 was the main product (40-70% mol/mol). CO, CH_4, C_2H_4, CO_2, and acetaldehyde were also obtained. In all cases, product distribution was sensitive to the ethanol conversion; an increase of acetaldehyde concentration related with decrease of ethanol conversion was found.

A comparative analysis of the reaction product distribution shows that for Ni/36Zr14Y and Ni/8Zr45Y a higher concentration of ethene was found (Fig. 5.8a and 5.8b). Moreover, these catalysts produced a lower concentration of H_2 and CO than those obtained for the other catalysts. The presence of ethene indicates that dehydration of ethanol may occur [16]

$$C_2H_5OH \rightarrow C_2H_4 + H_2O \qquad (5.1)$$

Ethene can polymerize on the surface of these catalysts and block the access to the active sites producing deactivation; this may explain the faster deactivation of Ni/36Zr14Y and Ni/8Zr45Y catalysts.

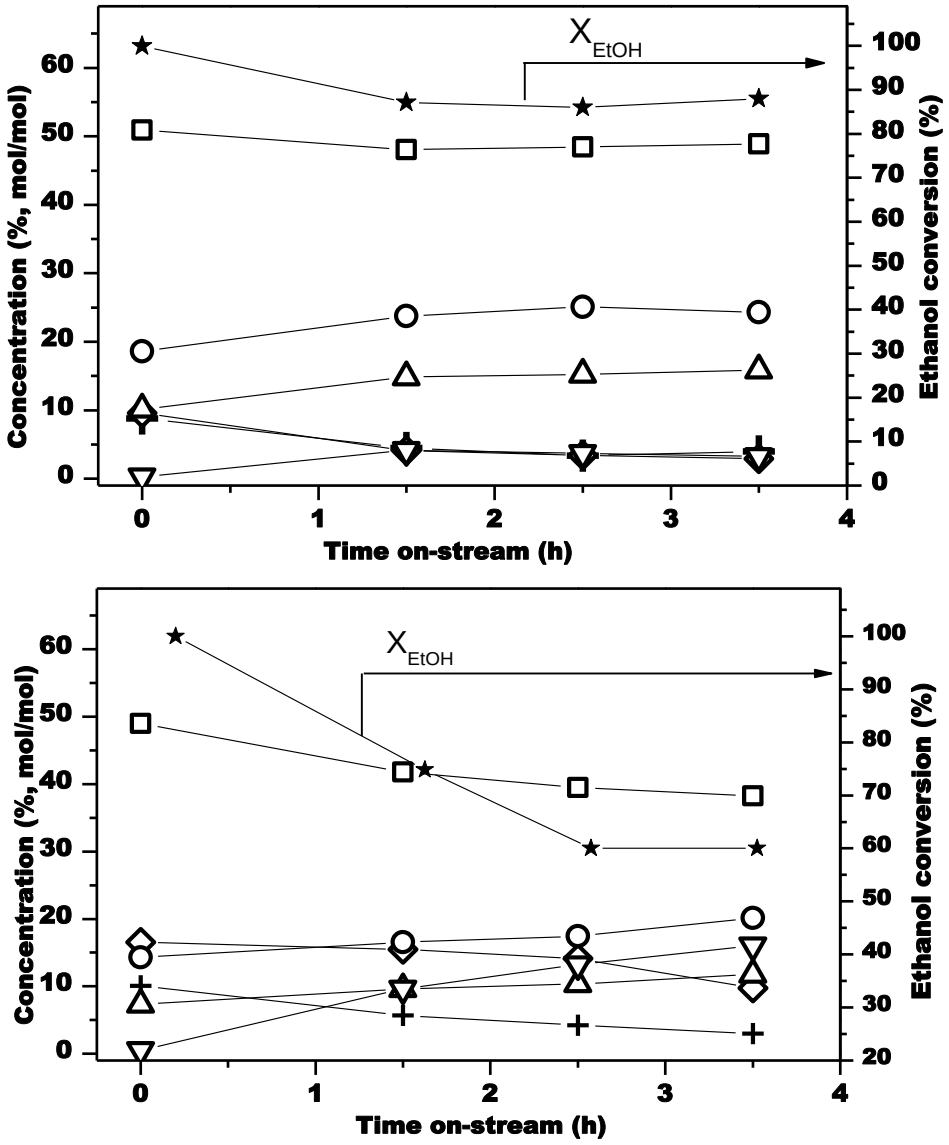

Figure 5.8a. Catalytic behaviour under ESR over Ni/35Zr14La (top) and Ni/36Zr14Y (bottom) catalysts. Molar concentrations of (□)H_2, (○)CO, (+)CO_2, (△)CH_4, (▽)CH_3CHO and (◊)C_2H_4 in the outlet gas are shown. Reaction conditions: GHSV = 8100 h^{-1}, m_{cat} = 200 mg, T = 600 °C; 1.0 EtOH/1.6 H_2O/22.8 (Ar+N_2), molar ratios

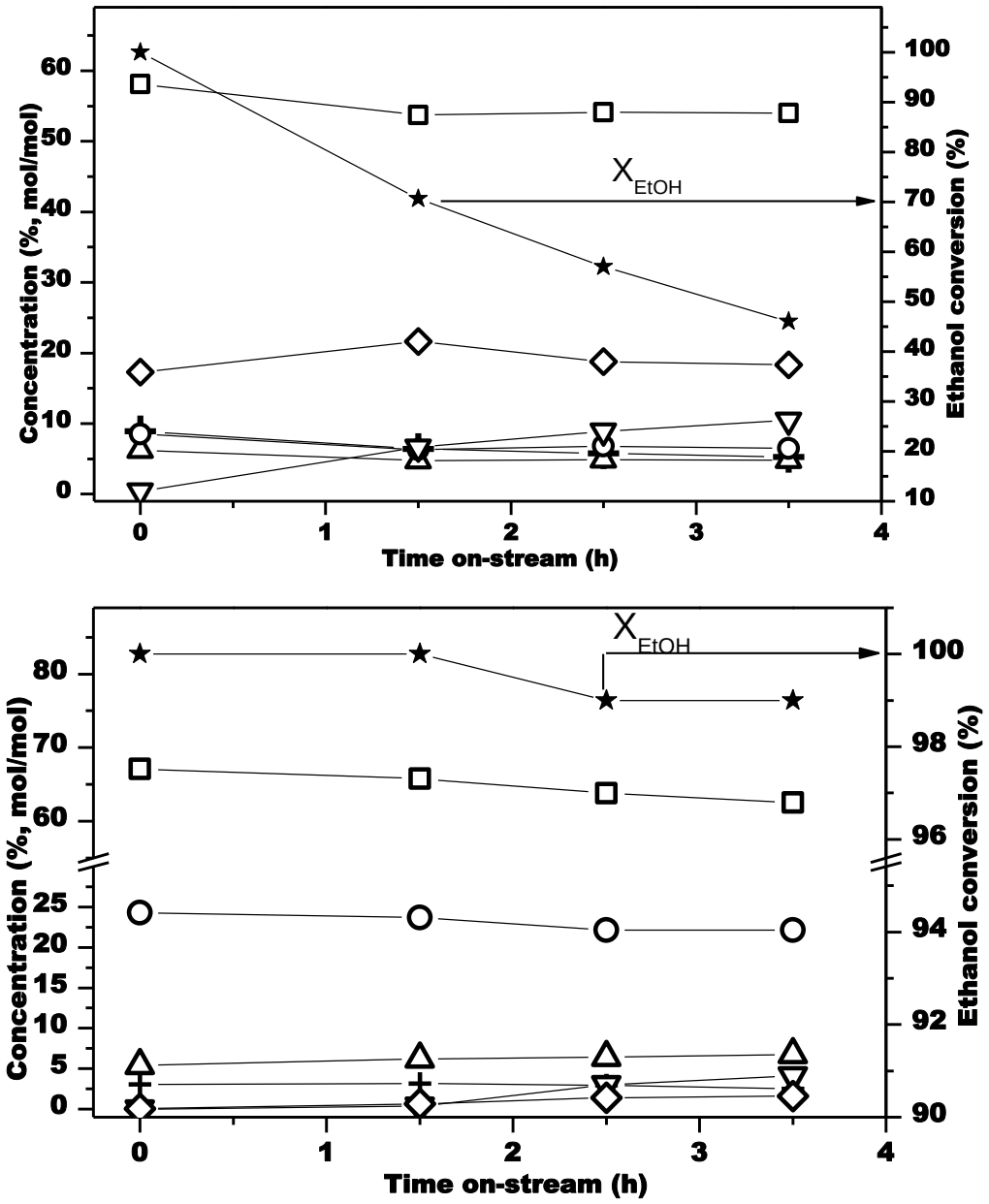

Figure 5.8b. Catalytic behaviour under ESR over Ni/8Zr45Y (top) and Ni/8Zr50La (bottom) catalysts. Molar concentrations of (□)H_2, (○)CO, (+)CO_2, (△)CH_4, (▽)CH_3CHO and (◊)C_2H_4 in the outlet gas are shown. Reaction conditions: GHSV = 8100 h^{-1}, m_{cat} = 200 mg, T = 600 °C; 1.0 EtOH/1.6 H_2O/22.8 (Ar+N_2), molar ratios

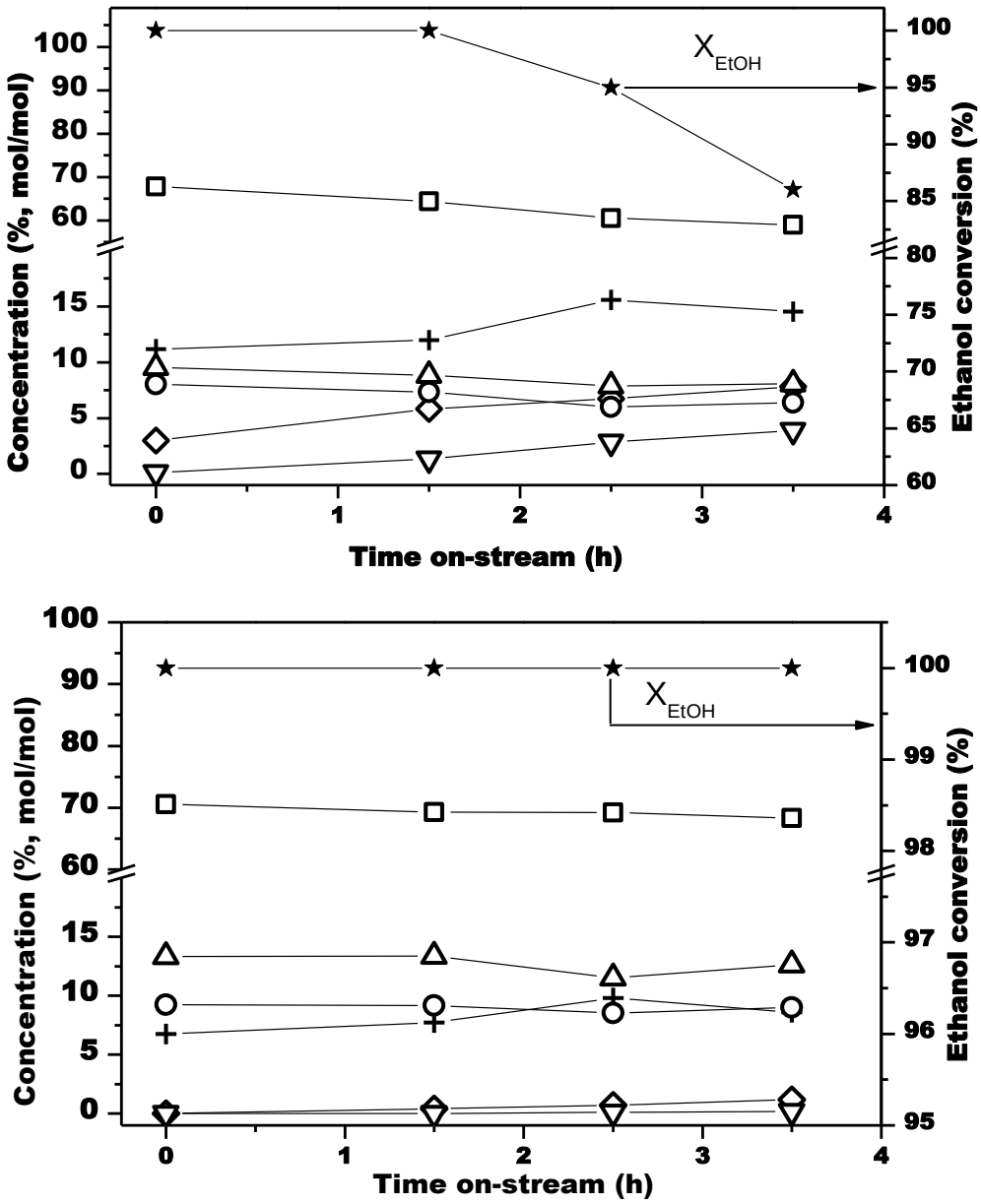

Figure 5.8c. Catalytic behaviour under ESR over Ni/12Zr29Y13La (top) and Ni/12Zr12Y31La (bottom) catalysts. Molar concentrations of (□)H_2, (○)CO, (+)CO_2, (△)CH_4, (▽)CH_3CHO and (◊)C_2H_4 in the outlet gas are shown. Reaction conditions: GHSV = 8100 h^{-1}, m_{cat} = 200 mg, T = 600 °C; 1.0 EtOH/1.6 H_2O/22.8 (Ar+N_2), molar ratios

The catalysts suffered partial deactivation under ESR conditions; the more stable being those with higher lanthanum content. In order to regenerate them, a catalytic test with two CO_2-treatments was performed; the first after 3.5 h on-stream and the second after 8.5 h of total accumulated reaction time. The CO_2-treatments were carried out as previously described in the Chapter 4 (p.88). In all cases, along CO_2-treatment CO was produced, similarly to Ni/Me_xO_y catalysts described in the Chapter 4.

Figure 5.9 shows detailed data of the ethanol conversion for the catalysts along the complete catalytic test. After the first CO_2-treatment, except for Ni/8Zr45Y, a complete ethanol conversion was recovered for all the catalysts. Afterwards, a second reaction period was carried out and deactivation of the catalysts was again observed. Following, the second CO_2-treatment resulted in the recovery of complete ethanol conversion for Ni/36Zr14Y, Ni/35Zr14La, Ni/8Zr50La and Ni/12Zr29Y13La catalysts.

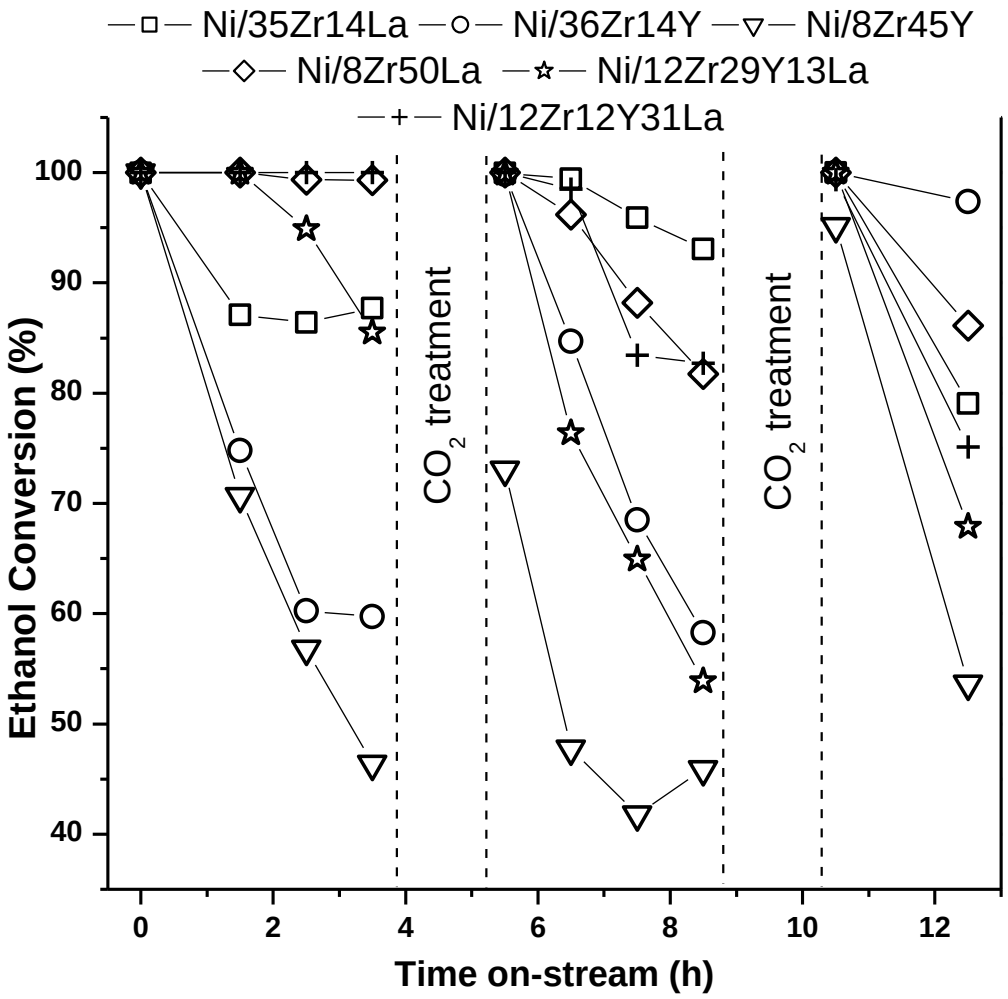

Figure 5.9. Ethanol conversion along time under ESR with CO_2-treatments over different catalysts (GHSV = 8100 h^{-1}, m_{cat} = 200 mg, T = 600 °C; 1.0 EtOH/1.6 H_2O/22.8 (Ar+N_2), molar ratios)

Figure 5.10 shows the profile of the H_2 concentration for all the catalysts during the catalytic test. During the first reaction period, the highest H_2 concentration was found for catalysts containing La and with low content of Zr (Ni/8Zr50La, Ni/12Zr29Y13La and Ni/12Zr12Y31La). After the first CO_2-

treatment, the catalysts with high La content maintained high H_2 concentration along the second reaction period. At the beginning of the last reaction period all the catalysts with low Zr content showed high (65-70% mol/mol) H_2 concentration. The complete distribution of products along time for all catalysts is given in the Annex (Fig. A.13-15).

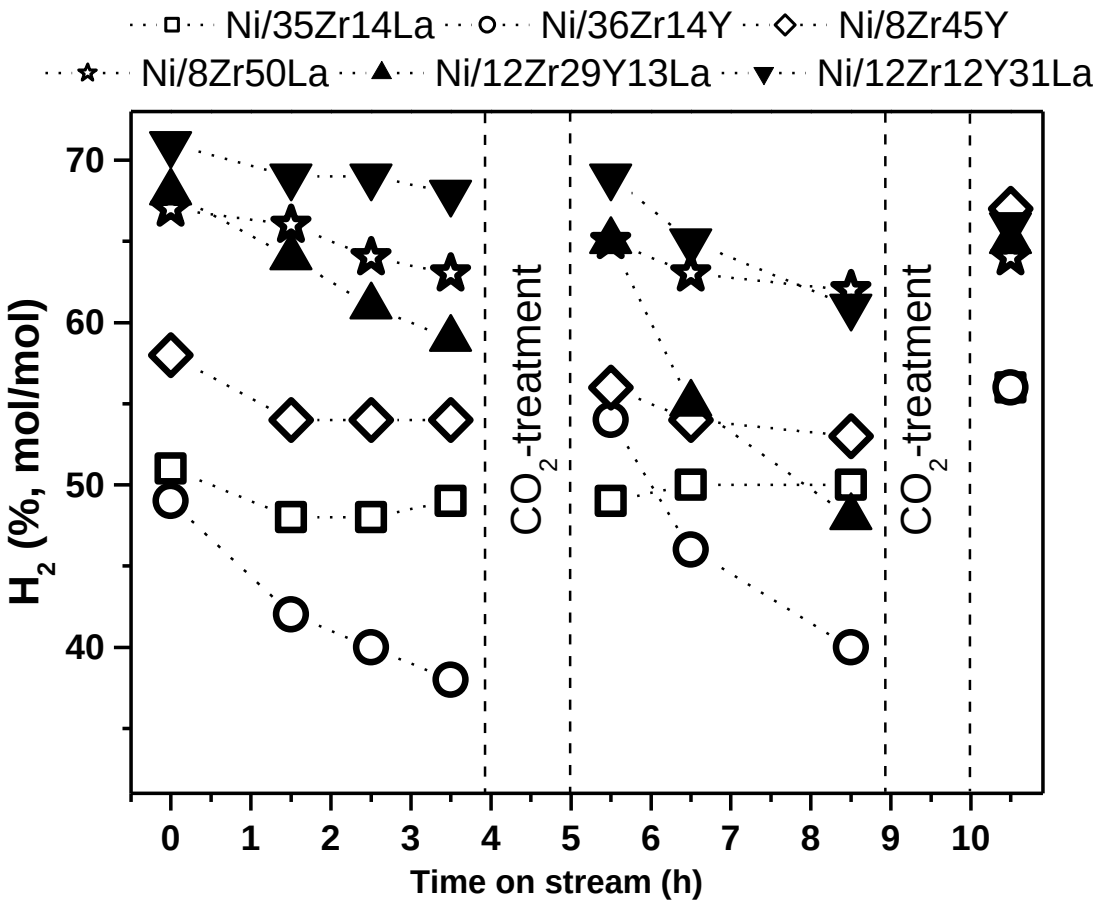

Figure 5.10. Variation of H_2 concentration along time under ESR with CO_2-treatment over different catalysts (GHSV = 8100 h^{-1}, m_{cat} = 200 mg, T = 600 °C; 1.0 EtOH/1.6 H_2O/22.8 (Ar+N_2), molar ratios)

Taking into account the deactivation process observed and the outstanding response to CO_2-treatments, the Ni/36Zr14Y catalyst was chosen for a long-time test with intermediate CO_2-treatments. Figure 5.11 presents the ethanol conversion and the product distribution under ESR during a 165-hour test. Along this experiment, the catalyst was regenerated 14 times (dashed vertical lines). Supposing that performed CO_2-treatments may not only gasify carbon deposits but also oxidize nickel, additional re-reduction was carried out, after 103 h on stream.

The performed CO_2-treatments allowed to regenerate the catalyst and to recuperate high ethanol conversion. However, along this reaction period it could be observed a progressive increase in the concentration of H_2 in the effluent as well as a parallel decrease in the CO concentration.

The carbon balance for this reaction showed a trend of rather stable mean carbon balance at about 95%, for the first 70 h (Fig. 5.12). However, from that point, the relation between carbon found in the outlet gas and carbon in the reactants continuously decreased. This is suggesting that, for this catalyst, the procedure used for the regeneration treatment could be useful only during a limited number of cycles.

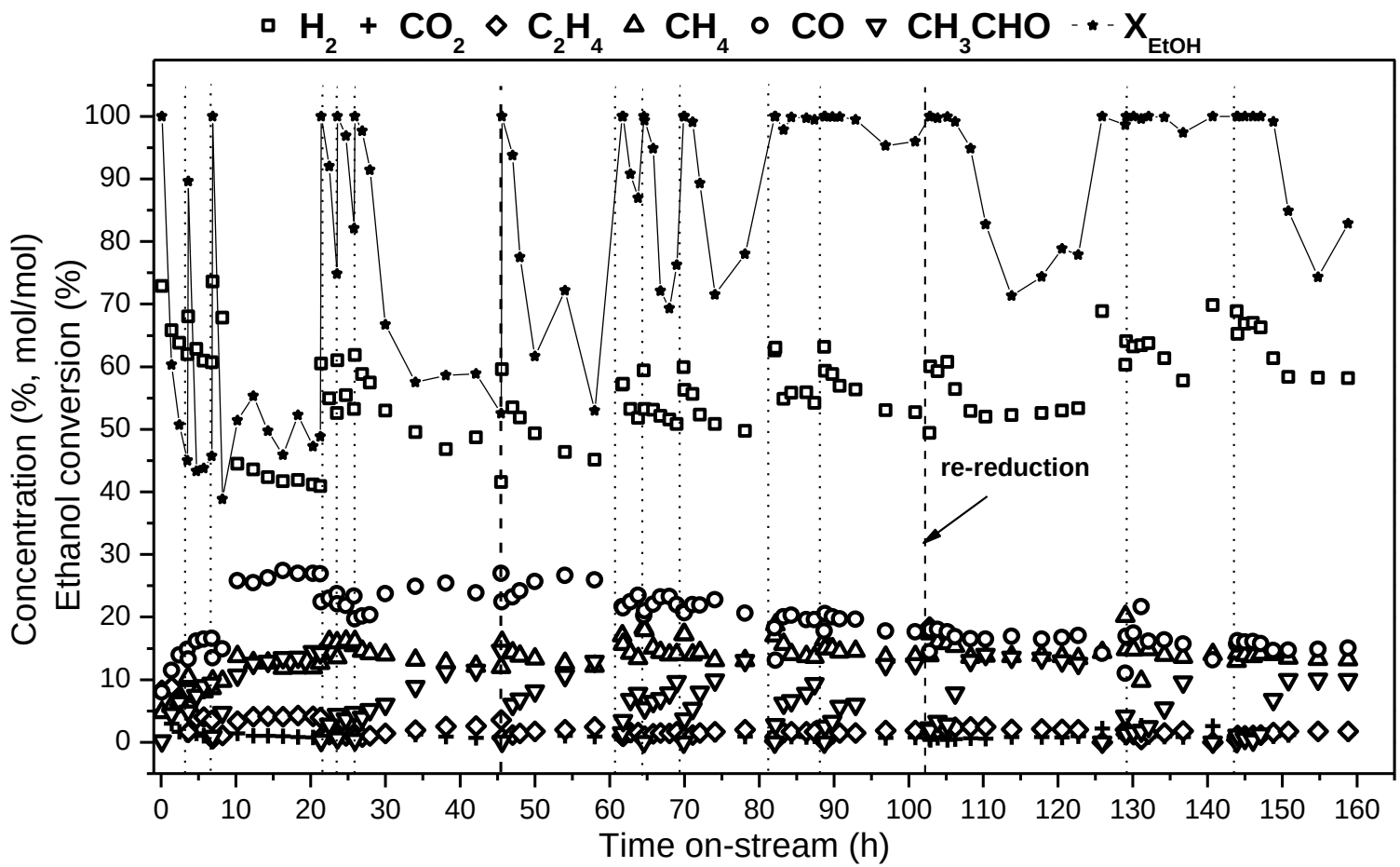

Figure 5.11. Catalytic behaviour under ESR over Ni/36Zr14Y catalyst for 165 hours with 14 breaks for regeneration with CO_2-treatment and one break for CO_2-treatment and re-reduction. Molar concentrations of H_2, CO, CO_2, CH_4, CH_3CHO and C_2H_4 in the outlet gas and ethanol conversion are shown. Dashed vertical lines indicate CO_2-treatment. Reaction conditions: GHSV = 8100 h^{-1}, m_{cat} = 200 mg, T = 600 °C; 1.0 EtOH/1.6 H_2O/22.8 (Ar+N_2), molar ratios

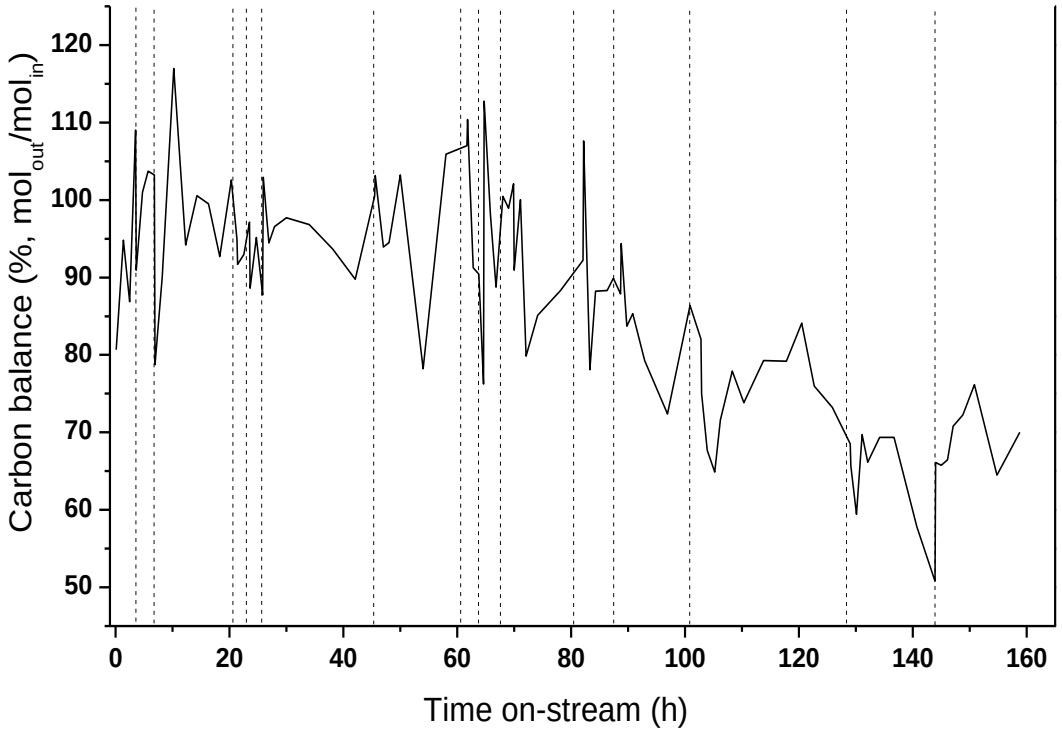

Figure 5.12. Carbon balance under ESR over Ni/36Zr14Y catalyst for 165 hours with 14 breaks for regeneration with CO_2-treatment and one break for CO_2-treatment and re-reduction. Dashed vertical lines indicate CO_2-treatment. Reaction conditions: GHSV = 8100 h^{-1}, m_{cat} = 200 mg, T = 600 °C; 1.0 EtOH/1.6 H_2O/22.8 (Ar+N_2), molar ratios

A long-time test (280 h) with different periodicity of CO_2-treatments was carried out using the Ni/12Zr29Y13La catalyst. In this test, the catalyst was working under ESR conditions during 230 h; several CO_2-treatments were applied. Then, during the last 50 h, it was periodically regenerated (every 4 h) in order to maintain complete ethanol conversion. During the first period, the ethanol conversion decreased along time but complete ethanol conversion was found after each CO_2-treatment. This test showed that

Ni/12Zr29Y13La can be useful for stable hydrogen production using periodical regenerating CO_2-treatments. A H_2-yield about 65% under complete ethanol conversion could be achieved. CH_4, CO_2 and CO were generated with stable distribution: 12%, 10% and 4% mol/mol, respectively; C_2H_x concentration was below 0.5% mol/mol. Figure 5.13 shows representative data of H_2-yield and the concentration of the other products formed when the ethanol conversion was recovered with the regeneration procedure. During the last 50 h, using the mentioned CO_2-treatment, complete ethanol conversion was maintained. All data of conversion and product distribution obtained during this long-time test are given in the Annex (Fig. A.16).

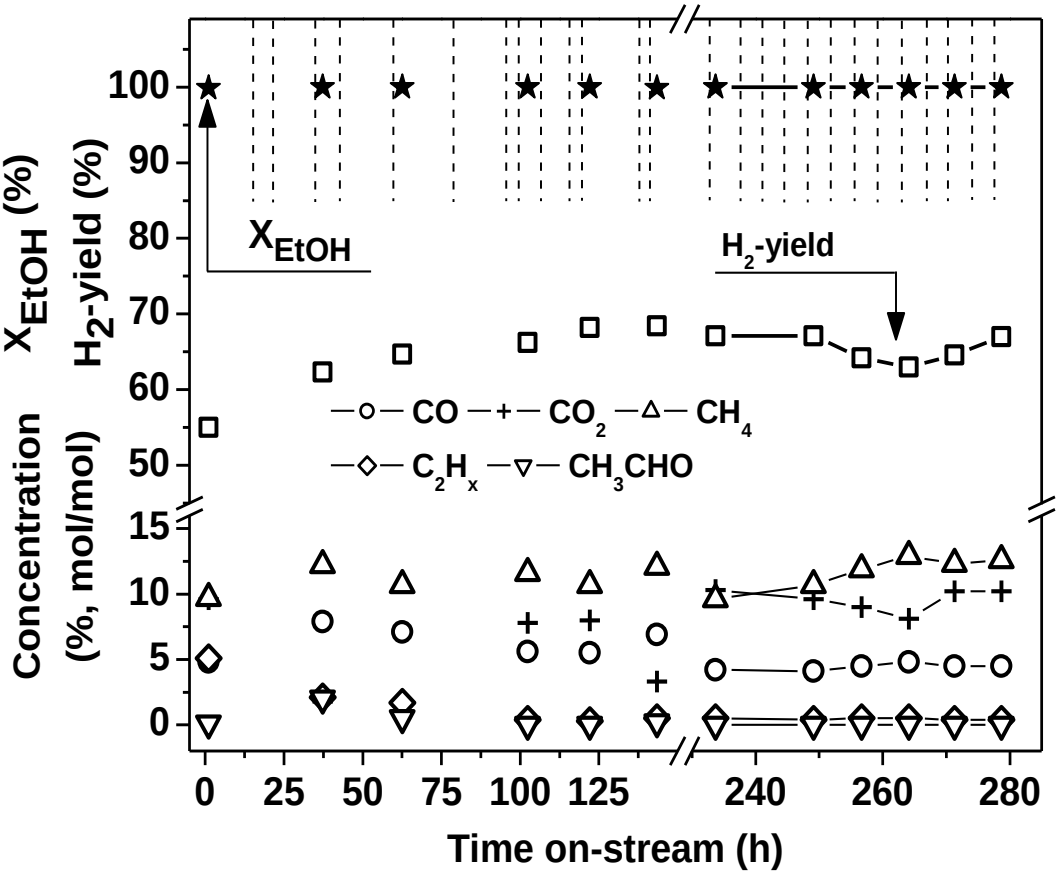

Figure 5.13. H_2-yield, ethanol conversion and product distribution obtained over Ni/12Zr29Y13La catalyst during ESR with CO_2-treatments (indicated by dashed lines) for 280 h. During the last 50 h, 1-hour CO_2-treatments were applied periodically every 4h. Reaction conditions: GHSV = 8100 h^{-1}, m_{cat} = 200 mg, T = 600 °C; 1.0 EtOH/1.6 H_2O/22.8 (Ar+N_2), molar ratios

The carbon balance determined for this reaction (Fig. 5.14) presents values between 30% and 80% during the stage of non-regular CO_2-treatment; and rather constant balance around 50% during the last 50 h with periodical CO_2-treatment and complete ethanol conversion.

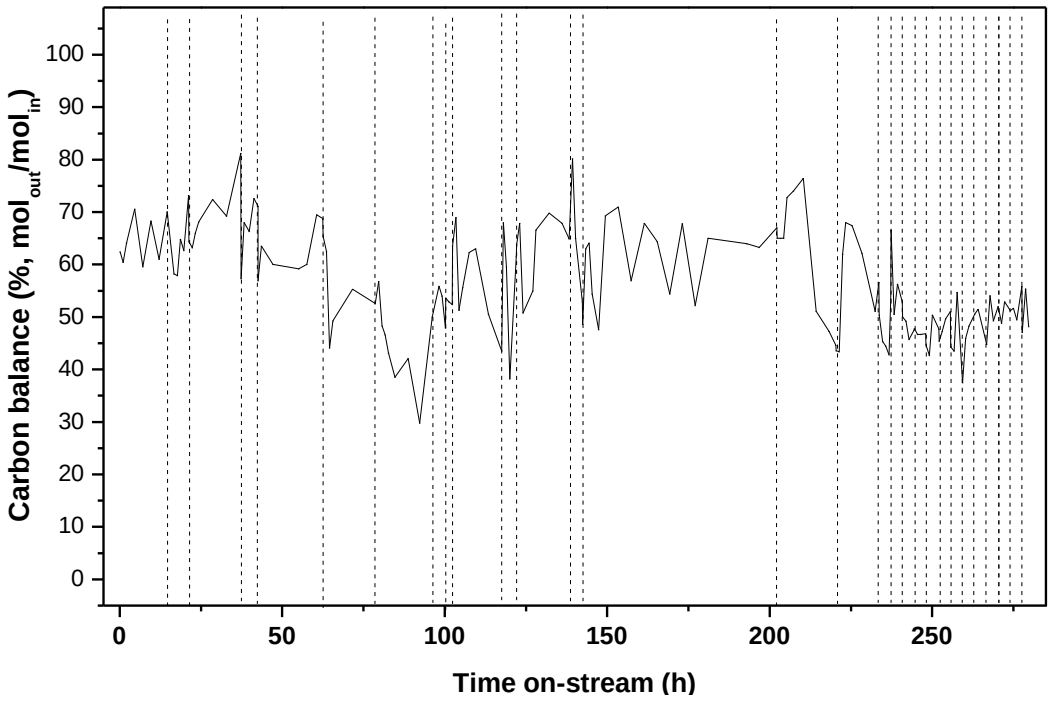

Figure 5.14. Carbon balance over Ni/12Zr29Y13La catalyst during ESR with CO_2-treatments (indicated by dashed lines) for 280 h. Reaction conditions: GHSV = 8100 h^{-1}, m_{cat} = 200 mg, T = 600 °C; 1.0 EtOH/1.6 H_2O/22.8 (Ar+N_2), molar ratios

The effect of the application time of CO_2-treatment was studied. Figure 5.15 shows hydrogen evolution after 1 h CO_2-treatment (standard) (A zone) and after extended CO_2-treatment, carried out during 9 h (B zone). The first CO_2-treatment was performed after 4 h on stream from the previous regeneration (ethanol conversion 72%). The second CO_2-treatment was performed after 18 h on stream from the previous regeneration (ethanol conversion 51%). Both treatments restored complete ethanol conversion. However, the short CO_2-treatment resulted in a shorter period of complete ethanol conversion.

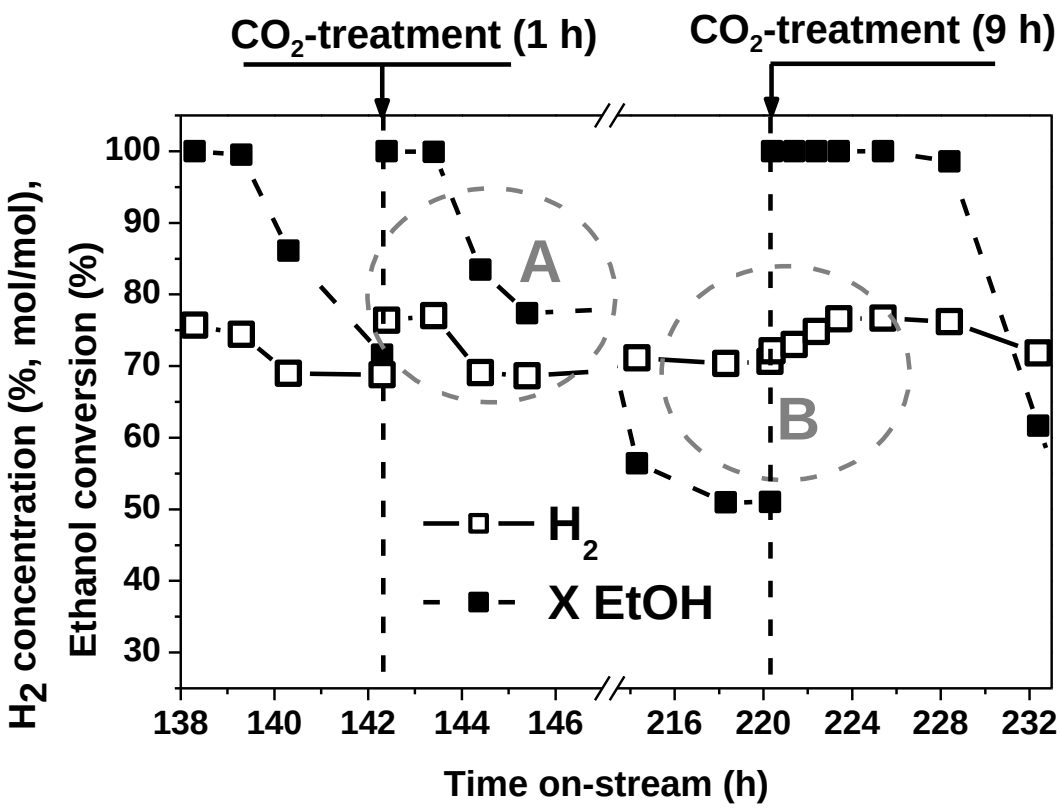

Figure 5.15. Effect of time of CO_2-treatment on ethanol conversion and hydrogen evolution under ESR over Ni/12Zr29Y13La

As shows Figure 5.15, after the short (1 h) CO_2-treatment, the H_2 concentration increased immediately and then decreased in the next 2 h. The longer treatment (9 h) resulted in a slow increase of hydrogen concentration during the first 4 h and then decreased. These observations suggest a relationship between the duration of the CO_2-treatment and the hydrogen production, and it could be related with a partial oxidation of the nickel phase if a prolonged CO_2-treatment is applied.

For deeper studies of possible oxidation of the nickel phase during CO_2-treatment, XRD analysis of spent Ni/36Zr14Y was carried out. Spent catalyst, after 165 h experiment (Fig. 5.11), was treated for 2.5 h with CO_2 during the last part of the experiment. Figure 5.16 presents the XRD pattern of spent catalyst, where both NiO and Ni^0 were detected. Although the XRD was done *ex-situ*, this result suggests that during the CO_2-treament, CO_2 not only reacts with carbon deposits but also can partially oxidize Ni^0 to NiO [17].

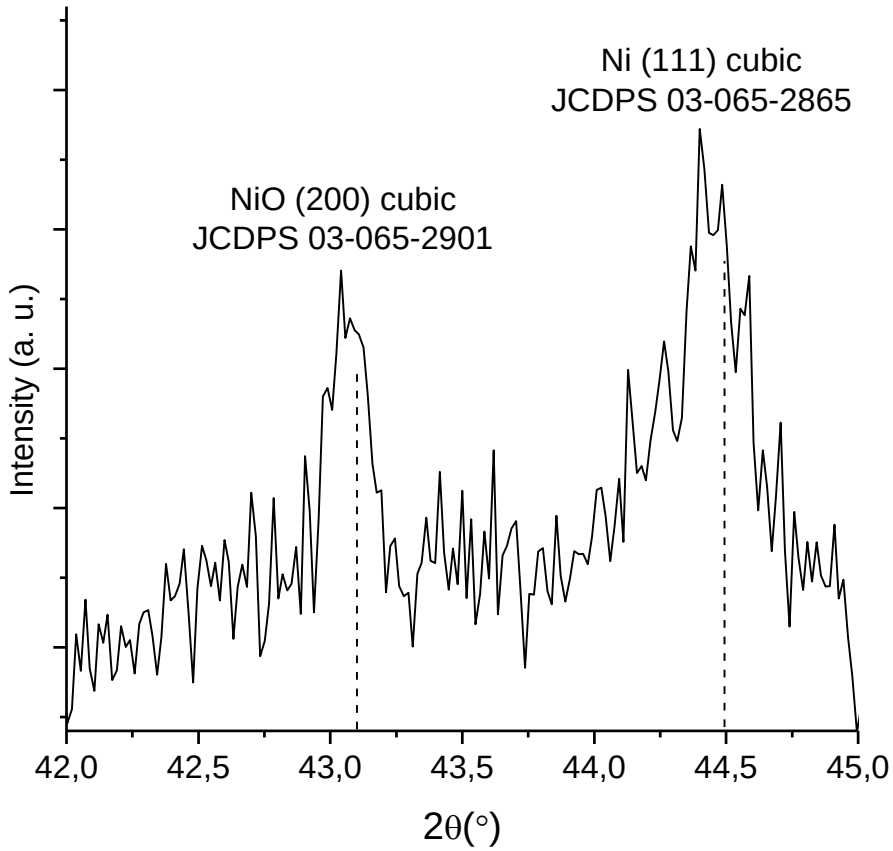

Figure 5.16. XRD pattern of spent Ni/36Zr14Y catalyst after 165 hours on stream, and a final 2.5h CO_2-treatment

5.3. Characterization of spent catalysts and carbon deposits

All catalysts were characterized after the standard catalytic test under substoichiometric ESR with two CO_2-treatments (3.5 h ESR, CO_2-treatment, 4.5 h ESR, CO_2-treatment, 2.5 h ESR).

The results of XRD analysis is shown in Figures 5.17a and 5.17b. The presence of Ni^0 was determined by this technique in all post reaction catalysts. The Ni^0 crystallite size was determined using the Debye-Scherrer method [3] and the (111) diffraction peak, giving the following results: Ni/35Zr14La – 39 nm, Ni/36Zr14Y – 27 nm, Ni/8Zr45Y – 9 nm, Ni/8Zr50La – 18 nm, Ni/12Zr29Y13La – 10 nm and Ni/12Zr12Y31La – 11nm.

After reaction, the catalysts with high yttrium content (Ni/8Zr45Y and Ni/12Zr29Y13La) showed a relative increase in the crystallinity of the support phase in respect with fresh calcined samples (Fig. 5.3); especially a strong crystallization of cubic Y_2O_3 phase was observed. For Ni/8Zr50La, clear peaks related to La_2O_3 were found.

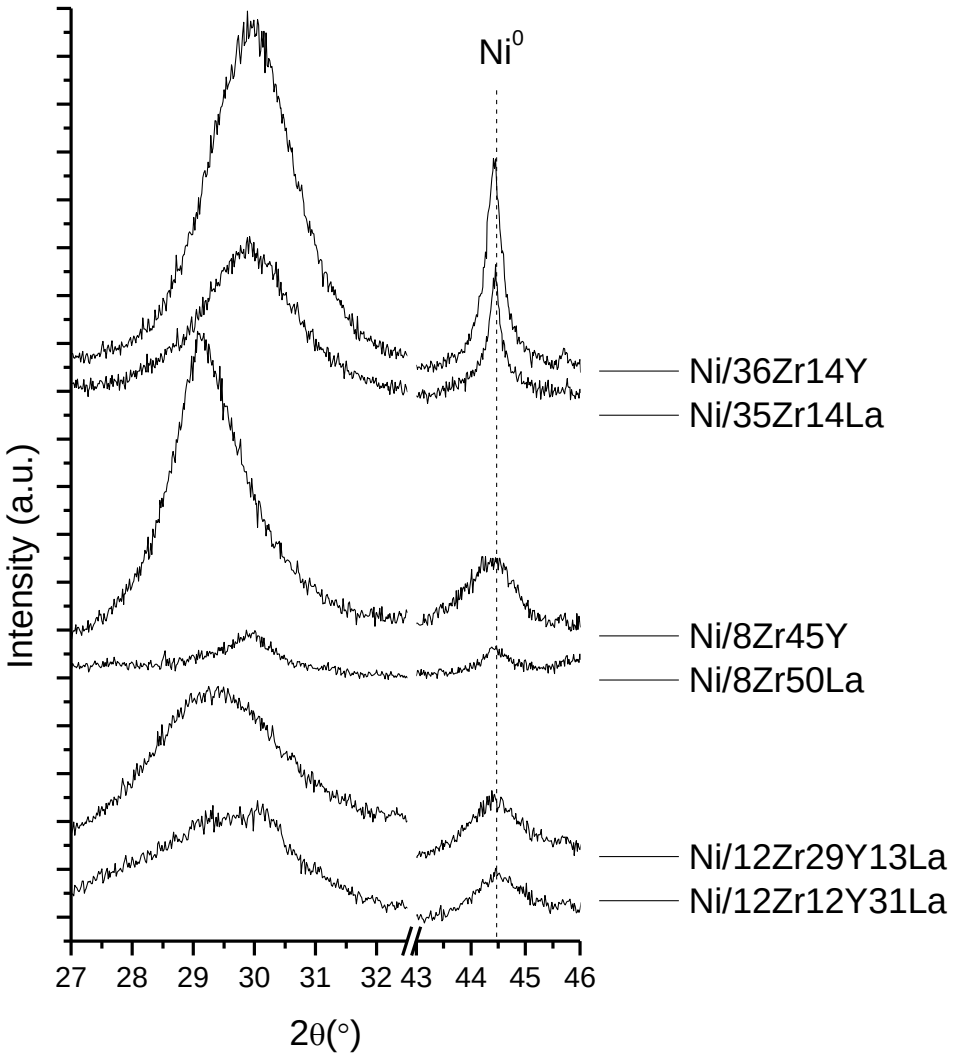

Figure 5.17a. XRD patterns of post-reaction Ni/ZrY, Ni/ZrLa and Ni/ZrYLa catalysts used under ESR with two CO_2-treatments, in the zones corresponding to the most intensive peaks of the supports (2θ=27-33°) and Ni^0 (2θ= 43-46°)

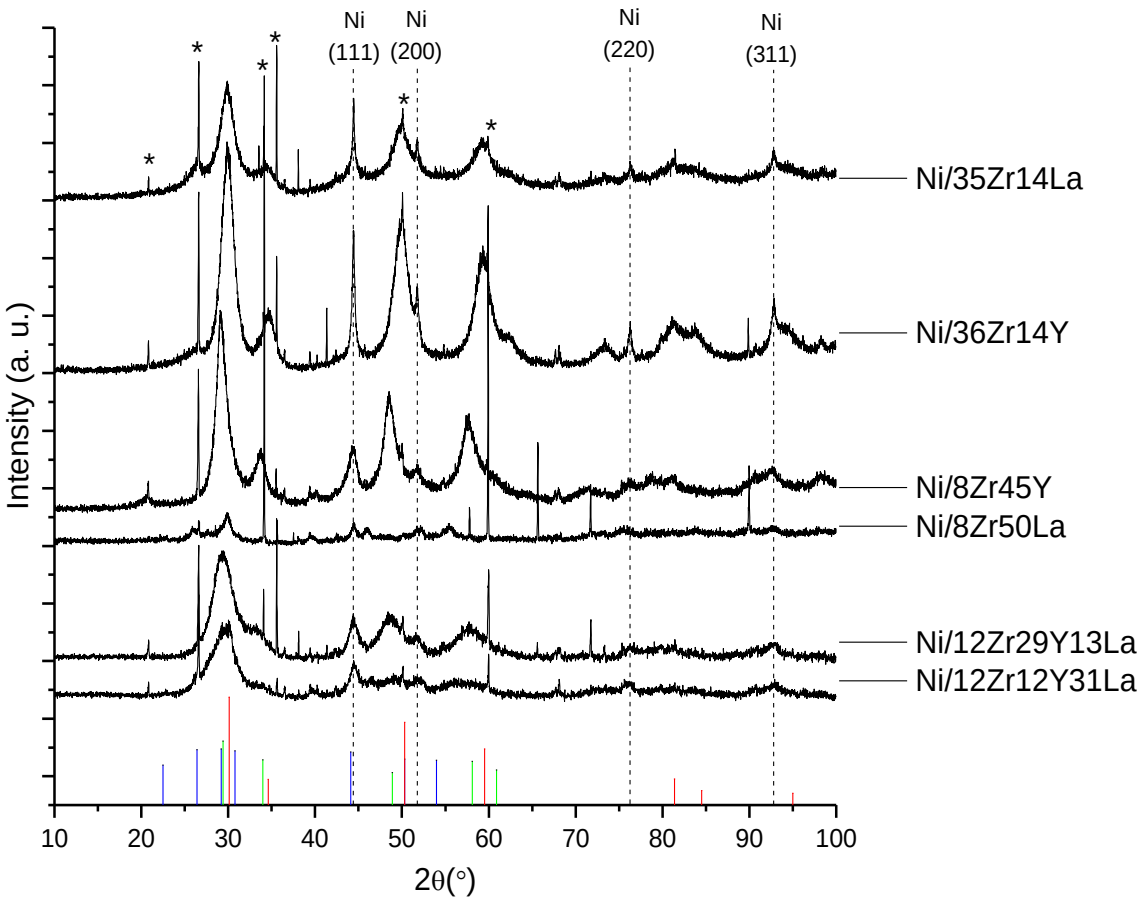

Figure 5.17b. XRD patterns of post-reaction Ni/ZrY, Ni/ZrLa and Ni/ZrYLa catalysts used under ESR with two CO_2-treatments; the dashed vertical lines indicate the position of the cubic Ni peaks (JCPDS 03-065-2865). In the bottom part, XRD patterns for recognized phases are presented: |-ZrO_2 tetragonal (JCPDS 00-024-1164), |-Y_2O_3 cubic (JCPDS 00-043-0661), |-$La_2O_2CO_3$ monoclinic (JCPDS 00-048-1113). The asterisks indicate quartz wool SiO_2 peaks

In order to determine the total amount of carbon deposits and their basic characteristics, TPO-MS analyses were carried out with spent catalysts after 10.5 h ESR tests with the two intermediate CO_2-treatments. The corresponding TPO profiles are shown in Figure 5.18. The area under each

TPO profile corresponds to the quantity of carbon deposits found during the analyses. TPO profiles of catalysts supported on binary systems and with high zirconium content, Ni/35Zr14La and Ni/36Zr14Y, presented mostly combustion at temperatures above 500 °C, indicating the main presence of highly ordered carbon deposits. For the other two catalysts supported on binary systems, the Ni/8Zr45Y catalyst exhibited only combustion about 400 °C, corresponding to the presence of amorphous carbon. Contrarily, Ni/8Zr50La catalyst exhibited only a high temperature peak, between 520 °C and 700 °C, suggesting the main presence of graphitic carbon in this case.

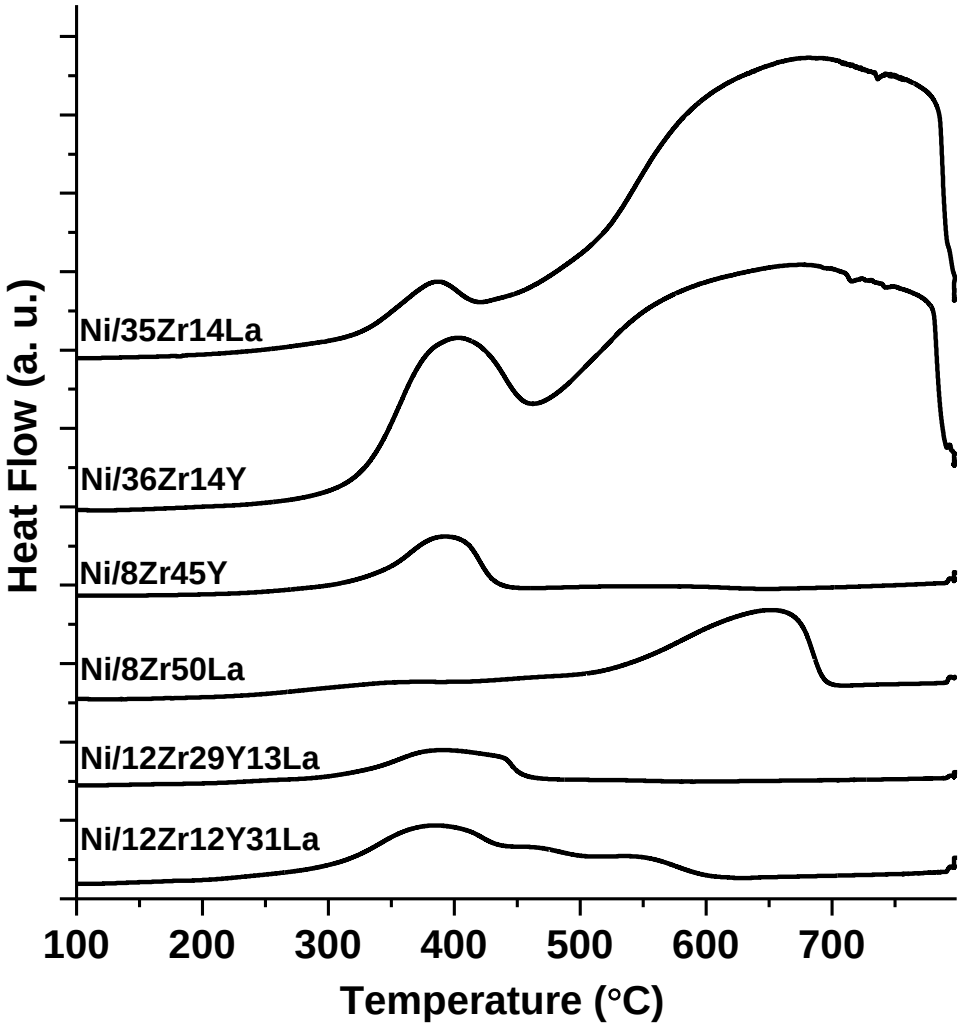

Figure 5.18. Heat flow profiles obtained during TPO-MS analysis of post-reaction catalysts after ESR with two CO_2-treatments

The TPO results of Ni/12Zr29Y13La and Ni/12Zr12Y31La catalysts showed a main peak starting at about 325 °C with maximum at ca. 400 °C. For Ni/12Zr12Y31La, the combustion peak extended up to 600 °C [18]. For both these catalysts, the lowest amount of carbonaceous deposits was found (Tab. 5.5). Moreover, for the Ni/12Zr29Y13La, which exhibited the highest

CO_2 adsorption enthalpy, only a carbon deposition rate of 0.12 mmol C/h·g_{cat} of poorly ordered nature was found. Table 5.5 presents the amount of carbon deposited, expressed as the carbon deposition rates, calculated from TPO-MS experiments. It can be seen that high content of zirconium favours formation of carbon deposits and this is in agreement with the results found for Ni/ZrO_2, previously studied. Thus, for Ni/35Zr14La and Ni/36Zr14Y, after the reaction conditions used, the highest amount of carbon deposits were found. An increase in yttrium or lanthanum content resulted in a smaller carbon formation.

Table 5.5. Carbon deposition rate determined form TPO-MS measurements and Raman I_G/I_D ratio after ESR with two CO_2-treatments

Catalyst	Carbon deposited (mmol C/h·g_{cat})	I_G/I_D
Ni/35Zr14La	2.61	0.49
Ni/36Zr14Y	2.52	0.54
Ni/8Zr45Y	0.33	0.54
Ni/8Zr50La	0.82	0.49
Ni/12Zr29Y13La	0.12	0.49
Ni/12Zr12Y31La	0.17	0.54

Raman spectroscopy was used to analyse the characteristics of carbon deposits. The Raman spectra in the carbon region are presented in Figure 5.19, and the corresponding I_G/I_D ratios, appear in Table 5.5. As can be seen, obtained results are similar to the results of Ni/Me_xO_y catalysts. In all cases, the I_G/I_D ratio presented values of approximately 0.5. The Raman analysis

did not establish significant differences between the carbon deposits formed for the different catalysts.

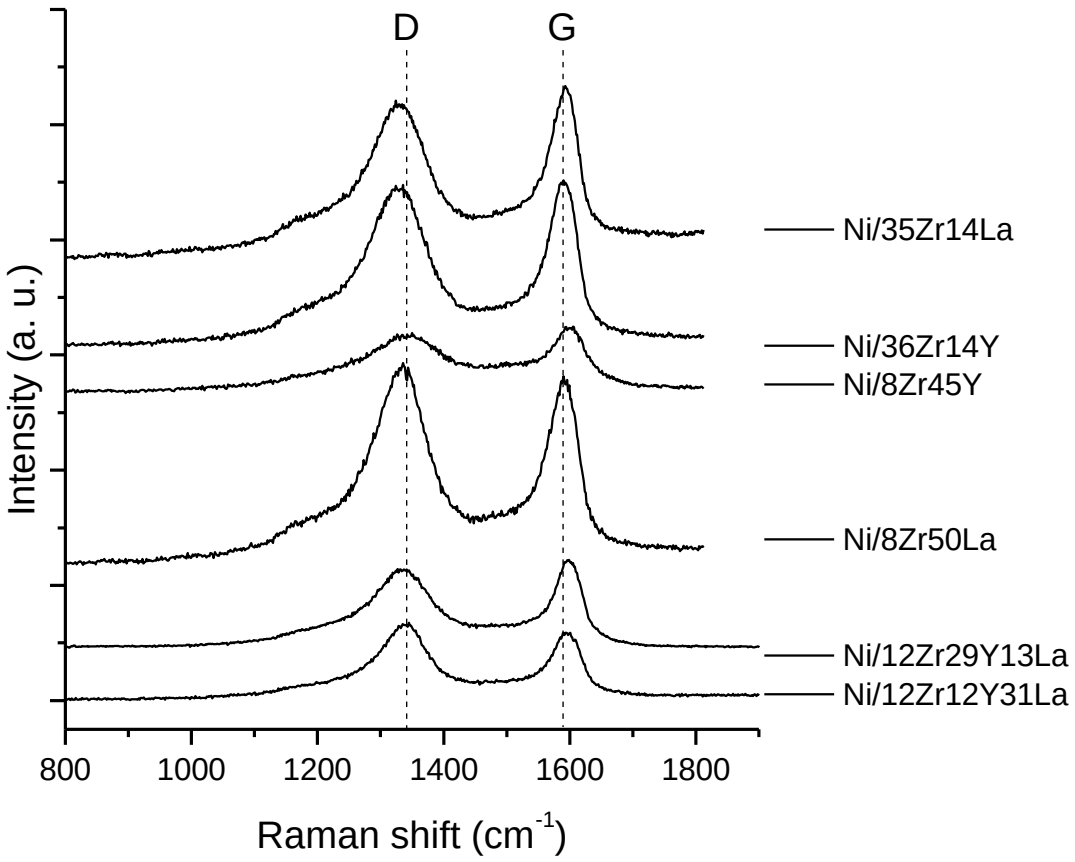

Figure 5.19. Carbon region of Raman spectra of post-reaction Ni/ZrY, Ni/ZrLa and Ni/ZrYLa catalysts after ESR with two CO_2-treatments

Analysis by infrared spectroscopy technique permits to know deeper the characteristics of carbon deposits, especially in terms related to the presence of partially hydrogenated carbonaceous species. Figure 5.20 shows the registered spectra corresponding to spent catalysts, analysed after the 10.5 h ESR experiment. The DRIFT spectra were analysed in the

region between 2750 cm^{-1} and 3150 cm^{-1}, where the presence of carbonaceous species containing CH_x groups could be detected. Bands in the 2750-3000 cm^{-1} can be attributed to the symmetric and asymmetric modes of *v*(C-H) stretching of aliphatic species. Bands above 3000 cm^{-1} are characteristic of the *v*(C-H) vibrations of olefinic/aromatic hydrocarbons [19].

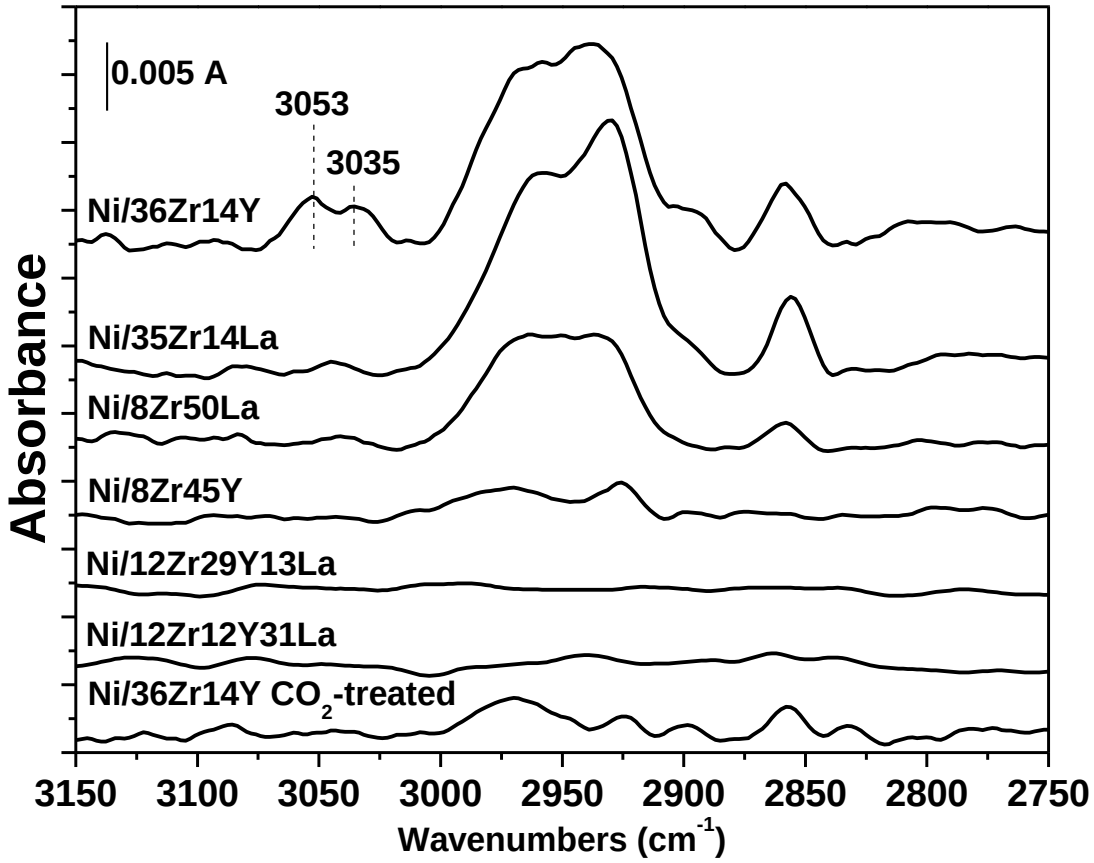

Figure 5.20. DRIFTS spectra of Ni/ZrY, Ni/ZrLa and Ni/ZrYLa catalysts after ESR with two CO_2-treatments; Ni/36Zr14Y CO_2-treated – spent catalyst after 165 h ESR test where the last step was prolonged CO_2-treatment

The spectra of Ni/12Zr29Y13La and Ni/12Zr12Y31La revealed negligible intensity *v*(C-H) bands. For Ni/36Zr14Y, Ni/35Zr14La, Ni/8Zr45Y and Ni/8Zr50La, bands were observed in the range 3000-2950 cm^{-1}, pointing to the presence of *v*(C-H) stretching modes of aliphatic hydrocarbon species. Moreover, for Ni/36Zr14Y, bands at 3035 cm^{-1} and 3053 cm^{-1}, corresponding to the presence of olefinic/aromatic species, are visible. This could be related with the abundant production of ethene determined for this catalyst.

In a separate experiment carried out for 165 h with Ni/36Zr14Y, the catalyst was treated with CO_2 at the end of the test, in order to know about the effects of CO_2-treatment on the carbon deposits removal. The spectra of this sample is labelled as "Ni/36Zr14Y CO_2-treated" in Figure 5.20. As can be seen, the corresponding spectra for this catalyst registered after the CO_2-treatment shows a large decrease of the bands in the *v*(C-H) region. In particular, the performed CO_2-treatment fully removed the bands above 3000 cm^{-1}, indicating a major removal of this kind of surface carbonaceous species.

5.4. References

[1] Bednarczuk L, Ramírez de la Piscina P, Homs N. H_2-production from CO_2-assisted ethanol steam reforming: The regeneration of Ni-based catalysts. Int J Hydrogen Energy 2015;40:5256–63. doi:10.1016/j.ijhydene.2015.01.061.

[2] Yermán L, Homs N, Ramírez de la Piscina P. Hydrogen production from oxidative steam-reforming of n-propanol over Ni/Y_2O_3–ZrO_2 catalysts. Int J Hydrogen Energy 2012;37:7094–100. doi:10.1016/j.ijhydene.2011.11.045.

[3] Debye P, Scherrer P. Interferences in irregularly oriented particles in Reontgen light. Phys Zeitschrift 1916;17:227–83.

[4] Biesinger MC, Payne BP, Lau LWM, Gerson A, Smart RSC. X-ray photoelectron spectroscopic chemical state Quantification of mixed nickel metal, oxide and hydroxide systems. Surf Interface Anal 2009;41:324–32. doi:10.1002/sia.3026.

[5] Edwards ER, Antunes EF, Botelho EC, Baldan MR, Corat EJ. Evaluation of residual iron in carbon nanotubes purified by acid treatments. Appl Surf Sci 2011;258:641–8. doi:10.1016/j.apsusc.2011.07.032.

[6] Akhavan O, Abdolahad M, Esfandiar A, Mohatashamifar M. Photodegradation of Graphene Oxide Sheets by TiO_2 Nanoparticles after a Photocatalytic Reduction. Society 2010;114:12955–9. doi:10.1021/jp103472c.

[7] Ma J, Sun N, Zhang X, Zhao N, Xiao F, Wei W, et al. A short review of catalysis for CO_2 conversion. Catal Today 2009;148:221–31. doi:10.1016/j.cattod.2009.08.015.

[8] Zawadzki A, Bellido JDA, Lucrédio AF, Assaf EM. Dry reforming of ethanol over supported Ni catalysts prepared by impregnation with methanolic solution. Fuel Process Technol 2014;128:432–40. doi:10.1016/j.fuproc.2014.08.006.

[9] Liu BS, Au CT. Carbon deposition and catalyst stability over La_2NiO_4/gamma-Al_2O_3 during CO_2 reforming of methane to syngas 2003;244:181–95.

[10] Barbero J, Peña MA, Campos-Martin JM, Fierro JLG, Arias PL. Support effect in supported Ni catalysts on their performance for methane partial oxidation. Catal Letters 2003;87:211–8. doi:10.1023/A:1023407609626.

[11] Liu JY, Lee CC, Wang CH, Yeh CT, Wang CB. Application of nickel-lanthanum composite oxide on the steam reforming of ethanol to produce hydrogen. Int J Hydrogen Energy 2010;35:4069–75. doi:10.1016/j.ijhydene.2010.01.141.

[12] Liu H, Wu H, He D. Methane conversion to syngas over Ni/Y_2O_3 catalysts - Effects of calcination temperatures of Y_2O_3 on physicochemical properties and catalytic performance. Fuel Process Technol 2014;119:81–6. doi:10.1016/j.fuproc.2013.11.001.

[13] Bellido JDA, Assaf EM. Nickel catalysts supported on ZrO_2, Y_2O_3-stabilized ZrO_2 and CaO-stabilized ZrO_2 for the steam reforming of ethanol: Effect of the support and nickel load. J Power Sources 2008;177:24–32. doi:10.1016/j.jpowsour.2007.11.006.

[14] Zhu J, Peng X, Yao L, Tong D, Hu C. CO_2 reforming of methane over Mg-promoted Ni/SiO_2 catalysts: the influence of Mg precursors and impregnation sequences. Catal Sci Technol 2012;2:529. doi:10.1039/c1cy00333j.

[15] Bonne M, Haneda M, Duprez D, Ozawa M. Effect of addition on Y_2O_3 in ZrO_2 support on n-butane Pt catalyzed oxidation. Catal Commun 2012;19:74–9. doi:10.1016/j.catcom.2011.12.021.

[16] Alberton AL, Souza MMVM, Schmal M. Carbon formation and its influence on ethanol steam reforming over Ni/Al_2O_3 catalysts. Catal Today 2007;123:257–64. doi:10.1016/j.cattod.2007.01.062.

[17] Hannachi Y, Mascetti J, Stirling A, Pápai I. Metal insertion route of the

Ni + CO_2 → NiO + CO reaction. J Phys Chem A 2003;107:6708–13. doi:10.1021/jp0351324.

[18] Padilla R, Benito M, Rodríguez L, Serrano A, Muñoz G, Daza L. Nickel and cobalt as active phase on supported zirconia catalysts for bio-ethanol reforming: Influence of the reaction mechanism on catalysts performance. Int J Hydrogen Energy 2010;35:8921–8. doi:10.1016/j.ijhydene.2010.06.021.

[19] Silverwood IP, Hamilton NG, Laycock CJ, Staniforth JZ, Ormerod RM, Frost CD, et al. Quantification of surface species present on a nickel/alumina methane reforming catalyst. Phys Chem Chem Phys 2010;12:3102–7. doi:10.1039/b919977b.

6. Conclusions

In this work, using active carbon as template and urea as precipitation agent, mesoporous Me_xO_y single (Al_2O_3, MgO, Y_2O_3, La_2O_3, ZrO_2), ZrO_2-Y_2O_3 and ZrO_2-La_2O_3 binary (36Zr14Y, 8Zr45Y, 35Zr14La, 8Zr50La) and ZrO_2-Y_2O_3-La_2O_3 ternary (12Zr29Y13La, 12Zr12Y31La) oxide-based systems were prepared. These systems were used as supports for the preparation of nickel-based catalysts. The presence of crystalline $La_2O_2CO_3$ was determined in Ni/La_2O_3 catalyst, and in 35Zr14La, 8Zr50La and 12Zr12Y31La supports; $La_2O_2CO_3$ could be formed in the last preparation step of the supports, by reaction of La_2O_3 with CO_2 formed during the combustion of active carbon at 600 °C.

A relationship between the surface area of Ni/ZrO_2-Y_2O_3, Ni/ZrO_2-La_2O_3 and Ni/ZrO_2-Y_2O_3-La_2O_3 and the Zr content in the catalysts was found. Catalysts with higher Zr content showed higher values of surface area, independently of the components of the support. The formation of small ZrO_2 particles could contribute to the surface area and avoid the crystallization and/or sintering of other phases in the catalysts. In Ni/36Zr14Y and Ni/35Zr14La, the presence of ZrO_2-Y_2O_3 and ZrO_2-La_2O_3 solid solutions is proposed.

The analysis of the reducibility of the catalysts showed that, for yttrium- and lanthanum-containing catalysts, the H_2 consumption values largely exceeded those expected for NiO reduction to Ni^0. This is related with the partial reduction of the supports due to the presence of superficial oxygen vacancies and/or with the presence of $La_2O_2CO_3$.

Ni/Me_xO_y (Me_xO_y = Al_2O_3, MgO, Y_2O_3, La_2O_3 and ZrO_2) catalysts were tested under substoichiometric ethanol steam reforming (ESR) (ethanol/H_2O = 1.0/1.6, molar ratio) followed by CO_2-assisted substoichiometric ethanol steam reforming (CDESR) (ethanol/H_2O/CO_2 = 1.0/1.6/1.6, molar ratios) at 600 °C. The behaviour of Ni/Me_xO_y under ESR/CDESR was compared with that under ESR.

In all cases, H_2 was the main product obtained (molar concentration 40-60 %). Although the distribution of carbon-containing products depended on the ethanol conversion, in general, acetaldehyde and CO were the most abundant carbon-containing products and smaller amounts of CH_4 and C_2H_4, and CO_2 under ESR, were also produced. The product distribution was not significantly affected by the CO_2 incorporation to the reactant mixture, CDESR conditions, for the catalysts studied.

The amount of carbon deposits formed during ESR was significantly lower for Y_2O_3-supported catalysts and Ni/La_2O_3 when compared with the other Ni/Me_xO_y catalysts. These catalysts showed a higher surface density of basic sites than that of remaining catalysts; the reaction between adsorbed CO_2 (formed during ESR) and carbon deposits could take place preferentially over these catalysts. Moreover, on Y_2O_3-supported catalysts, the presence of active surface oxygen species could help to oxidize carbon deposits.

Ni/La_2O_3 showed a lower amount and less ordered carbon deposits after ESR/CDESR (0.060 mmol C/h·g_{cat}) than after ESR (0.191 mmol C/h·g_{cat}) catalytic tests. Under CDESR the formation of surface $La_2O_2CO_3$ species

close to Ni particles could be favored; these species could react with carbon deposits forming CO and La_2O_3. On the other hand, Ni(K)/Y_2O_3 showed a much higher amount of carbon deposits after ESR/CDESR (0.230 mmol C/h·g_{cat}) than after ESR (0.074 mmol C/h·g_{cat}); for this catalyst a competition between CO_2 and H_2O for the adsorption sites during CDESR could exist.

CO_2-treatments during ESR at 600 °C were useful for the regeneration of deactivated catalysts. In all cases, a CO_2-treatment partially (or totally) restored the catalytic performance. CO_2 can act as a mild oxidant removing part of the carbonaceous deposits through their oxidation to CO (reverse Boudouard reaction); this behaviour is related with the basic characteristics of the catalysts.

Except for Ni/Al_2O_3, the application of a CO_2-treatment during ESR over Ni/Me_xO_y catalysts produced a diminution of the total carbonaceous deposits. This effect was more significant for Ni/Y_2O_3 and Ni/La_2O_3, which showed high density of CO_2 adsorption sites and high value of mean enthalpy of CO_2 adsorption.

Ni/ZrO_2-Y_2O_3, Ni/ZrO_2-La_2O_3 and Ni/ZrO_2-Y_2O_3-La_2O_3 catalysts were tested under ESR (ethanol/H_2O = 1.0/1.6, molar ratio) at 600 °C, with intermediate CO_2-treatments. For these catalysts, periodic CO_2-treatments proved to be also useful for regeneration of deactivated catalysts. During ESR, Ni/ZrO_2-Y_2O_3 showed higher deactivation than Ni/ZrO_2-La_2O_3 did.

The characteristics and amount of carbon deposits found after the catalytic test (ESR with CO_2-treatments) are related with the CO_2 adsorption properties of catalysts. For Ni/ZrO_2-Y_2O_3 and Ni/ZrO_2-La_2O_3 catalysts, an increase in La or Y content resulted in a higher surface density of basic sites and in a smaller amount of carbon found after the catalytic test.

After the catalytic test, Ni/ZrO_2-Y_2O_3-La_2O_3 showed significantly lower amount of carbon deposits than Ni/ZrO_2-Y_2O_3 and Ni/ZrO_2-La_2O_3. For Ni/ZrO_2-Y_2O_3-La_2O_3 catalysts, the presence of yttrium and lanthanum species, diluted with small ZrO_2 particles, can result in an appropriate balance of surface oxygen defects and formation of surface lanthanum carbonate oxide species under the reaction conditions used. The lowest and less ordered carbon deposits were found for the Ni/12Zr29Y13La catalyst, which presented the highest CO_2 adsorption enthalpy and an intermediate value of surface density of basic sites.

Using periodic CO_2-treatments for regeneration, a continuous operation of Ni/12Zr29Y13La under 100% ethanol conversion, with a H_2-yield of about 65%, during a long-term ESR experiment was achieved.

Annex

Table A.1. Amounts of the corresponding nitrates ($Mg(NO_3)_2 \cdot 6H_2O$, $Al(NO_3)_3 \cdot 9H_2O$, $Y(NO_3)_3 \cdot 6H_2O$, $La(NO_3)_3 \cdot 6H_2O$ and $ZrO(NO_3)_2 \cdot H_2O$), urea, active carbon and water used in the preparation of single metal oxide supports

Support	Salt [g]	Urea [g]	Active carbon [g]	Water [mL]
MgO	55.198	55.88	15	750
Al_2O_3	101.375	44.14	15	750
Y_2O_3	50.916	19.97	15	750
La_2O_3	39.620	13.64	15	750
ZrO_2	30.341	18.32	15	750

Table A.2. Amounts of nitrates, urea, active carbon and water used in the preparation of binary and ternary oxide systems. The numbers before the element indicate its weight percent content determined by chemical analysis of related catalysts

Support	$ZrO(NO_3)_2 \cdot H_2O$ [g]	$Y(NO_3)_3 \cdot 6H_2O$ [g]	$La(NO_3)_3 \cdot 6H_2O$ [g]	Urea [g]	Active carbon [g]	Water [mL]
35Zr14La	16.186	-	5.365	11.61	10	500
36Zr14Y	16.186	6.835	-	12.43	10	500
8Zr45Y	4.049	27.138	-	13.18	10	500
8Zr50La	4.047	-	21.275	9.85	10	500
12Zr29Y13La	6.067	16.976	5.340	12.26	10	500
12Zr12Y31La	6.096	6.806	13.345	11.13	10	500

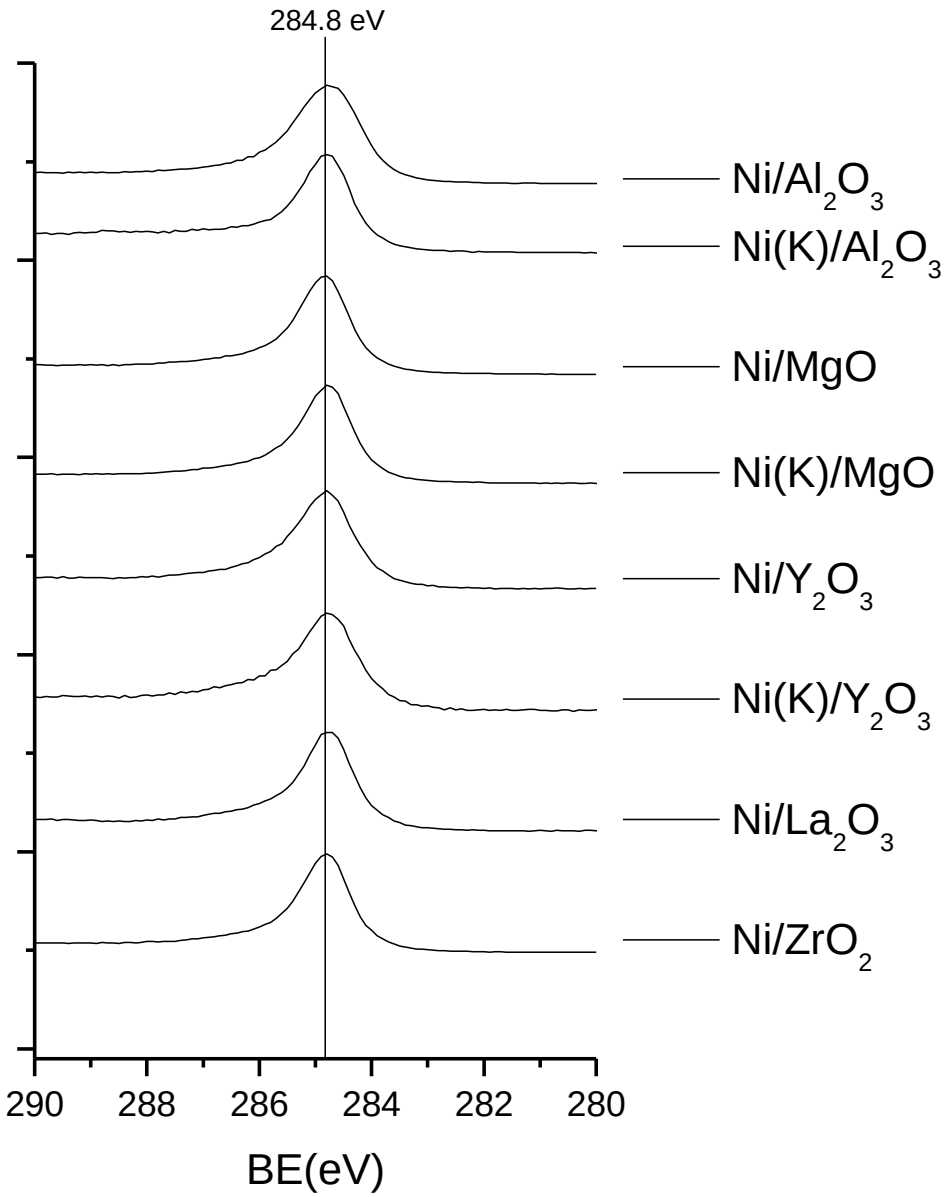

Figure A.1. XPS spectra of C1s region of post-reaction Ni/Me_xO_y catalysts after ESR

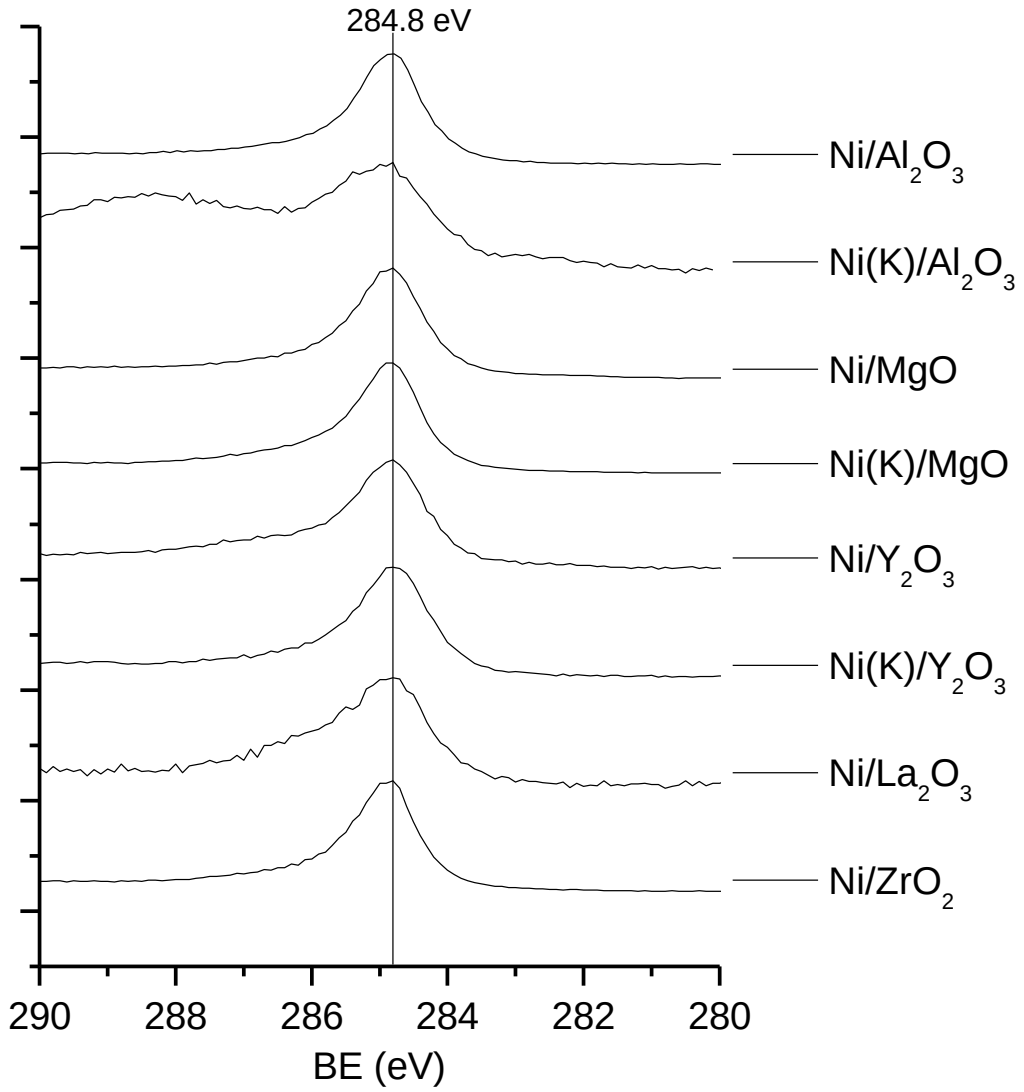

Figure A.2. XPS spectra of C1s region of post-reaction Ni/Me_xO_y catalysts after ESR with CO_2-treatment

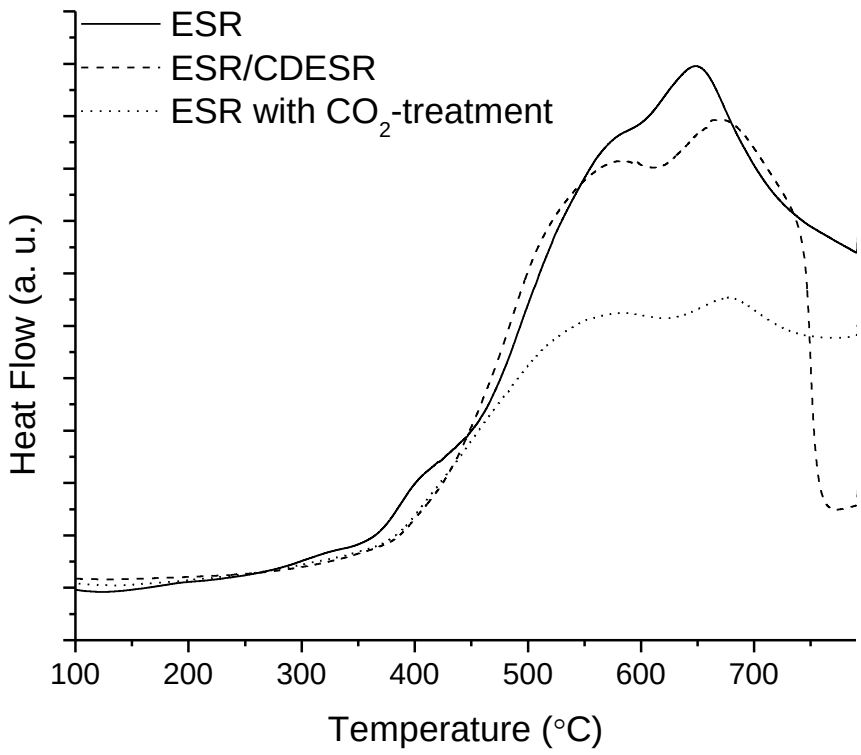

Figure A.3. Heat flow profiles obtained during TPO-MS analysis of post-reaction Ni/Al_2O_3 catalysts after ESR, ESR/CDESR and ESR with CO_2-treatment

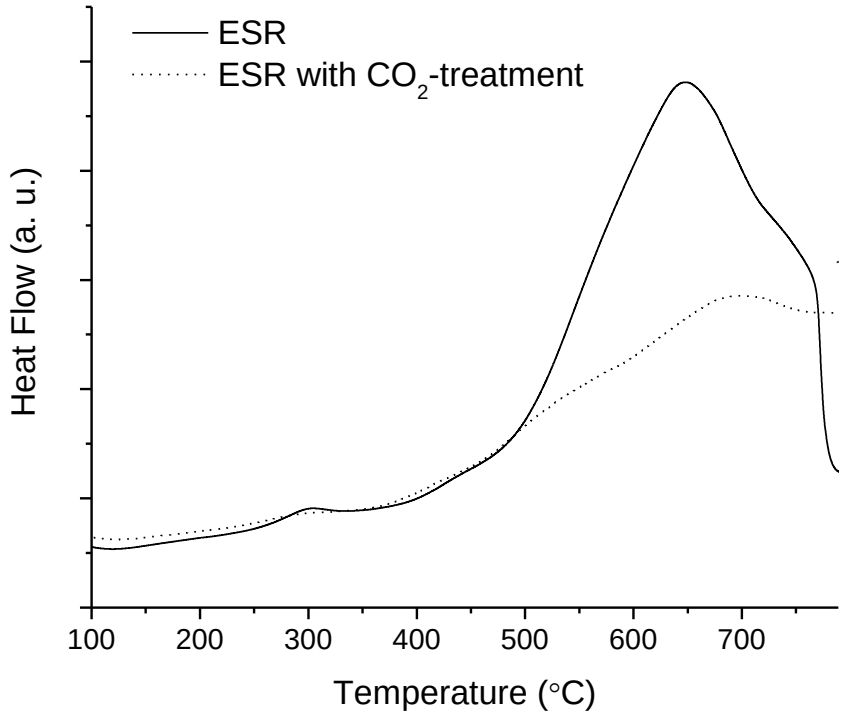

Figure A.4. Heat flow profiles obtained during TPO-MS analysis of post-reaction Ni(K)/Al_2O_3 catalysts after ESR and ESR with CO_2-treatment

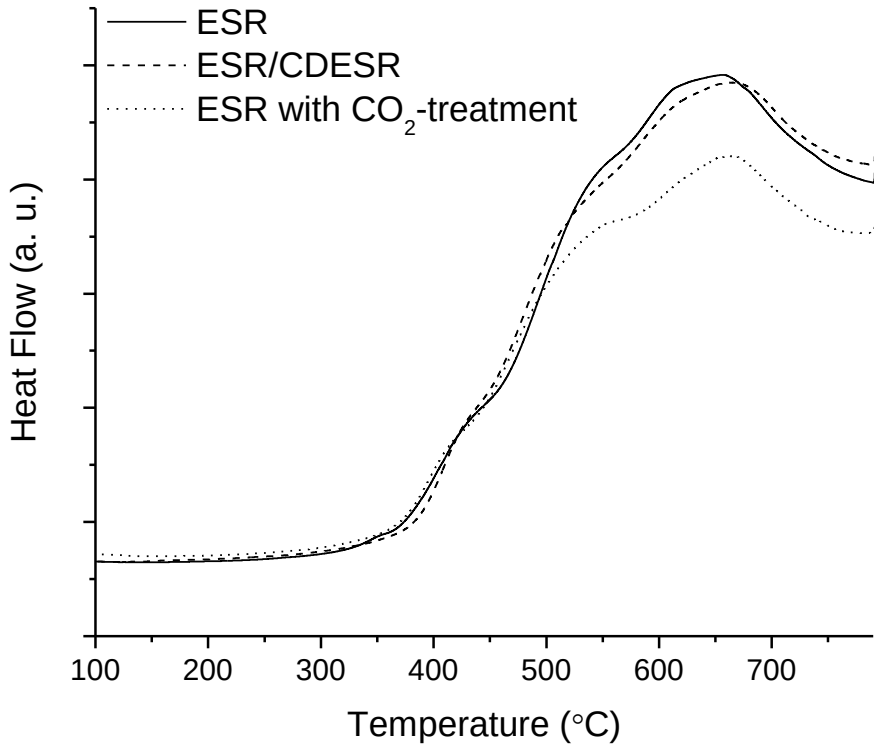

Figure A.5. Heat flow profiles obtained during TPO-MS analysis of post-reaction Ni(K)/MgO catalysts after ESR, ESR/CDESR and ESR with CO_2-treatment

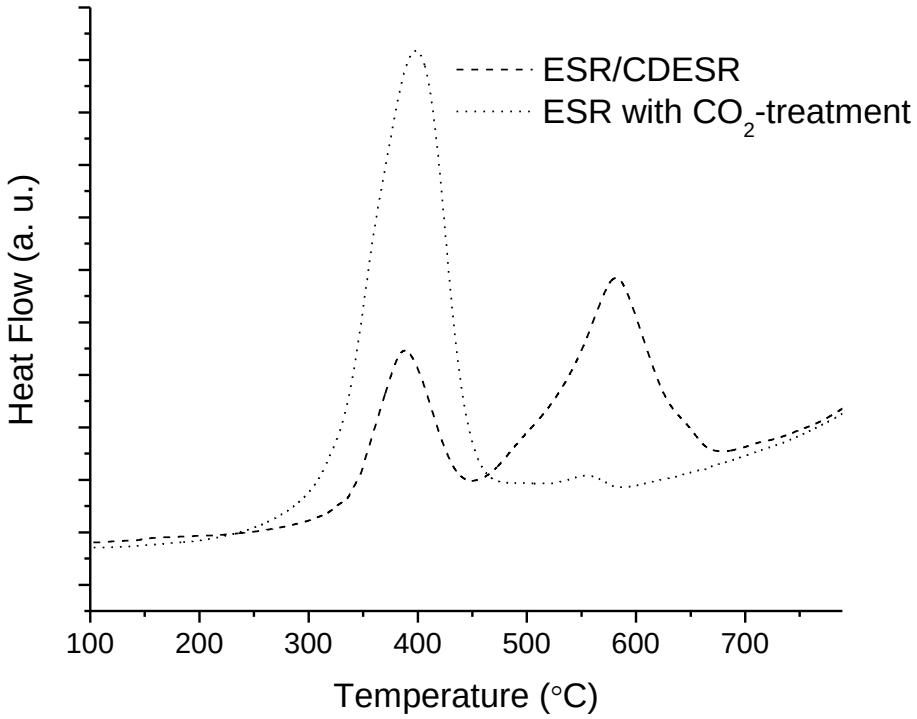

Figure A.6. Heat flow profiles obtained during TPO-MS analysis of post-reaction Ni(K)/Y_2O_3 catalysts after ESR/CDESR and ESR with CO_2-treatment

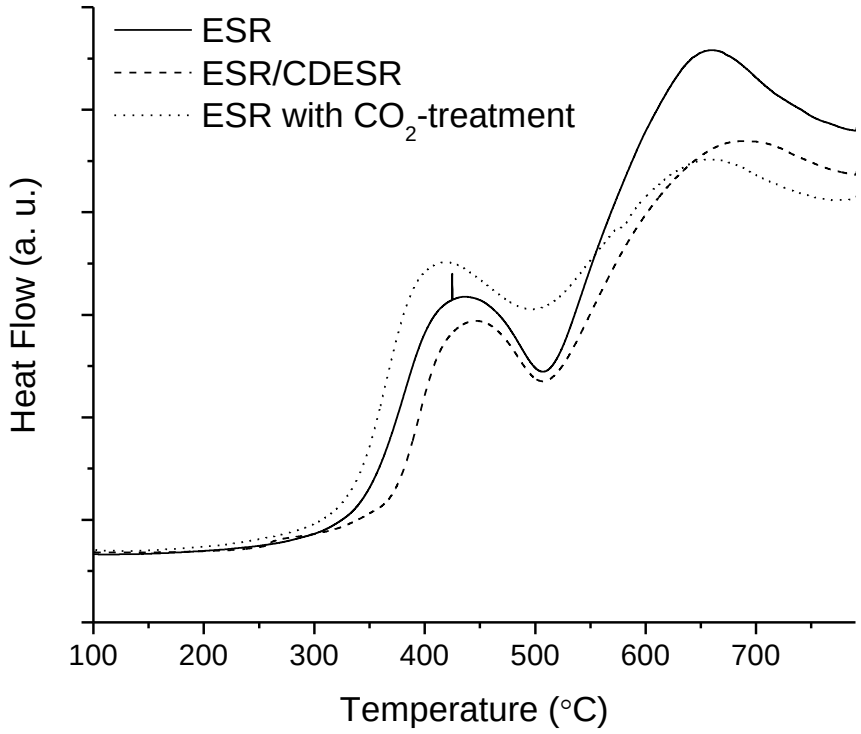

Figure A.7. Heat flow profiles obtained during TPO-MS analysis of post-reaction Ni/ZrO_2 catalysts after ESR, ESR/CDESR and ESR with CO_2-treatment

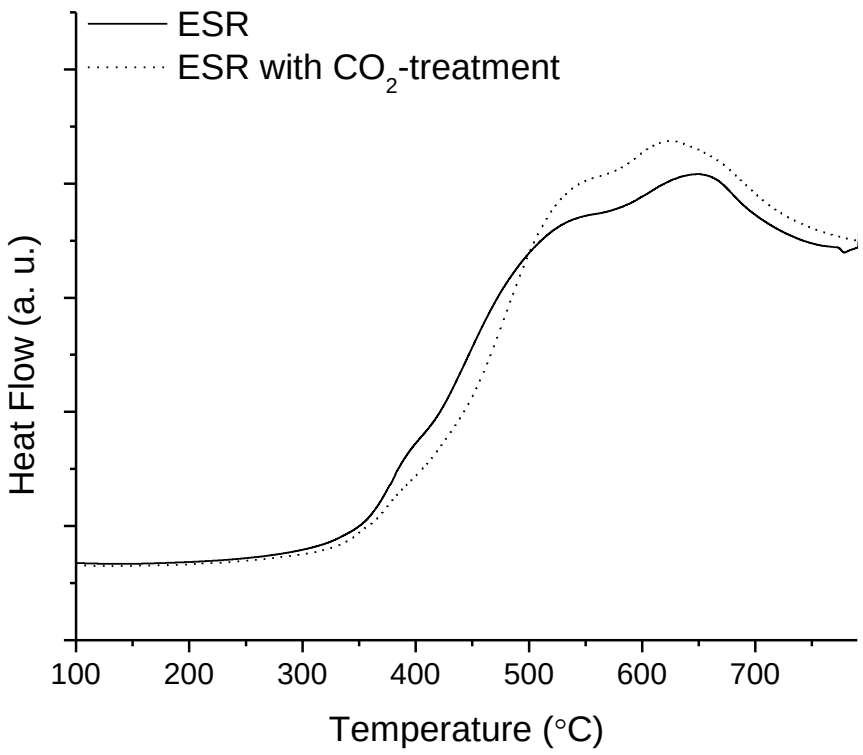

Figure A.8. Heat flow profiles obtained during TPO-MS analysis of post-reaction Ni/MgO catalysts after ESR and ESR with CO_2-treatment

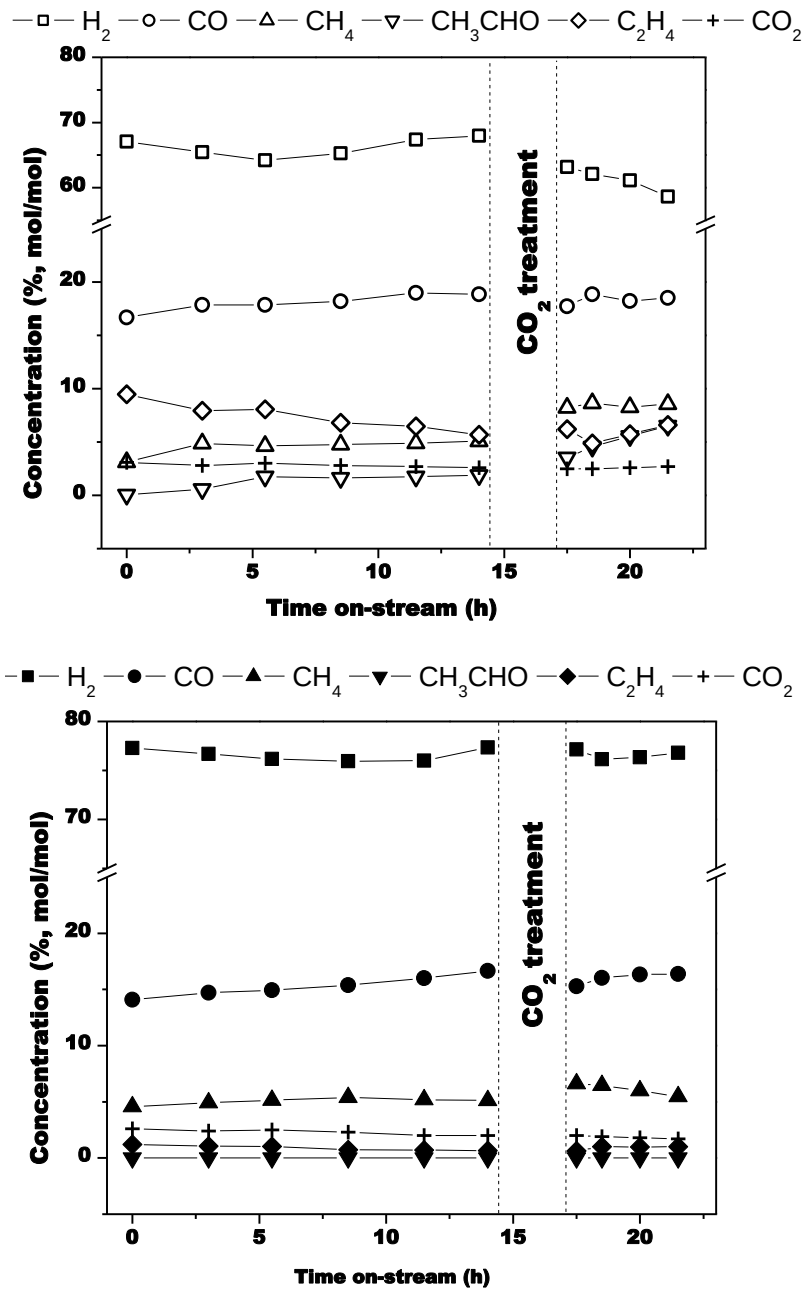

Figure A.9. Effect of the CO_2-treatment on the product distribution obtained over Ni/Al_2O_3 (top) and $Ni(K)/Al_2O_3$ (bottom). Molar concentrations of (□) H_2, (○) CO, (△) CH_4, (▽) CH_3CHO, (◇) C_2H_4 and (**+**) CO_2 in the outlet gas are shown. Reaction conditions: GHSV = 8100 h^{-1}, m_{cat} = 200 mg, T = 600 °C; 1.0 EtOH/1.6 H_2O/22.8 ($Ar+N_2$), molar ratios, for 18 hours with 2-hours break for CO_2-treatment.

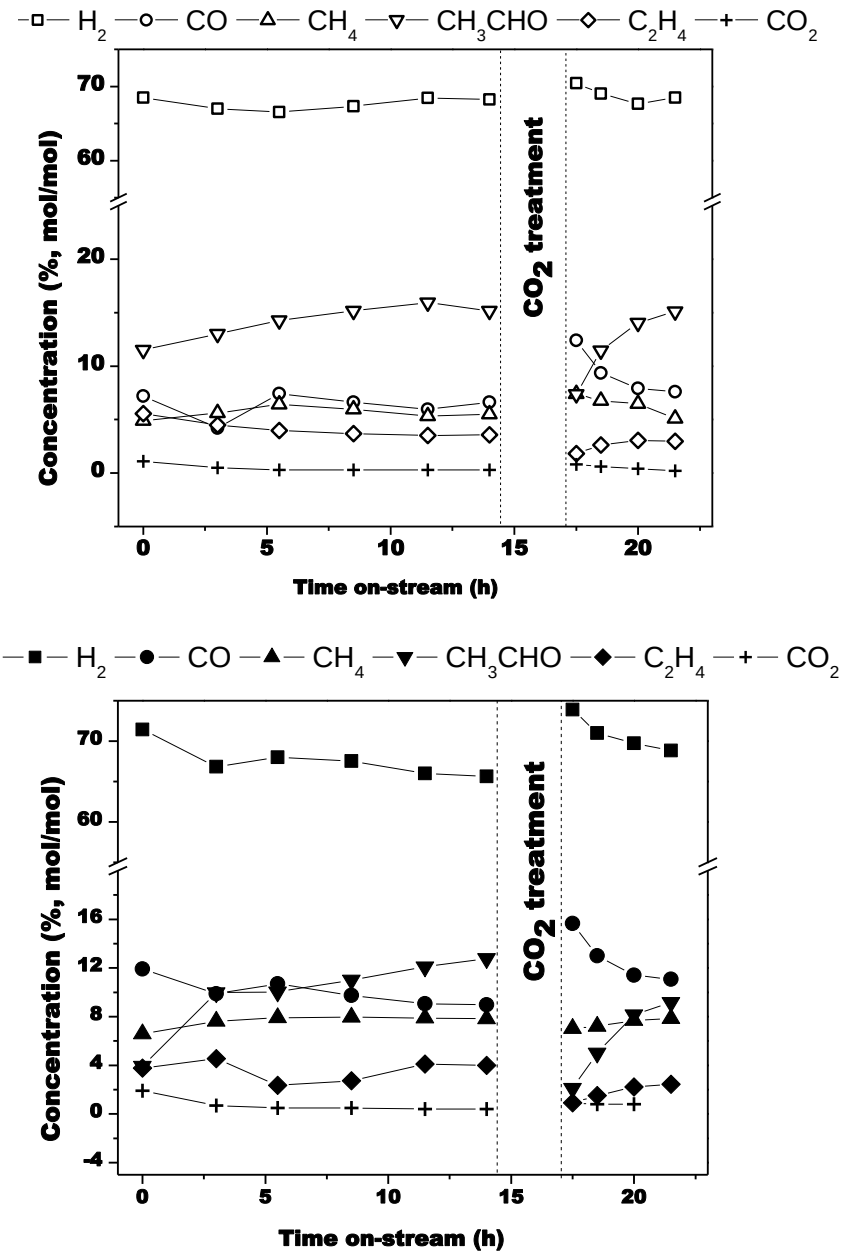

Figure A.10. Effect of the CO_2-treatment on the product distribution obtained over Ni(K)/MgO (top) and Ni(K)/MgO (bottom). Molar concentrations of (□) H_2, (○) CO, (△) CH_4, (▽) CH_3CHO, (◇) C_2H_4 and (**+**) CO_2 in the outlet gas are shown. Reaction conditions: GHSV = 8100 h^{-1}, m_{cat} = 200 mg, T = 600 °C; 1.0 EtOH/1.6 H_2O/22.8 ($Ar+N_2$), molar ratios, for 18 hours with 2-hours break for CO_2-treatment.

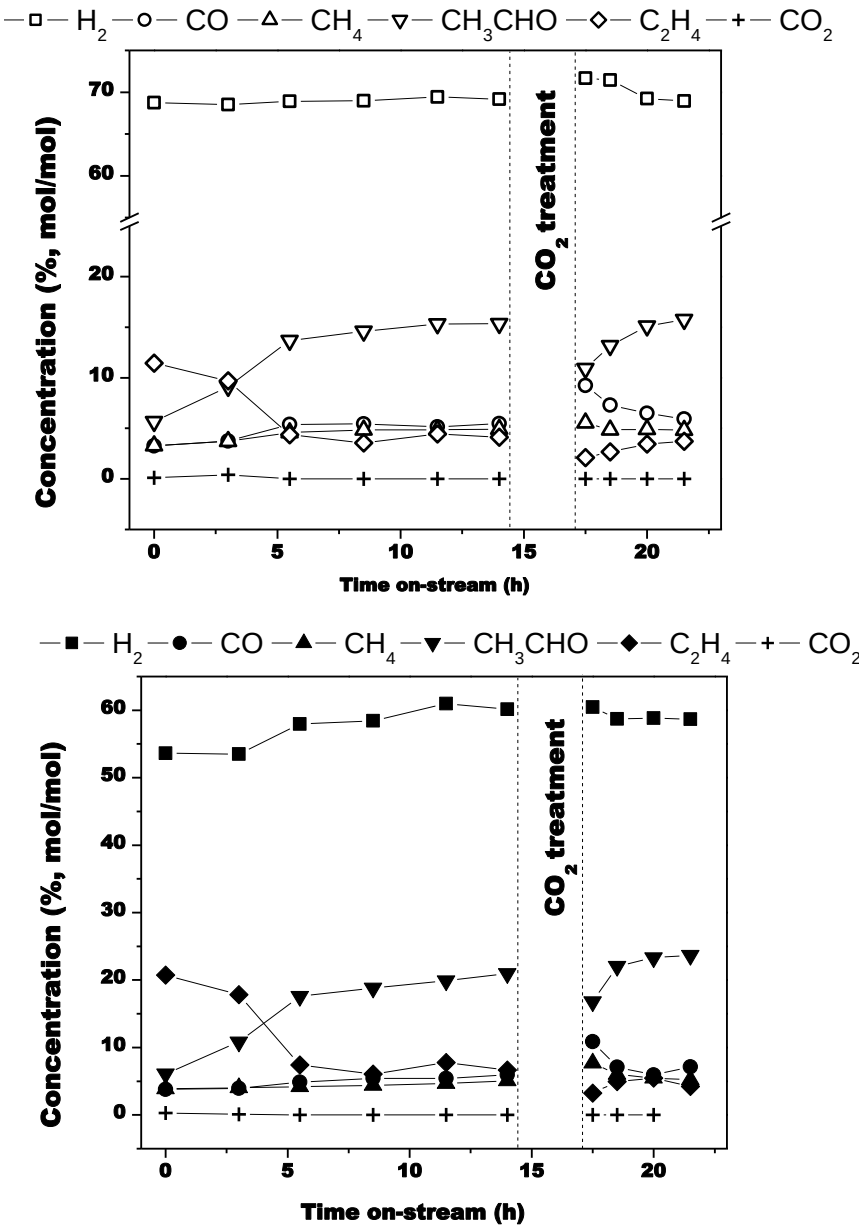

Figure A.11. Effect of the CO_2-treatment on the product distribution obtained over Ni(K)/Y_2O_3 (top) and Ni(K)/Y_2O_3 (bottom). Molar concentrations of (□) H_2, (○) CO, (△) CH_4, (▽) CH_3CHO, (◇) C_2H_4 and (**+**) CO_2 in the outlet gas are shown. Reaction conditions: GHSV = 8100 h^{-1}, m_{cat} = 200 mg, T = 600 °C; 1.0 EtOH/1.6 H_2O/22.8 (Ar+N_2), molar ratios, for 18 hours with 2-hours break for CO_2-treatment.

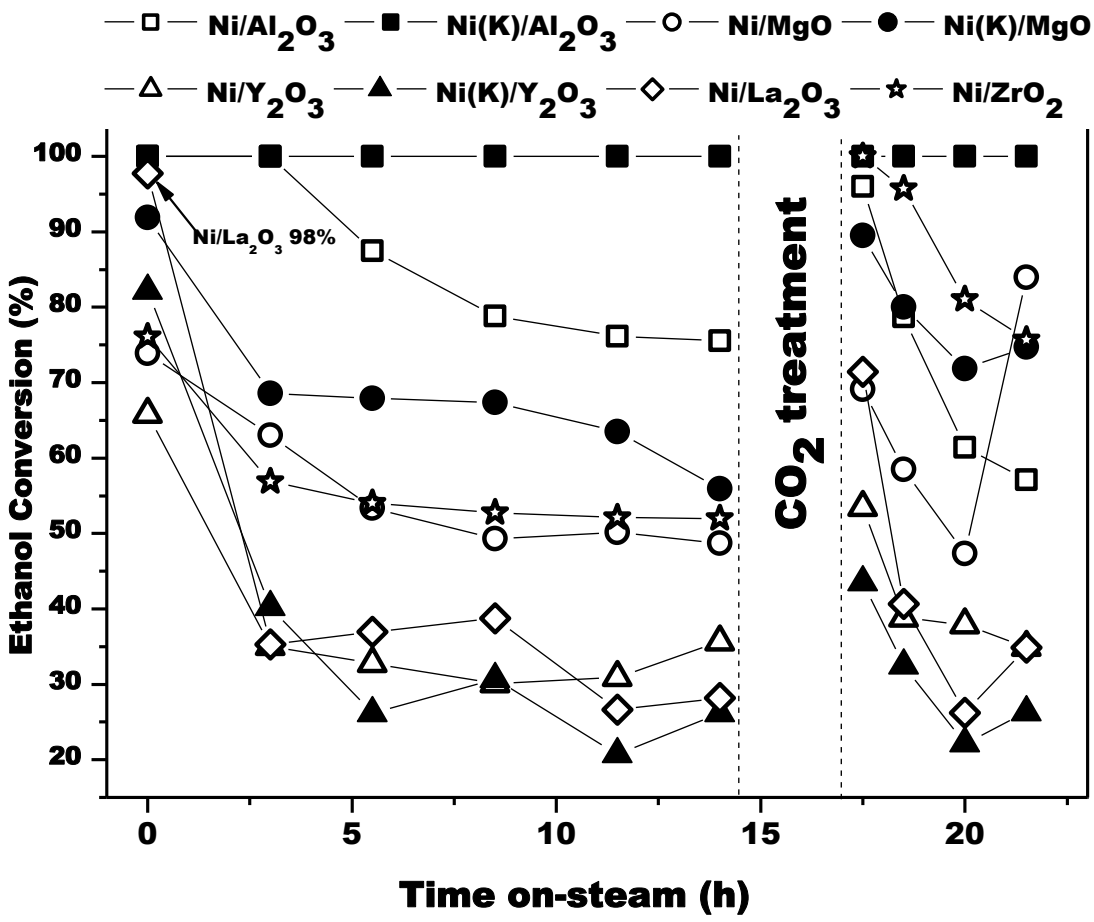

Figure A.12. Effect of the CO_2-treatment on the ethanol conversion over different catalysts. Reaction conditions: GHSV = 8100 h^{-1}, m_{cat} = 200 mg, T = 600 °C; 1.0 EtOH/1.6 H_2O/22.8 (Ar+N_2), molar ratios, for 18 h with 2-hours break for CO_2-treatment.

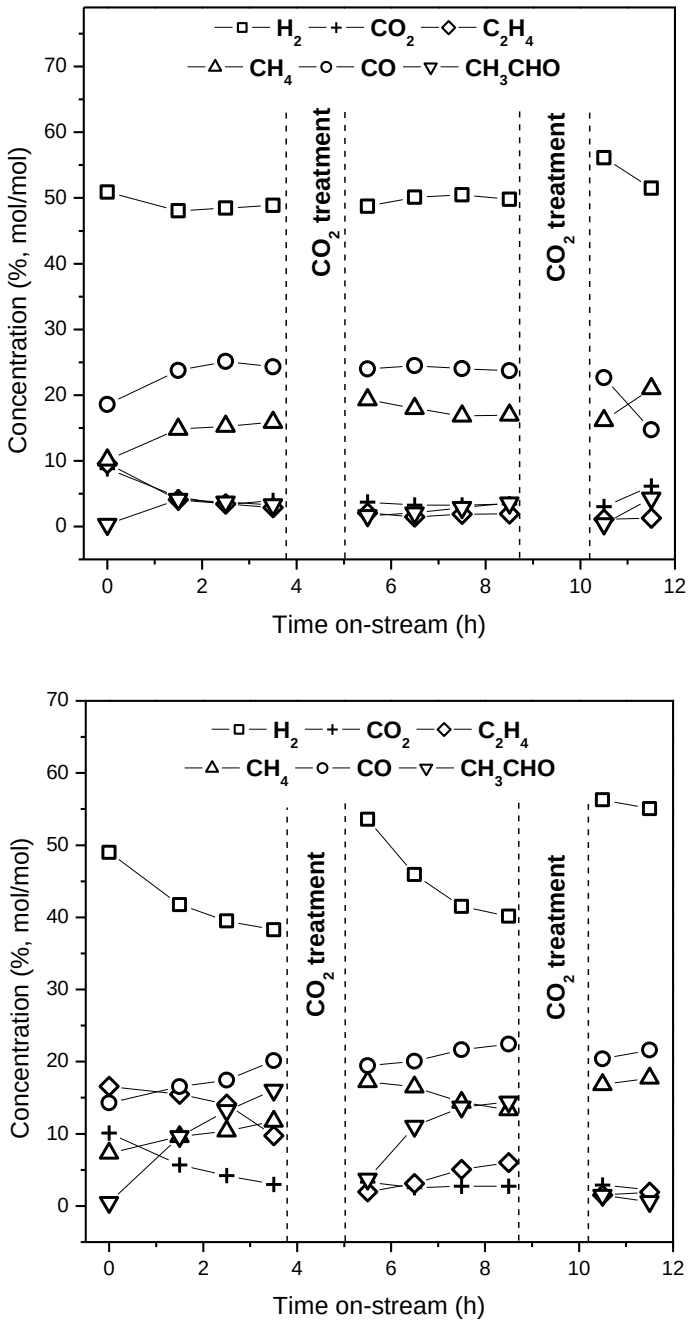

Figure A.13. Catalytic behaviour under ESR over Ni/35Zr14La (top) and Ni/36Zr14Y (bottom) catalysts. Reaction conditions: GHSV = 8100 h^{-1}, m_{cat} = 200 mg, T = 600 °C; 1.0 EtOH/1.6 H_2O/22.8 (Ar+N_2), molar ratios, for 10.5 hours with two 1-hour breaks for CO_2-treatments.

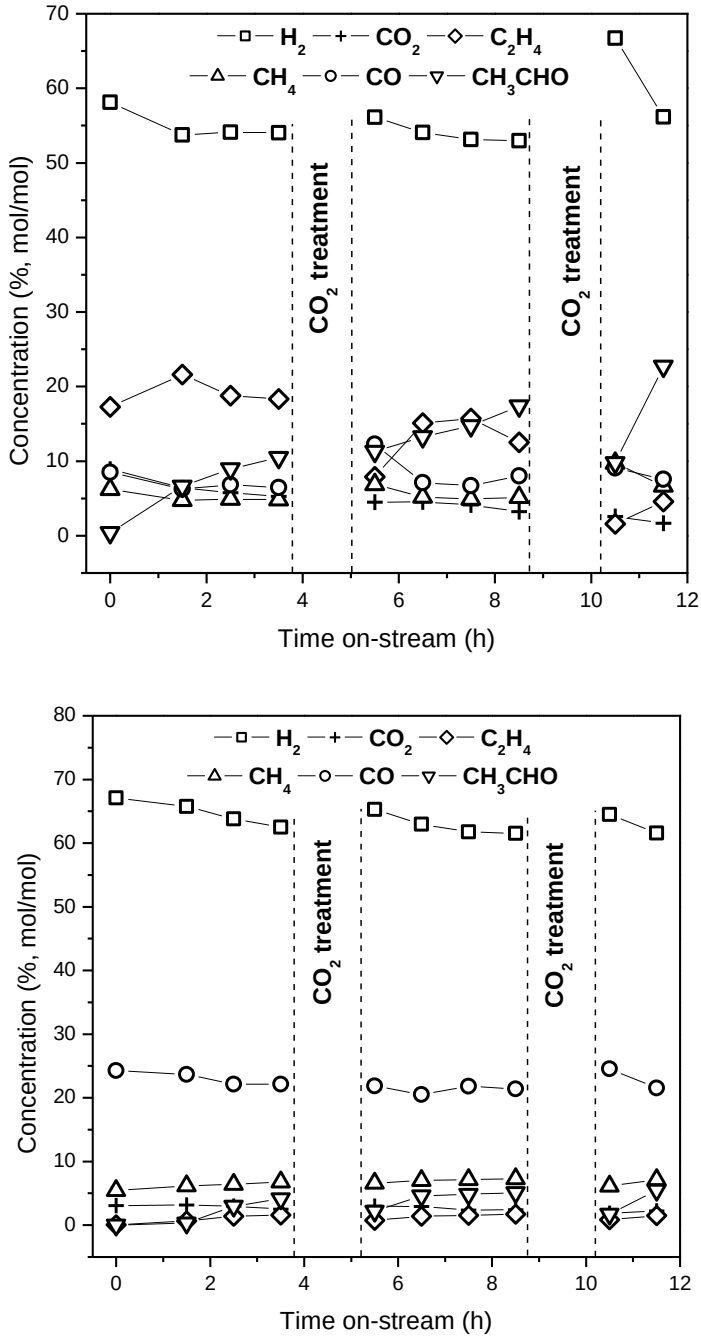

Figure A.14. Catalytic behaviour under ESR over Ni/8Zr45Y (top) and Ni/8Zr50La (bottom) catalysts. Reaction conditions: GHSV = 8100 h^{-1}, m_{cat} = 200 mg, T = 600 °C; 1.0 EtOH/1.6 H_2O/22.8 (Ar+N_2), molar ratios, for 10.5 hours with two 1-hour breaks for CO_2-treatments.

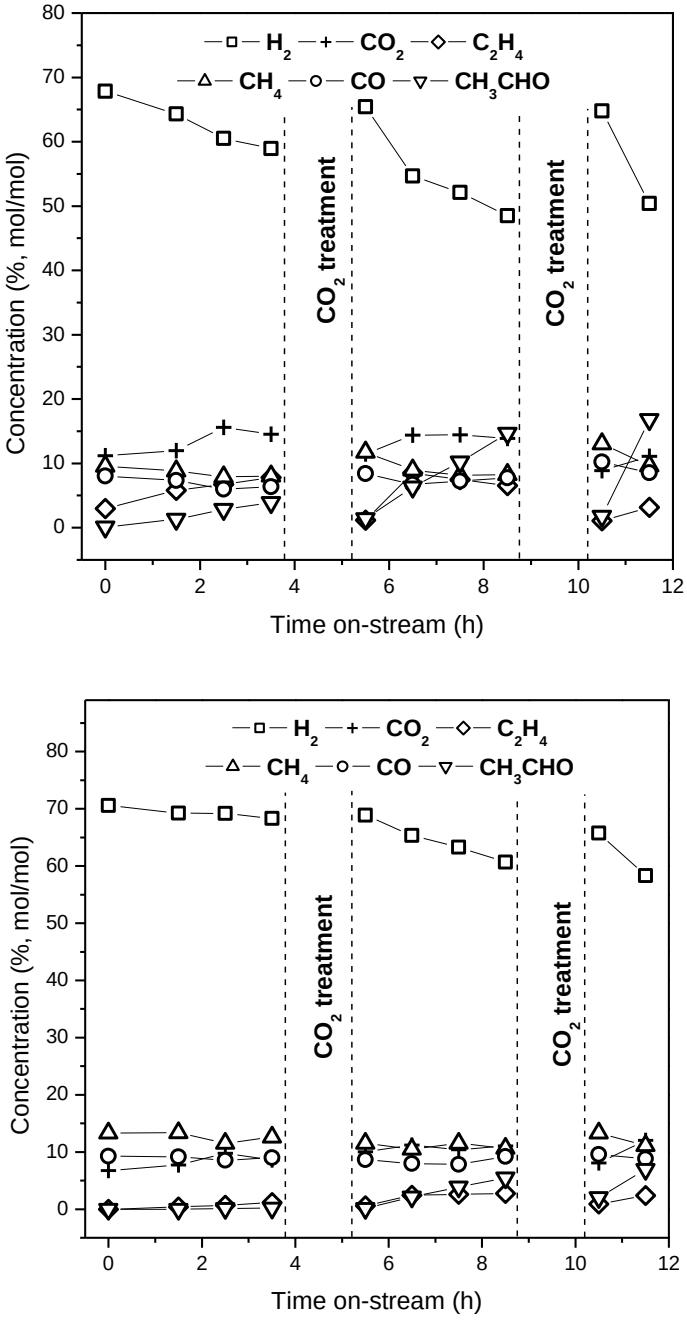

Figure A.15. Catalytic behaviour under ESR over Ni/12Zr29Y13La (top) and Ni/12Zr12Y31La (bottom) catalysts. Reaction conditions: GHSV = 8100 h^{-1}, m_{cat} = 200 mg, T = 600 °C; 1.0 EtOH/1.6 H_2O/22.8 (Ar+N_2), molar ratios, for 10.5 hours with two 1-hour breaks for CO_2-treatments.

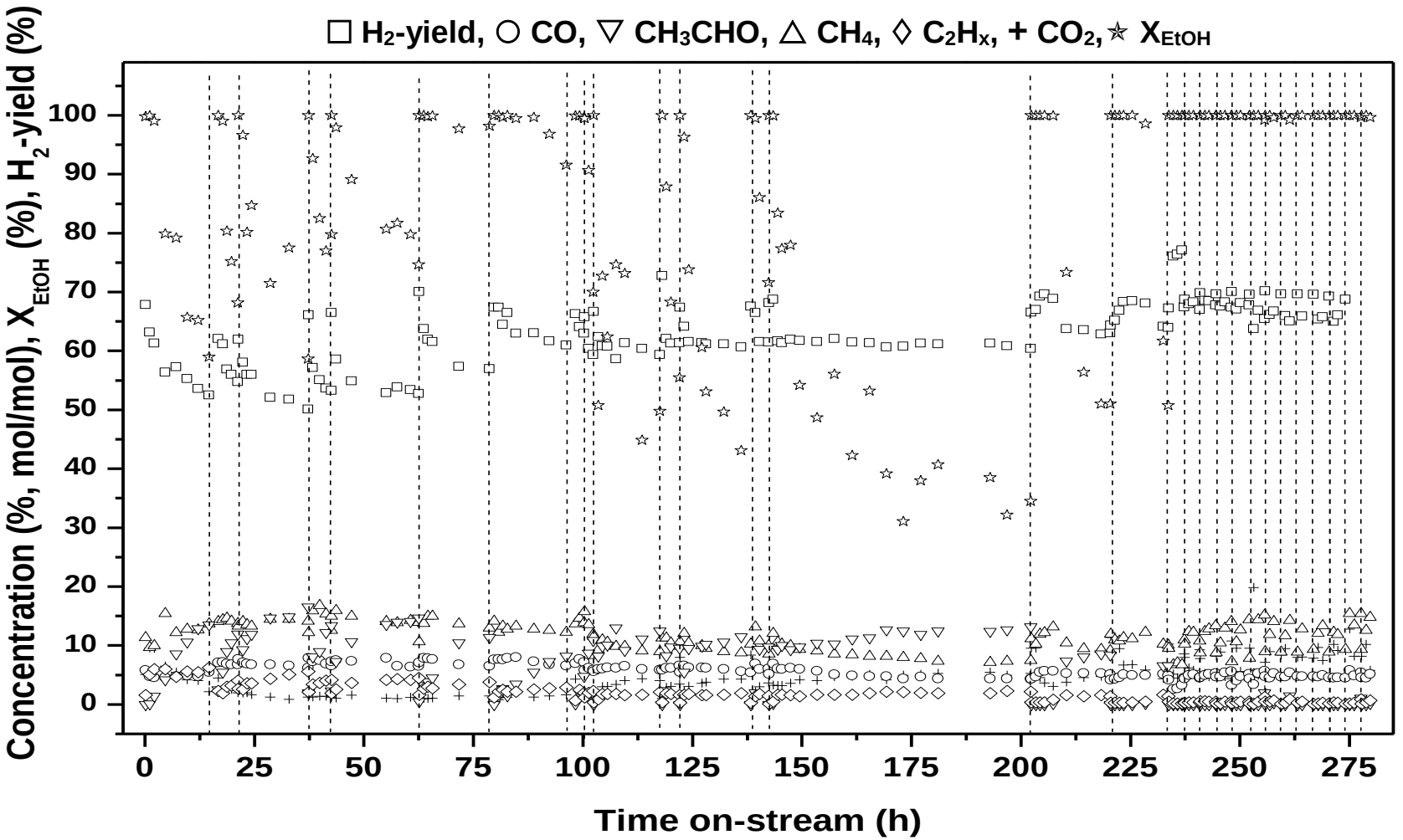

Figure A.16 H_2-yield, ethanol conversion and product distribution obtained over Ni/12Zr29Y13La catalyst during ESR with CO_2-treatments (indicated by vertical dashed lines) for 280 h. During the last 50 h, 1-hour CO_2-treatments were applied periodically every 4 h. GHSV = 8100 h^{-1}, m_{cat} = 200 mg, T = 600 °C; 1.0 EtOH/1.6 H_2O/22.8 ($Ar+N_2$), molar ratios